University of Alberta

The Design of Instrumentation for Force Measurement During Scoliosis Surgery

By

Kajsa Kelly Duke

A thesis submitted to the Faculty of Graduate Studies and research in partial fulfillment of the requirements for the degree of Masters of Science.

Department of Mechanical Engineering
&
Department of Biomedical Engineering

Edmonton, Alberta

Spring 2001

National Library of Canada
Acquisitions and Bibliographic Services
395 Wellington Street
Ottawa ON K1A 0N4
Canada

Bibliothèque nationale du Canada
Acquisitions et services bibliographiques
395, rue Wellington
Ottawa ON K1A 0N4
Canada

Your file Votre référence

Our file Notre référence

The author has granted a non-exclusive licence allowing the National Library of Canada to reproduce, loan, distribute or sell copies of this thesis in microform, paper or electronic formats.

L'auteur a accordé une licence non exclusive permettant à la Bibliothèque nationale du Canada de reproduire, prêter, distribuer ou vendre des copies de cette thèse sous la forme de microfiche/film, de reproduction sur papier ou sur format électronique.

The author retains ownership of the copyright in this thesis. Neither the thesis nor substantial extracts from it may be printed or otherwise reproduced without the author's permission.

L'auteur conserve la propriété du droit d'auteur qui protège cette thèse. Ni la thèse ni des extraits substantiels de celle-ci ne doivent être imprimés ou autrement reproduits sans son autorisation.

0-612-60422-5

Canada

University of Alberta

Library Release Form

Name of Author:	**Kajsa Kelly Duke**
Title of Thesis:	**The Design of Instrumentation for Force Measurement During Scoliosis Surgery**
Degree:	**Master of Science**
Year this Degree Granted:	**2001**

Permission is hereby granted to the University of Alberta Library to reproduce single copies of this thesis and to lend or sell such copies for private, scholarly or scientific research purposes only.

The author reserves all other publication rights in association with the copyright in the thesis, and except as herein before provided, neither the thesis nor any substantial portion thereof may be printed or otherwise reproduced in any material form whatever without the author's prior written permission.

Kajsa Duke

Kajsa Duke
51424C Hwy 60
Spruce Grove, Alberta
T7Y 1C8

Date: Jan. 30, 2001

University of Alberta

Faculty of Graduate Studies and Research

The undersigned certify that they have read, and recommend to the Faculty of Graduate Studies and Research for acceptance, a thesis entitled **The Design of Instrumentation for Force Measurement During Scoliosis Surgery** submitted by **Kajsa Kelly Duke** in partial fulfillment of the requirements for the degree of **Master of Science**

Dr. Ken Fyfe (Supervisor)

Dr. Richard Snyder (Co-supervisor)

Dr. David Budney

Dr. Brian Fleck

Dr. Terry Hrudey

Date: JAN 29, 2001

To my parents

Abstract

Scoliosis surgery involves fixation of various hooks, screws and rods to straighten the 'S' shaped spine. The procedure is controlled by the surgeons' skill and feel, as they are unaware of the applied forces. The object of this thesis was to design instruments capable of measuring forces and moments applied during scoliosis surgery.

An instrument called the Gripper, housing strain gauges, was fit over a rod rotator to measure the forces and moments. The Gripper was tested on 17 patients where the average maximum force and moments applied were 39 (±14) N and 8 (±1) Nm respectively.

Finite element analysis (FEA) was used to aid in designing a hook capable of measuring the forces at the vertebral level. Preliminary results, from the Plate hook, show the largest moments are applied on insertion and removal of the hook, reaching a maximum of 1.1 Nm. The largest axial force observed was 370 N. Time traces of forces and moments produced by the Gripper and the Plate hook provided insight on scoliosis surgery mechanics.

Acknowledgements

I am indebted to many people for their help in the completion of this thesis. The first group to whom I owe gratitude is Jim Raso's group at the Glenrose Hospital. Any electronics or programming help was always available from Narc, Doug, Edmond and Mark. The surgeons Marc Moreau and Jim Mahood were patient as they kept waiting to see some dramatic breakthrough. The Glenrose also gave me many opportunities to grow, through an exchange to Paris and by presenting my work at various conferences. In general it is a great place to work, from summer bar-B-Q's to Hearts games to experiences in the cadaver lab.

From the mechanical engineering department I need to thank Ken Fyfe who accepted me and the project without really knowing what he was getting into. While the "retired" Dave Budney has continued to provided support and design ideas. Help with manufacturing, calibrating and general trouble shooting was provided by Bernie, Dave, Ian and Terry. I know who really keeps the MecE department running, and for that I need to thank Lynda, Gail, Doris and Helen.

The friendship and help from fellow Mec/BME girls such as Alice, Monica, Tonya, Kristen and Allison. Many other friends and fond memories have tempted me to never leave this university. My family must be thanked, for they were always very supportive and proud of my work. Finally, I need to thank Demetri for his friendship, "crazy theories and common sense".

Contents

Chapter 1 Background 1

1.1 Anatomy 1
1.1.1 Vertebral Column 2
1.1.2 Vertebral Anatomy 2
1.2 Scoliosis 3
1.2.1 Scoliosis in General 3
1.2.2 Progression 3
1.2.3 Treatment of Scoliosis 3
1.3 Surgical Instrumentation and Procedure 4
1.3.1 Surgical Instrumentation 5
1.3.2 Pre-op planning 5
1.3.3 Hook Placement 6
1.3.4 Convex Hook Placement 6
1.3.5 Rod Insertion 6
1.3.6 Rod Rotation Maneuver 7
1.4 Qualitative Prediction of Mechanical Forces Applied to the Spine 7

2 Literature Review 22

2.1 Surgical Complications 22
2.1.1 Failure in Harrington Rod Systems 22
2.1.2 Failure of Cotrel Dubousset (CD) System 23
2.2 Biomechanical Tests 25
2.2.1 Pedicle Screw Pullout 25
2.2.2 Pedicle Screw Insertional Torque 25
2.2.3 Pullout of Hooks 25
2.3 *In-vivo* Force Measurements 27
2.4 Chapter Discussion and Future Directions 29

3 The Gripper 32

3.1 Background 32
3.2 Materials and Methods 33
3.3 Results 36
3.3.1 Calibration 36
3.3.2 Surgical Tests 36
3.4 Chapter Summary 38

4 FEA and Hook Design 50
4.1 Introduction 50
4.2 FEA Background 51
4.3 Material and Methods 51
4.4 FEA Results of the Three Designs 53
4.5 FEA of Plate 54
4.6 Magnitude of Plate Strains 55
4.7 Analytical formulas of the Plate 56
4.8 Probable Error 60
4.9 Comparison of FEA, Excel and Gauge Output of the Plate 62

5 Using the Plate Hook **71**
5.1 Introduction 71
5.2 Manufacturing of hook 71
5.2.1 Material selection 71
5.2.2 Hook geometry 72
5.2.3 Other consideration 73
5.3 Calibrating the Hooks 74
5.3.1 Initial results 74
5.3.2 Axial Calibration 74
5.3.3 Moment Calibration 76
5.4 Using the plate hook 76
5.4.1 Surgical Case 1 77
5.4.2 Noise Test 77
5.4.3 Surgical Case 2 78
5.4.4 Failure of Plate B 78
5.4.5 Failure of Plate C 79
5.4.6 Surgical Case 3 79

6 Conclusions 99
6.1 Chapter 1 99
6.2 Chapter 2 99
6.3 Chapter 3 100
6.3.1 Conclusions from Gripper Study 100
6.3.2 Future work with Gripper 100
6.4 Chapter 4 101
6.5 Chapter 5 101
6.5.1 Conclusions of Plate Hook Design 101
6.5.2 Future Work with Plate Hook 103
6.6 Closing Remarks 103

References **105**

Appendix A Electronics and DAC System **108**
A.1 Bridge Circuits 108
A.2 DAC System 109
A.3 LabWindows 110

Appendix B Finite Element Type Selection 112
B.1 Introduction 112
B.2 Materials and Method 112
B.3 Results 113
B.4 Conclusions 113

List of Figures

	page
Figure 1.1: Vertebral column anatomy	9
Figure 1.2: Vertebra anatomy	10
Figure 1.3: Fixation of pedicle screws	11
Figure 1.4: Scoliosis	12
Figure 1.5: Radiograph of patient with scoliosis. Cobb angle measures 73°	13
Figure 1.6: Various hooks	14
Figure 1.7: Vertebral screw	14
Figure 1.8: Pre and post op x-ray of scoliosis patient	15
Figure 1.9: Hook placement	16
Figure 1.10: Rod contouring	16
Figure 1.11: Rod insertion	17
Figure 1.12: Rod rotation maneuver	17
Figure 1.13: Maintenance of kyphosis in sagittal plane	18
Figure 1.14: The Cartesian coordinate system as oriented with respect to the spine	19
Figure 1.15: Schematic of axial pull-out force	20
Figure 1.16: Schematic of axial push-in force	20
Figure 1.17: Schematic of compressive force	21
Figure 1.18: Schematic of distraction force	21
Figure 3.1: The Gripper	39
Figure 3.2: FBD of entire Gripper system in horizontal clamped position	40
Figure 3.3: FBD of resultant force (F_c) and moment (M_c) within Gripper sleeve	41
Figure 3.4: Free body, shear force & bending moment diagrams for cantilever beam	42
Figure 3.5: Gripper force calibration	43
Figure 3.6: Inclinometer calibration	44
Figure 3.7: Sample I of Gripper force and inclination data	45
Figure 3.8: Sample IIa of Gripper force and inclination data	46
Figure 3.9: Sample IIb of Gripper force and inclination data	47
Figure 3.10: Amount of Cobb angle correction vs force	48
Figure 3.11: Cobb angle correction versus force for AIS patients only	49
Figure 4.1: Sofamor Danek CD pedicle hook	65
Figure 4.2: The force and constraints applied to the standard CD hook	66
Figure 4.3: The three modeled designs	67
Figure 4.4: The constrained membrane	68
Figure 4.5: Schematic representation of plate subjected to four major forces	69
Figure 4.6: Free body, shear Force, and bending moment diagrams for simply supported beam	70

Figure 5.1: Prototype "plate" hook 81
Figure 5.2: The raw voltage, resultant force and moment for bend, bend, push, pull test 82
Figure 5.3: Calibration setup 83
Figure 5.4: Raw voltage from tension compression axial calibration 84
Figure 5.5: Calculated plate force vs applied Instron force 85
Figure 5.6: Calibrated plate force vs applied Instron force 86
Figure 5.7: Moment calibration setup 87
Figure 5.8: Raw voltages from Case 1 88
Figure 5.9: Edited results from Case 1 89
Figure 5.10: A close up look at the moments applied during hook insertion 90
Figure 5.11: The moments and force present on removal of the hook in Case 1 91
Figure 5.12: Force present while rod pusher is used 92
Figure 5.13: Noise test with various equipment in empty OR 93
Figure 5.14: Raw voltages, calculated forces and moments from Case 2 94
Figure 5.15: Insertional moment and failure of Plate 95
Figure 5.16: Test of Plate B in Instron Machine 96
Figure 5.17: Ambient noise comparison 97
Figure 5.18: Results of OR Case 3 98

Figure A.1: Wheatstone bridge circuit electronic schematic 111
Figure B.1: FEA model of cantilever beam 114

List of Tables

Table1.1: Treatment of various severity's of scoliosis 4

Table 4.1: Summary of three hooks and design criteria 54
Table 4.2: Variables and their respective value and errors. 61
Table 4.3: Strain results from three methods. Error/standard deviation in brackets. 63

Table 5.1: Mechanical properties of three plates 73

Table A.1: Electronic components 108
Table A.2: Software selectable gain 110
Table B.1: Bending test results 113

Chapter 1 Background

The object of this thesis work was to design instruments that can be used to measure the forces applied during scoliosis surgery. Scoliosis surgery involves the fixation of various instruments such as hooks, screws and rods into the spine to straighten the deformed 'S' shaped scoliotic curve. Presently the surgeons are unaware of the amount of force applied during surgery. They requested that this force be quantified.

This thesis begins by providing a general background into scoliosis and the surgical procedure. Chapter 2 reviews the relevant research discussing complications, *in-vitro* biomechanical tests and *in-vivo* force measurements. Chapter 3 presents the Gripper, which is the first instrument designed to measure the force applied during the rod rotation maneuver a corrective step during scoliosis surgery. In order to measure the force applied to the vertebra, an instrumented hook was designed and the process is discussed in Chapter 4. Once the general Plate hook design was selected, it was manufactured and tested as discussed in Chapter 5. Finally, in Chapter 6, conclusions and future directions are discussed.

Chapter 1 provides the necessary medical background to understand this thesis work. It begins by discussing the anatomy of the vertebral column and the vertebra itself. This is followed by a general discussion of scoliosis and some treatment options frequently prescribed. The surgical instrumentation and surgical procedure used to treat scoliosis are discussed in detail followed by a discussion of predicted forces applied during the surgical procedure. The goal of this section is to provide an understanding of the biomechanics involved in surgical correction of scoliosis.

1.1 Anatomy

To become acquainted with the basic anatomy of the spine, the anatomy of the vertebral column and a typical vertebra are discussed.

1.1.1 Vertebral column

The vertebral column is divided into four major components (Figure 1.1). At the top is the cervical spine or neck. The thoracic region consists of the vertebra to which ribs attach. The lower back is called the lumbar region and the part that fuses to the pelvic is the sacrum and coccyx. Scoliotic deformities occur in the thoracic and lumbar region of the spine. Scoliosis is often recognized as an "S" shaped curvature viewed from the back. During the surgical procedure, portions of the thoracic and lumbar regions are fused. In some severe cases, where the mobility of the patient is not of prime concern, the lumbar section in fused to the sacrum.

In a normal spine (Figure 1.1b) there is natural curvature in the sagittal plane. A slight kyphosis (hunchback) is present in the thoracic region and lordosis (sway back) is present in the lumbar region. Natural curves in this plane must be maintained while correcting the scoliosis curve in order to maintain proper balance of the patients.

1.1.3 Vertebral Anatomy

The basic anatomy of a vertebra can be seen in Figure 1.2a depicting a superior view of the vertebra (looking down). The most predominant part of the vertebra is the spinous process (Figure 1.2b). This part this part can be felt as bumps along the spine. The bodies of the vertebrae carry the majority of the load and are separated by intervertebral disks. Other important landmarks to note on the vertebra are the lamina, pedicles and transverse processes. In scoliosis surgery the lamina are important for the seating of the hooks. The pedicles form the sides of the arch that protects the spinal cord. For instrument fixation, pedicle screws are anchored through the pedicles and into the body of the vertebra (Figure 1.3). Pedicle hooks attach similarly to laminar hooks expect that the tip is notched to fit around a pedicle. Other hooks can anchor to the transverse processes. Details of the surgical instrumentation are discussed later in this chapter.

1.2 Scoliosis

This section is to provide a general definition of scoliosis. Described are the differences between the various classifications of scoliosis. Progression of scoliosis is mentioned, as this is important in selecting the various treatments.

1.2.1 Scoliosis in general

In the past, scoliosis has been defined as a lateral curvature of the spine. More recently the attention has focused on scoliosis as a three dimensional deformity (Dubousset 1994, Aubin 1999). With the three dimensional deformity, there is often rotation of the vertebra which presents itself as a rib hump (Figure 1.4). From the sagittal view (from the side) there is often flat back associated with scoliosis. Although the presence of a three dimensional deformity is now widely recognized, the clinical definition of scoliosis is a curve of over 10^{o} as measured from an AP radiograph using the Cobb angle (Figure 1.5). Scoliosis is often secondary to some neuromuscular disease such as muscular dystrophy. There is however a large percentage of scoliosis ($\approx$80%) that develops in otherwise healthy children for no known cause. This type of scoliosis is classified as idiopathic. Adolescent idiopathic scoliosis (AIS) is the most common spinal deformity (Longstein 1994). From school screening studies, the prevalence of scoliosis is between 1.5 and 3%.

1.2.2 Progression

The onset and progression of AIS is most common in children during the adolescent growth spurt. Its progression is multivariable but primarily based on the child's maturity and the type and severity of the curve. Curve progression is less of a risk after menarche. Larger double curves are more likely to progress than small single curves (Longstein 1994), but it is still very difficult for the doctor to predict whether or not a curve will progress.

1.2.3 Treatment of Scoliosis

A sound understanding of the progression of the scoliotic curve is necessary to provide the best treatment. The treatment of scoliosis varies at different clinics

throughout the world. The most common forms of treatment are observation, bracing and surgical fusion. Table 1.1 summarises the treatment of scoliosis.

Table1.1: Treatment of various severity's of scoliosis

Curve (degrees)	Maturity	Treatment
< 20	low maturity	observation
20-30	low maturity	bracing
30-40	growth remaining	bracing
<45-50	no growth remaining	nothing
>45-50	any age	surgical fusion

Other non-operative treatments are used at some centres such as electrical stimulation, exercise, biofeedback, and manipulation, all of which have not yet been proven to alter the natural history of AIS. For surgical correction, the minimum number of vertebra should be fused to leave the patient as mobile as possible.

In the 1960's, Harrington (1962) introduced the first widely used spinal instrumentation system. It consisted of a distraction rod attached with hooks to the lamina. This rod stabilized the spine so that fusion could occur. Since then, various systems have emerged consisting of various hooks, screws, wires, rods, and plates. The system most commonly used at the University of Alberta to treat AIS is the Cotrel Doubouset (CD) system by Sofamor Danek. The surgical procedure of this system needs to be understood in detail to predict the mechanical forces applied to the spine. Details of this procedure are provided in the following section.

1.3 Surgical Instrumentation and Procedure

A description of the surgical instrumentation used during scoliosis surgery is necessary prior to a description of the procedure. According to Polly (1996), posterior spinal instrumentation can be subdivided into two areas: longitudinal and attachment

members. Longitudinal members include rods, plates and wires. Attachment members include hooks, screws and wires.

1.3.1 Surgical Instrumentation

Rods are conformable in 3-D and are the longitudinal member used in the Sofamor Danek CD system. Plates work best for single level correction (Polly, 1996). They are attached via bone screws whose attachment site is the limiting factor due to the quality and geometry of the bone. Plates are seldom used in scoliosis surgery and will not be further discussed.

Hooks are named based on their site of placement (Figure, 1.6). Laminar hooks can either be placed cephalad, facing up or caudialy, facing down. Pedicle hooks can be placed from T2-T10 and are only placed facing up. Transverse process hooks are placed in the thoracic spine facing either up or down. Laminar hooks are stronger then pedicle hooks, but intrude into the spinal canal. Pedicle hooks are less intrusive and transverse process hooks and do not intrude at all into the spinal cannel. All screws are bone screws. They can be placed into either the body, pedicle, facet or fusion mass (Figure 1.7).

1.3.2 Pre-op Planning

Considerations must be made including: patient size, compliance, age, bone quality etc. Geometry must also be considered such as segment of spine, size of spine, alignment and attachment sites. Prior to the surgery, the hook and screw placement sites are selected and laid out on the pre-op x-ray (Figure 1.8).

The patient is placed in the prone position, face down, on the table. An incision is made down the centre of the patient's back and all the muscles posteriorly attached to the vertebra are removed to expose the vertebra.

The following surgical procedure would be used in a typical right thoracic adolescent idiopathic scoliosis. The procedure has been modified from a surgical technique given by Dr. Zeller and Dr. Dubousset (1996).

1.3.3 Hook Placement

It can be seen in Figure 1.9 that a one level pediculo-transverse claw is inserted at T5. The term "claw" is used when two hooks are used around either one or sometimes two vertebral levels. The top hook in the claw is always down facing while the bottom hook is up facing. Compression is applied between the two hooks to securely seat the hooks and provide a strong construct. A pedicle hook is inserted at T7. The down going hook at T10 is a supralaminar hook. A compression claw is inserted at the T12 -L1 level.

1.3.4 Convex hook placement

The upper claw is the same as on the concave side. A pedicle hook is inserted at the apex at T8. For the reversed hooks at T12-L1, enough bone should be resected to allow for easy insertion of the wide blade hooks (Figure 1.10).

Rod contouring is then preformed for the concave rod. The contour is chosen according to the expected sagittal contour after reduction and does not necessarily follow the coronal aspect of the sagittal curve.

1.3.5 Rod Insertion

A large facet excision is done prior to insertion of the rod. The rod is first inserted at either end of the instrumentation wherever it "fits best". The first hex nut in then inserted to secure the rod to the hook. Rotating the rod further allows placement of the cephalad hook. A hook holder is then placed at T10. The rod is inserted as seen in Figure 1.11 with the help of the translator-introducer.

The translator-introducer preformed a translation maneuver, which is the first part of the correction.

1) The lateral hook holder part grasps the hook.
2) The rod pusher part is assembled into the hook holder part.
3) A translation maneuver is preformed. Two translators on adjacent hooks may be used to enhance the maneuver.
4) The rod pusher is then driven down into the body of the hook.
5) The plug is then inserted through the cannulation of the rod pusher part and driven into the hook.

This controlled maneuver diminishes the risk of laminar breakage through excessive force application.

1.3.6 Rod Rotation Maneuver

The rod rotator is fixed to the rod that is held loosely within the hooks. The rod rotators may have to be replaced several times during rotation due to slipping and because of the low profile of the system. The rod rotation maneuver takes the scoliosis curvature and rotates it into the sagittal plane. Figure 1.12 schematically represents the rotation of the rod. The goal of the maneuver is to correct the scoliosis while maintaining the patients kyphosis avoiding the flat back syndrome that was common with previous systems. Figure 1.13 demonstrates how the kyphosis is improved in the sagittal plane. At the end of the maneuver, the hex nuts are retightened. Compression is applied at the level of the caudal claw to enhance its action against kyphosis. The convex rod is then placed into the hooks. Low profile transverse connectors are then placed. This is followed by final decortication and grafting. The rod length should be checked before closing.

1.4 Qualitative Prediction of Mechanical Forces Applied to the Spine

It is difficult to predict the mechanical forces applied to the spine for many reasons. The first is that the surgical procedure is lengthy and the actual applied forces are expected to change throughout the procedure. The second is that there are many hooks and screws that serve as attachment sites to the vertebra distributing the load of the rod in an indeterminate manner. The muscles and ligaments in the spinal column are elastic and could react to the instrumentation in a dynamic manner relaxing and tensing up in response to the forces created by the instrumentation.

To begin with, one of the most critical stages during scoliosis surgery, when using CD instrumentation, is the rod rotation maneuver. Recall that the rod rotation maneuver takes the scoliosis curvature and rotates it into the sagittal plane. During the rotation

maneuver, the force applied by the surgeon is distributed through a lengthy path before having an effect on the spine. A certain amount of force and moment is applied to the end of the rod rotator in order to rotate the rod, which is loosely connected to the hooks and screws, which in turn act on the vertebra to transform the scoliotic curve into a kyphotic curve.

Since the ultimate purpose of the surgeon is to change the shape of the spine, an understanding of the forces at the vertebral level is useful. A general orientation of the forces is first discussed. A Cartesian coordinate system of *xyz* has been standardised to the spine as shown in Figure 1.14. There is a risk of hooks and screws pulling out from their attachment site. This type of force, called axial pull-out force, is directed in the negative *x* direction and is schematically represented in Figure 1.15. There is also a risk of the force being in the positive *x* direction, axial push-in as shown in Figure 1.16. In order to properly seat the hooks, compression and distraction forces are applied along the *z* direction. Compression requires two hooks moving closer to one another and distraction requires that hooks be pushed away from one another as shown in Figures 1.17 and 1.18 respectively.

There is some trauma to the vertebra while the hooks and screws are inserted. In the case of the screws, there must be sufficient torque to cut through the bone and drive the screw through the pedicle and into the vertebral body. Upon hook insertion, force is required to wedge the hooks between the tight space between the upper and lower vertebra. The next force applied to the hooks occurs during rod insertion. The amount of force on the vertebra will vary depending on the shape of the rod and how well it "fits" into the hooks. If the rod were a "perfect fit", it would apply no load on the hooks and there would be no correction of the curve. During rod rotation, the apex of the curve is rotated into a kyphosis. A resultant pullout force on the hook at the apex is plausible as the kyphosis is maintained.

Another stage of concern is when the hex nuts are tightened. This stage should show an increase in overall force, as there is less play in the instrumentation. The finishing touches are to apply compression and distraction where necessary. Compressive forces should be noted between the hooks forming the hook claw and distraction forces present while moving distally from the apex of the curve.

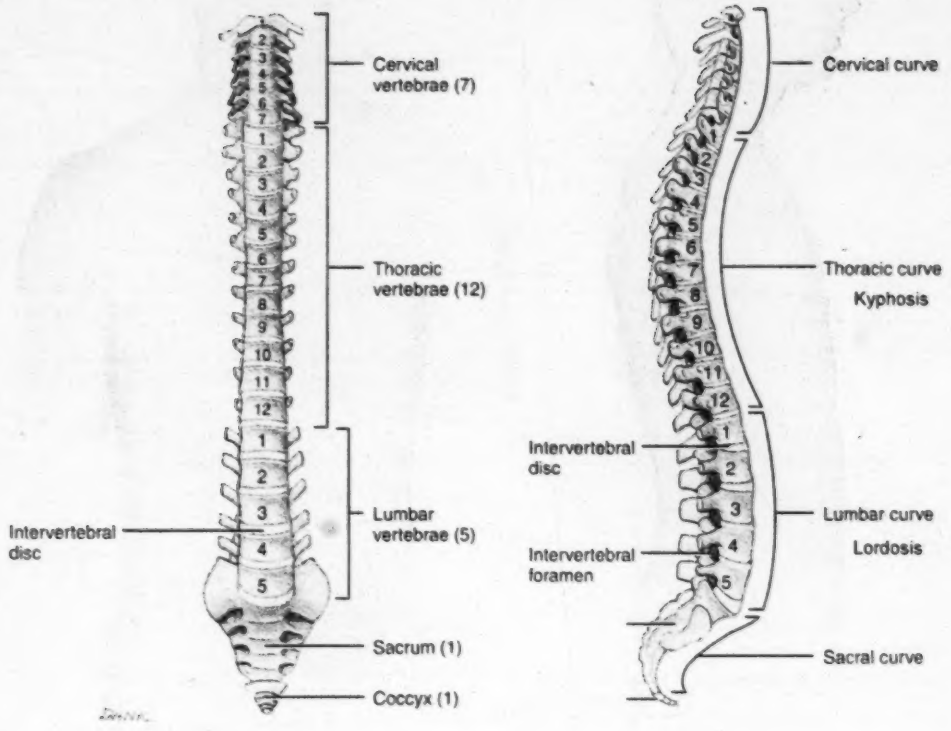

a) Anterior view b) Sagittal view

Figure 1.1 Vertebral column anatomy (Modified from Tortora, 2000)

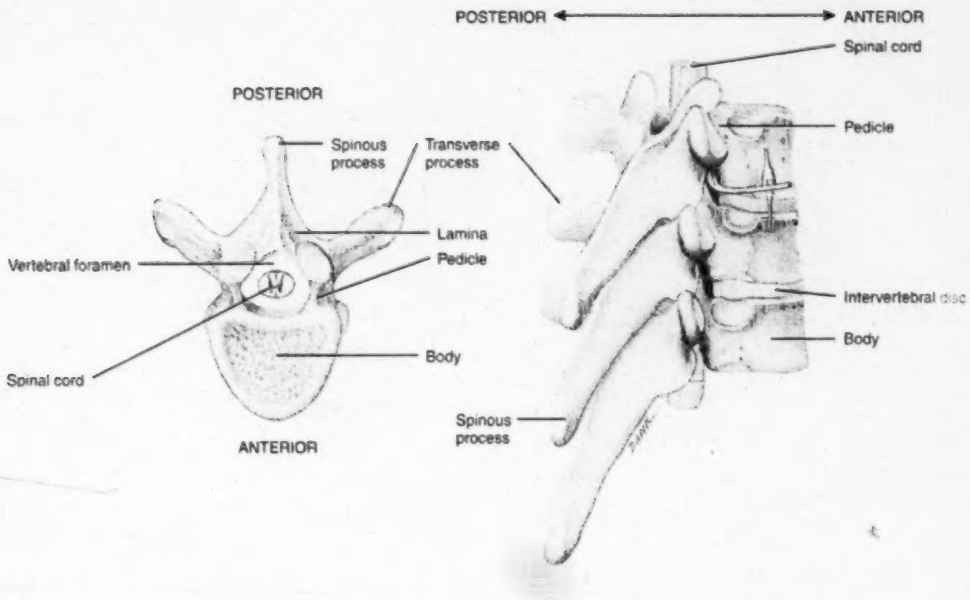

a) Posterior view b) Right side view

Figure 1.2 Vertebra anatomy. (Modified from Tortora, 2000)

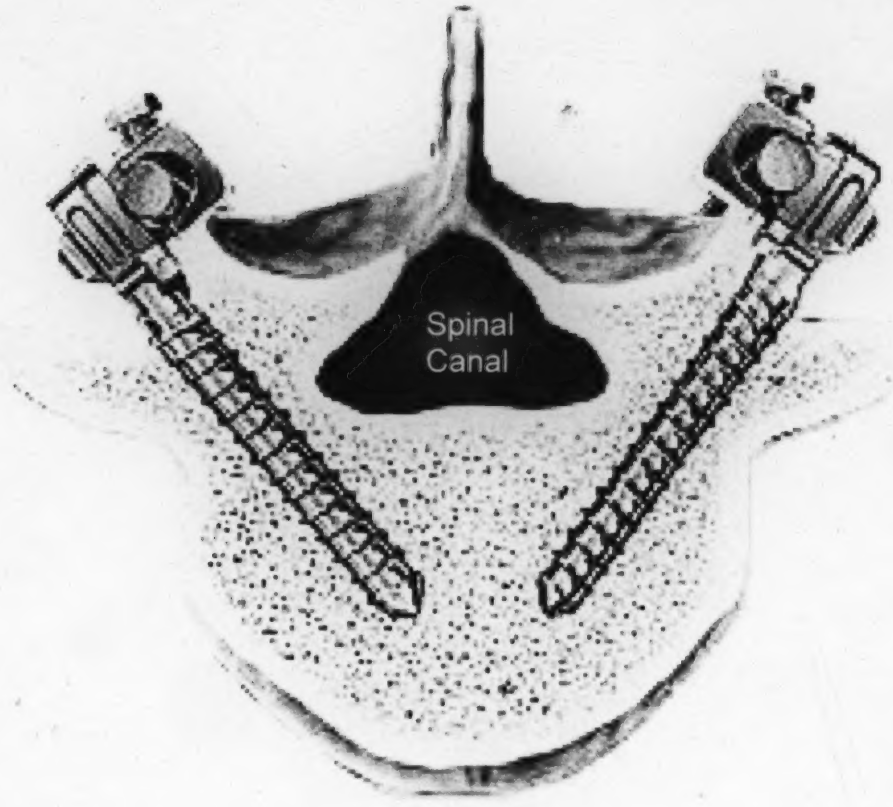

Figure 1.3 Fixation of pedicle screws

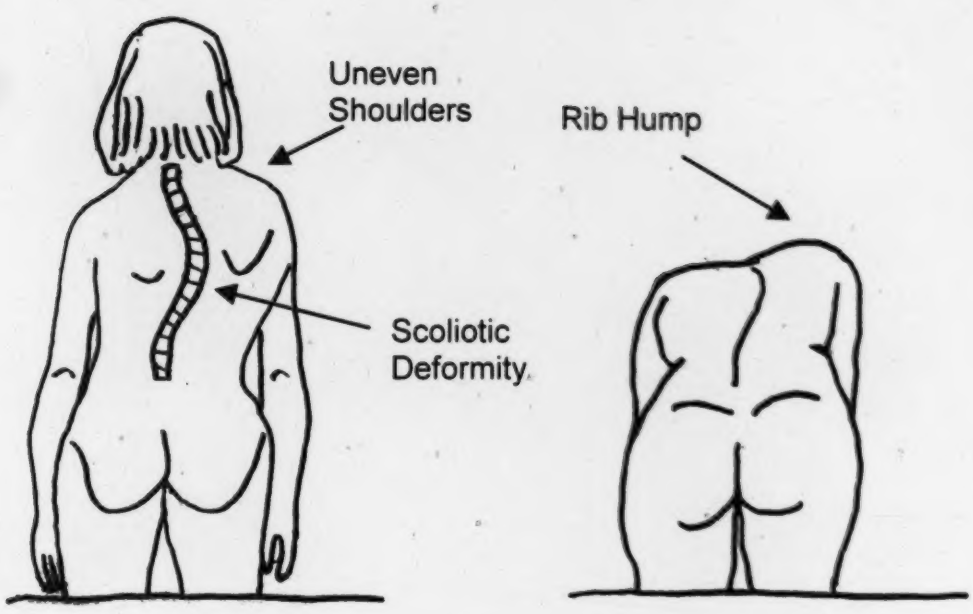

Figure 1.4: Scoliosis as viewed from the back and the predominance of the rib hump.

Figure 1.5: Radiograph of patient with scoliosis. Cobb angle measures 73°.

Wide blade small groove hook 84101SH

Wide blade hook 84101H

Pedicle Hook 84190H

Figure 1.6: Various Hooks

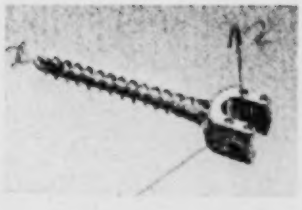

Pedicle Screw 84045L35H

Figure 1.7: Vertebral Screw

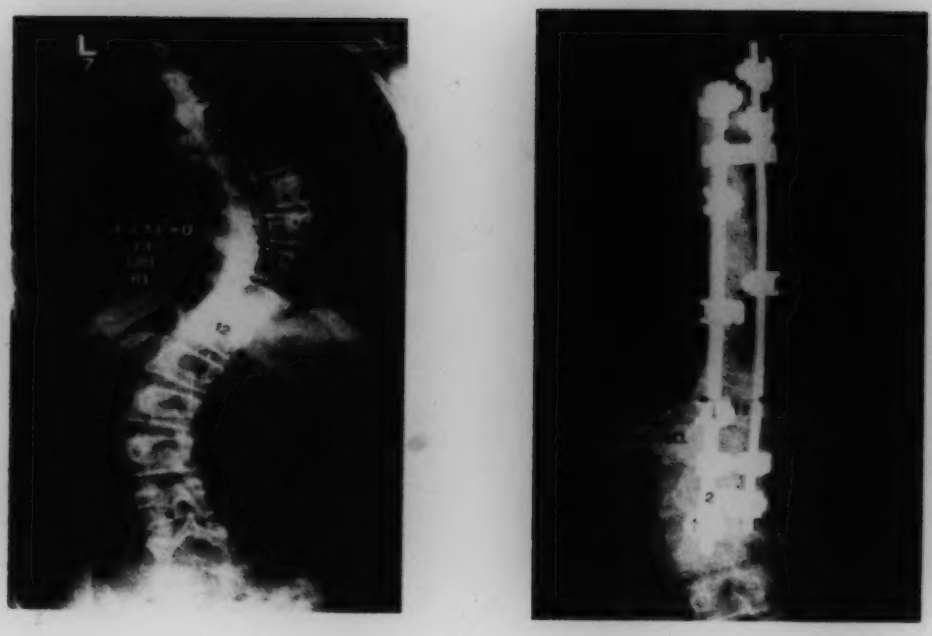

Figure 1.8: Pre and post op x-ray of scoliosis patient.

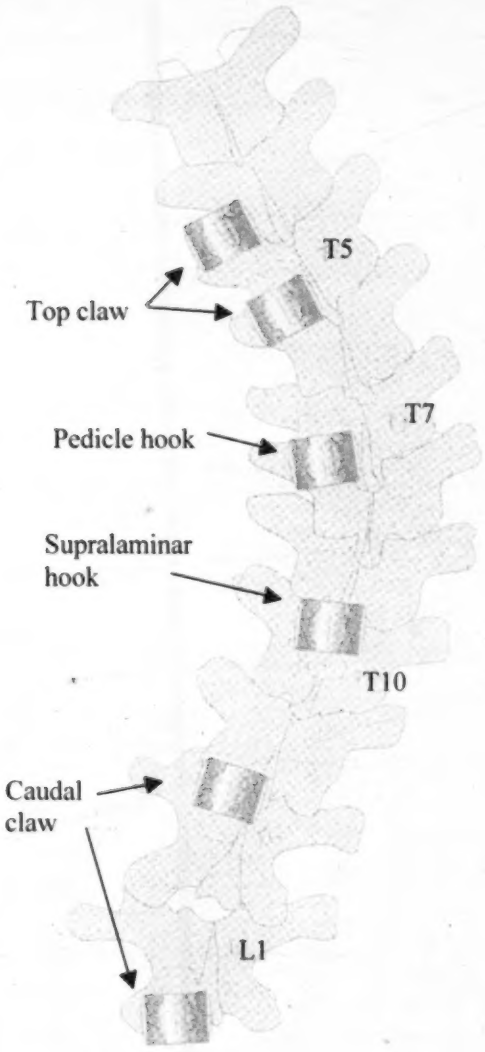

Figure 1.9: Hook placement

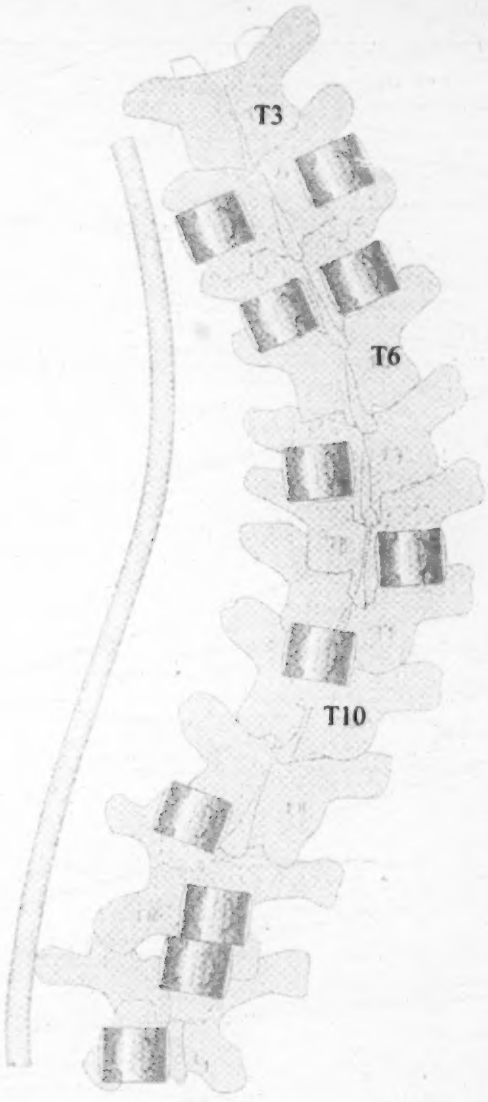

Figure 1.10: Rod contouring

(Modified from Zeller and Dubousset, 1996)

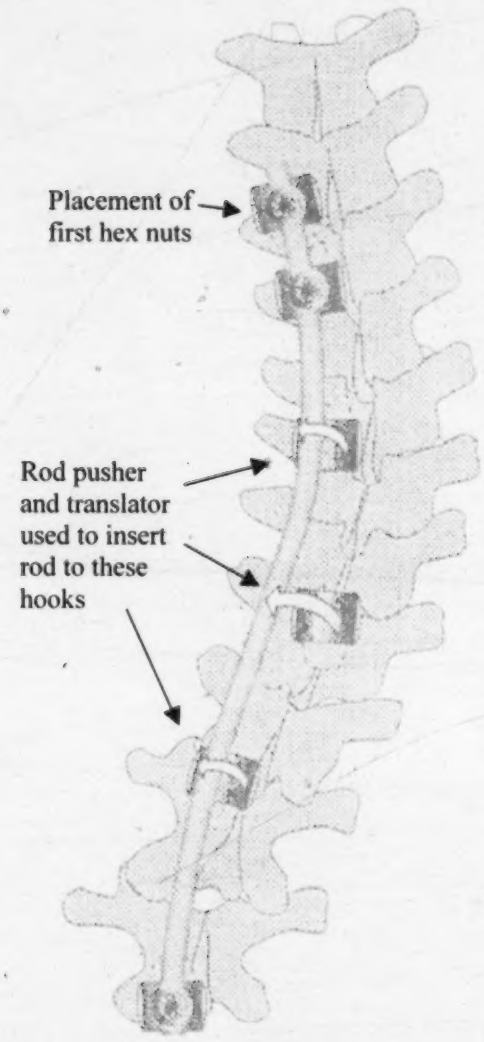

Figure 1.11: Rod insertion

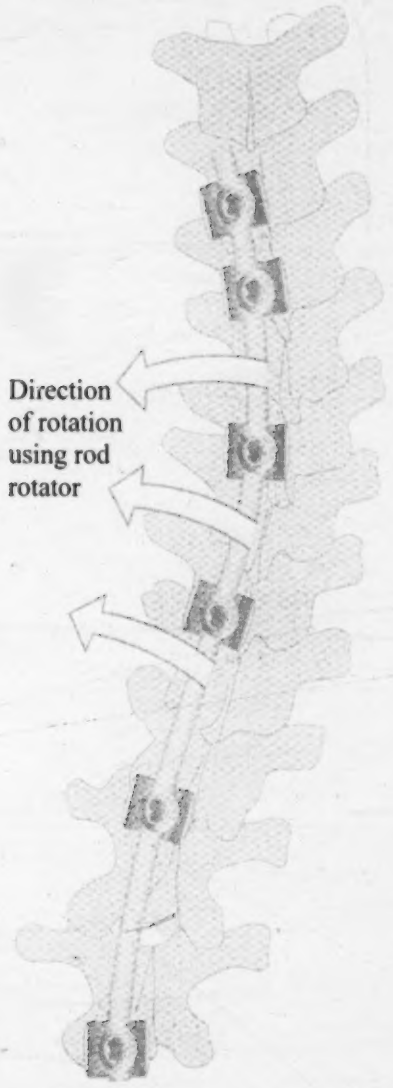

Figure 1.12: Rod rotation maneuver

(Modified from Zeller and Dubousset, 1996)

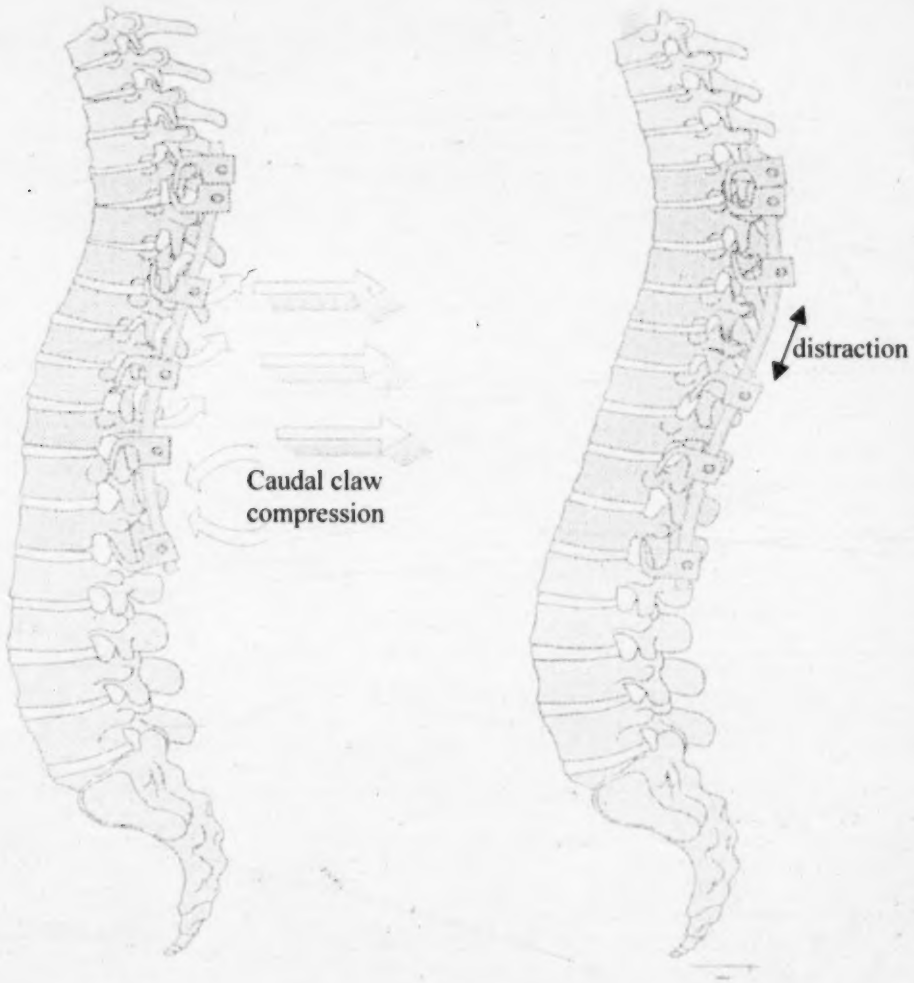

Figure 1.13: Maintenance of kyphosis in sagittal

(Modified from Zeller and Dubousset, 1996)

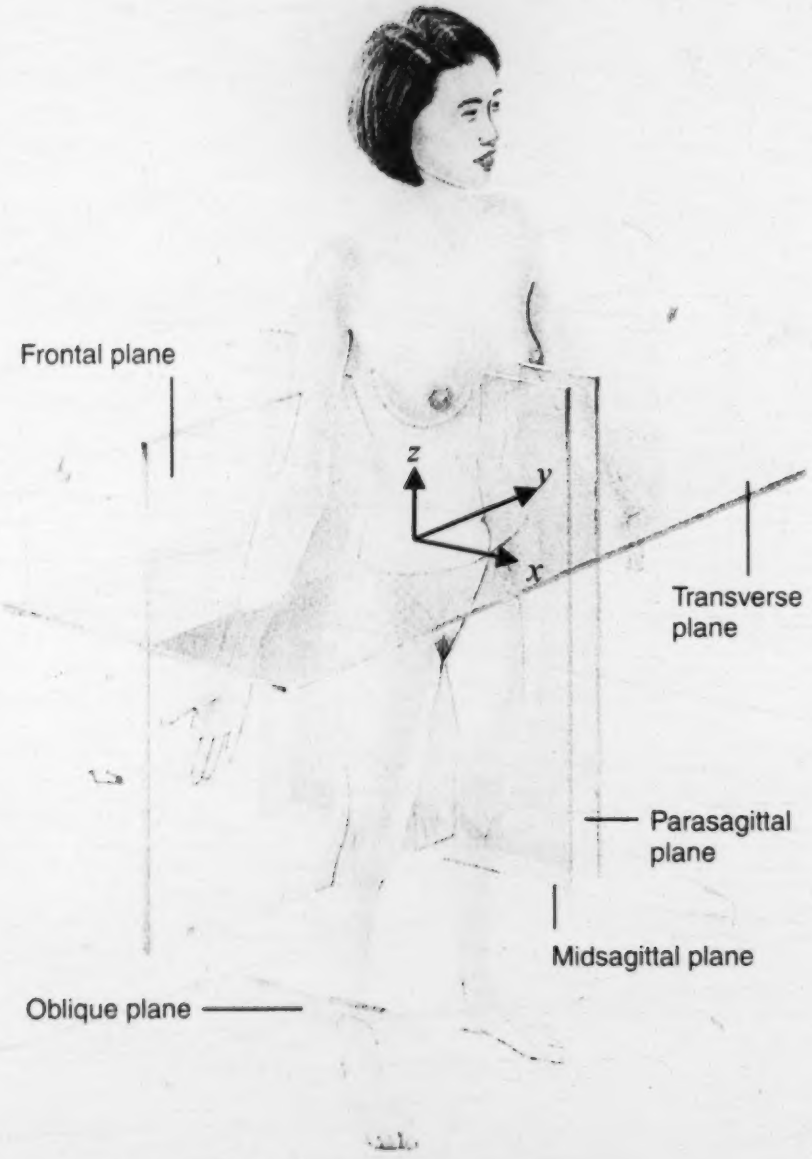

Figure 1.14: The Cartesian co-ordinate system as oriented with respect to the spine

(Modified from Tortora, 2000)

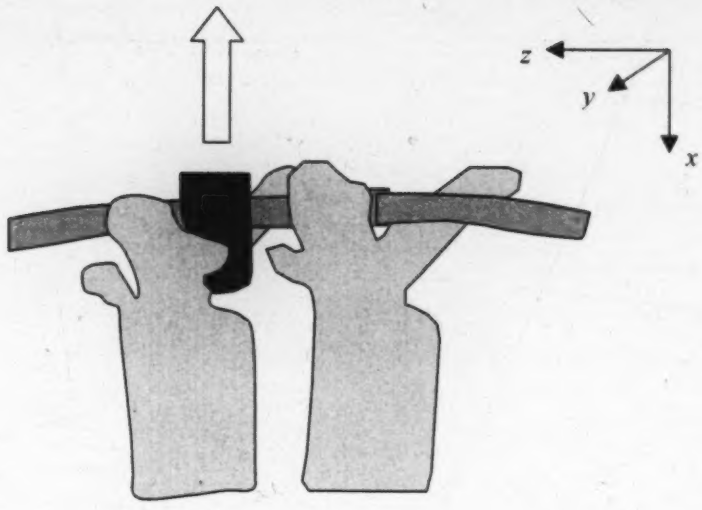

Figure 1.15: Schematic of axial pull-out force

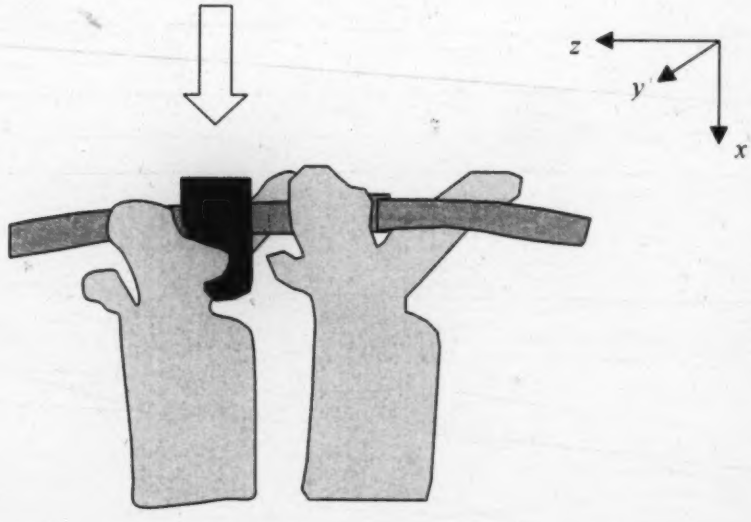

Figure 1.16: Schematic of axial push-in force

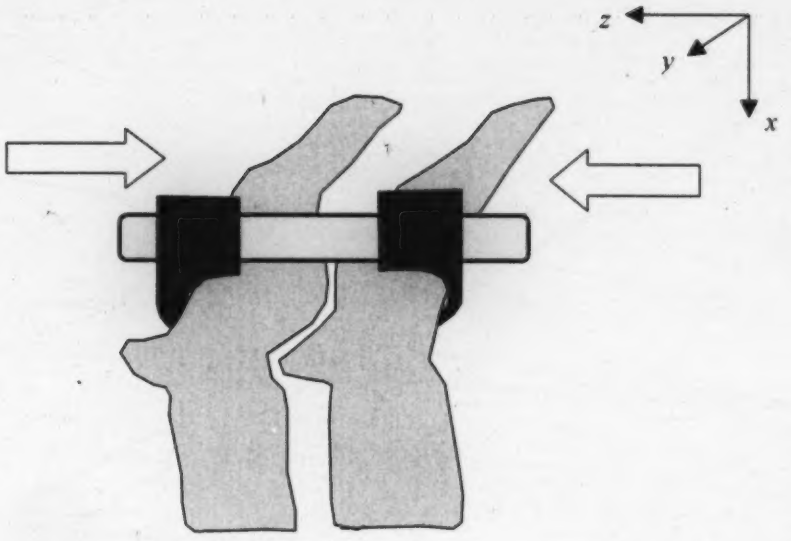

Figure 1.17: Schematic of compressive force

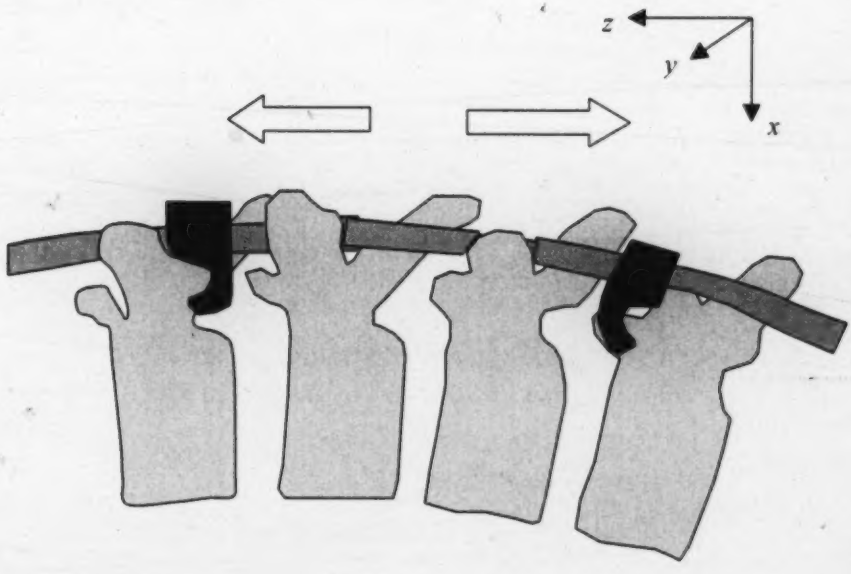

Figure 1.18: Schematic of distraction force

Chapter 2 Literature Review

This chapter gives the background into the relevant research that has occurred in scoliosis treatment. The literature review will focus on three main sections. The first section deals with clinical surgical complications that have been noted with scoliosis surgery. The next section discusses various biomechanical tests that have been performed to better understand instrumentation failure mechanisms. The final section is a review of *in-vivo* force measurements that have been recorded. In conclusion, a general discussion of the review, areas where further research is needed and the goal of this thesis research are presented.

2.1 Surgical Complications

It is difficult to review the complications of scoliosis surgery since not all complications are reported. There are a number of risks associated with scoliosis surgery. Due to the length of time required to complete the surgery, blood loss is a possible concern. There is also the risk of infection and in some rare cases rejection of the implant material. Another complication is mechanical failure of the implant or, more commonly, mechanical failure at the bone implant interface. The goal of this thesis work is to develop tools to increase our understanding of the biomechanics involved in scoliosis surgery. A sound understanding of the biomechanics applied during corrective surgery will help to reduce the risk to the future patient.

2.1.2 Failure in Harrington Rod Systems

Major complications with Harrington rod instrumentation were mechanical failure of the instrumentation such as the rod breaking or disengagement of the hooks (McAfee 1985). Also a concentration of hook forces at the lamina resulted in fixation failure due to fracture of the lamina (Freedman 1986). Redesign of the instrumentation and hook geometry helped to address these problems with the Harrington rod system.

2.1.2 Failure of Cotrel Dubousset (CD) System

The Harrington rod system approached scoliosis as a two dimensional deformity. Within the past twenty years however, attention has focused on scoliosis as a three dimensional deformity. To better address the three dimensional deformity of the spine, several new systems have been designed. The system that is most commonly used at the University of Alberta Hospital is the CD system (Sofamor Danek) (Cotrel 1988). The mechanical risks to the patient, associated with the Harrington rod system, have decreased as the CD system consists of several laminar and pedicle hooks or pedicle screws, which are placed at multiple levels along the spine. This more evenly distributes the forces along the spine, hence, reducing the load per vertebra and the risk of hook pullout.

Even with the changes to the system, hook pullout and disengagement has been reported with the CD system (Guidera 1993, Van Ooy 1992, Cotrel 1988). Not only is hook pullout a problem but so is hook push-in. This is associated with the hook being pushed in to the canal, which increases the possibilities of spinal cord damage. One such case has been reported as a late complication (Rittmeister 1999). Two cases of neurological complications immediately after insertion of lumbar hooks were reported by Been (1994).

Guidera et al. (1993) performed a retrospective study on 52 patients. There were 17 complications in this group including hook pullout, prominent hardware, infection, pseudarthrosis and the first two reported cases of broken CD instrumentation rods. The rod failures occurred more than one year post-op and the fatigue failure was secondary to pseudarthrosis. Three patients had displaced hooks. The cause for hook displacement can be one or more of the following, inadequate contouring of the rod, improper placement of the laminar or pedicle hooks or osteoporotic bone allowing hook pullout. One of these patients, with cerebral palsy and osteoperotic bone, had multiple hook pullouts and loss of correction. The entire surgery was revised with a different system and based on this experience the authors are no longer using CD instrumentation in osteoperotic neuromuscular patients.

Van Ooy et al. (1992) published the results of the CD operation on 38 patients. There were complications in a total of eight patients. Two cases had complete implant loosening and required revisional surgery. Four had shifting at the upper level, one had dislocation of the convex lower hook and a final complication was erosion at several hook sites.

Cotrel, one of the fathers of the CD system, reported on the results of 250 patients (Cotrel 1988). Two patients developed neurological complications. Concerning the hooks themselves, six patients suffered dislodgement of the upper hooks while two patients encountered transverse process fractures.

As mentioned previously, hook push-in is also a complication of CD surgery. Been et al. (1994) reported on two cases of neurological complications occurring immediately after hook insertion. During both cases, spinal cord function was monitored with posterior tibial nerve somatosensory cortical evoked potentials (PTN-SCEPs). In the first case a hook was inserted at T11 and shortly after the SCEP signal was absent. The hook was removed but the SCEP signal was still absent so the operation discontinued. Postoperative examination revealed incomplete paraplegia below T12. Fortunately at four to ten months after surgery the patient was neurologically normal. The patients curve had progressed and still required scoliosis surgery. CD instrumentation was placed and no neurological complications were present after her second surgery. During a second case a laminar hook was inserted on the concave side at the L4 level. Ten minutes after hook insertion the signal from the SCEP was absent. The hook was removed and the signal returned. They again tried to place the hook and the signal disappeared, returning again on removal. To avoid complications only the thoracic curve was instrumented and there were no neurologic complications after surgery. Rittmeister et al. (1999) reported on a late neurological complication of scoliosis surgery. Eight years after surgery a woman presented with neural deficits. A left sided compression of the cauda by a laminar hook at L2 was observed on a CT scan. The hook was surgically removed and the patient was discharged and neurologically recovered two weeks after surgery.

2.2 Biomechanical Tests

To deduce the risk to the patient and to better understand the biomechanics involved in instrumentation failure, a number of *in-vitro* biomechanical tests have been performed.

2.2.1 Pedicle Screw Pullout

The in-vitro pullout of pedicle screws has been extensively examined. (Refer to Berleman et al. (1995) for a review of the literature up to 1994.) In cadaver studies Heller found that the ultimate load to failure for a pedicle screw was 658 N (Heller 1999).

2.2.2 Pedicle Screw Insertional Torque

Another interesting characteristic of the screws that has been measured is the insertional torque required for screw placement. Zdeblick et al. (1993) used a custom designed digital torque screwdriver and recorded the maximum torque generated. They found that a linear relation existed between both insertional torque for taping or inserting a screw and the number of cycles to ultimate pullout. An inverse linear relationship was found between the pedicle width and cycles to failure. There was no relationship found with the number of cycles to failure and bone mineral density. In general, an insertional torque during tapping of less then 4 inch-pounds (452 Nmm) leads to early pedicle screw pullout (Zdeblick 1993).

2.2.3 Pullout of Hooks

There is less data available on the pullout strength of hooks. (Berleman 1995, Coe 1990, Ruland 1990, Hasegawa 1997) The pull-out strength of the hooks is of great importance for this thesis work, which is trying to measure the forces applied to the

hooks. The results of the various literature are quite different, and in some cases contradictory.

Berleman et al. (1995) performed biomechanical testing of cadaveric specimens (mean age 55y) on four different implant types. They believe that, during surgery, pedicle hooks might be subjected to considerable three dimensional forces. The implants they compared were a Universal Spine System (USS) pedicle hook with one screw, a prototype pedicle hook with two screws, a Cotrel-Dubousset (CD) pedicle hook with screw and a USS 5mm pedicle screw. Two different posterior pull-out tests were performed on each implant. One test was classified as constrained while the other was unconstrained. The pedicle screw was the strongest fixation device in the constrained test with a failure load of 1650 N. The CD hook had the lowest failure load for each test; 743 and 464 N for the constrained and unconstrained tests respectively. It is important to note that the CD hooks used by Berleman et al. were slightly modified in that they had a 3mm diameter set screw that pressed into the laminar surface providing more stability and anchorage.

The results of Coe et al. (1990) differ from those of Berleman. Coe tested the posteriourly directed failure load of four different implants including Drummond spinous process wires, Harrington laminar hooks, CD transpedicular screws and Steffee VSP transpedicular screws. The various implants were tested on cadaver spines ranging in age form 54 to 87 years. The mean load causing failure for the Harrington laminar hooks was 646 N. This falls within the range of Berleman's results for the constrained and unconstrained CD hook. However, contrary to Berleman's failure load of 1650 N, Coe found the CD pedicle screw to be the weakest with a tensile failure load of 345N. This large discrepancy in failure loads of the CD pedicle screws could be the result of varying bone mineral density (BMD), however, there does not appear to be a difference in BMD. The average BMD for Berleman was 0.825 and, though the raw data are not given, from a plot of BMD versus pullout strength the mean BMD for Coe falls between 0.7 and 0.9. The large discrepancy in CD screw pullout force may be due to some difference in testing apparatus, which is not apparent from reading the articles. Another explanation may be the variability in cadaver specimens as those used by Berleman were relatively young with a mean age of 55 years.

To get another idea as to the amount of pullout load required to cause failure of laminar hooks the work of Ruland et al. (1991) was reviewed. They did comparative load to failure tests of five different instrumentation types including a single CD laminar hook and a single CD pedicle screw. The tests were again done on cadaveric spinal segments. The results showed the mean load to failure to be 809 (99.4) N and 863 (108) N for the laminar hook and screw respectively.

A common procedure to reduce the risk of pullout of the upper hook is to create a hook claw around a vertebra with one upfacing pedicle hook and a down facing transverse process or lamina hook. On an upper thoracic vertebra there is often little room for both hooks and with two hooks there is little room for secure bone graft to develop. Using calf thoracic vertebra Roach et al. (1990) analyzed the pullout load to failure of single level claws and double level claws tested using a MTS machine. The load to failure for the double level construct was 442 N, which was statistically greater, than the pullout of the single level claw, 313N. The failure load for the hook claws is lower than the pull-out values of the three previously mentioned studies, which is surprising since the idea behind the claw was to more evenly, distribute the forces on a vertebra. The lower failure loads may be attributed to calf spines used in this study versus cadaver spines used in the previous three.

2.3 *in vivo* Force Measurements

The measurement of *in vivo* forces during scoliosis surgery is not a novel idea. However, most of the work was done many years ago. Almost all of the previous studies look at measuring the distraction forces applied during the Harrington rod procedure. In the past twenty years, scoliosis has been recognized as a three dimensional deformity and therefore, being treated in more then just the frontal plane. As a result, systems that evaluate the three dimensional deformity, such as the Cotrel Dubousset system, are more widely used. However, in attempting to measure the forces applied during today's surgical procedure, it is important to review how forces were previously measured.

Waugh et al. (1966) first performed the *in vivo* implementation of strain gauges to spinal instrumentation. Strain gauge readings for three patients were taken during, and for a period of about twenty four hours after surgery. The highest recorded force was 69kp (677N), which occurred after surgery while patient one was vomiting. (1 kp is a kilopond, which is equal to 9.81 N) In patient three, the distraction force was increased to 38 kp (373N) at which point failure occurred. Waugh concluded that the applied distraction force during surgery should not exceed 30 to 40 kp (294-392N).

Nachemson et al. (1969) instrumented a distracter with a leaf spring and a pointer scale. The spring gives a reading between zero to forty kiloponds (0-392 N). The device was used on over sixty patients without fractures except one case where 50 kp (491N) was intentionally exceeded. Though this device does not provide a continuous recording of the applied force it was obviously a useful tool in preventing fractures.

Elfstrom et al. (1973) were able to record the forces in the Harrington distraction rod for a two week period following surgical instrumentation. Telemetry recordings of the force in the rod were monitored in 11 patients in a number of positions, maneuvers and physical exercises. From their results they were able to concur with Waugh (1966) that no more then 30 to 40 kp (294-392N) of axial distraction should be exerted on any patient during surgery. They also provided guidelines for the recovery of the patient and how to minimize certain activities to avoid complications within the first two weeks post op. Another interesting trend they witnessed was a decline in the axial force over time. The maximum forces were witnessed during surgery. There was a rapid decline in the first three days and the forces stabilized at about 25% of their maximum after twelve days.

McBride at al. (1979) instrumented a standard outrigger and distracter with strain gauges. The strain gauges were connected in a Wheatstone bridge circuit and data was collected continuously. Continuous recording was provided better data collection than previous studies. Their results for twenty patients were presented as percentages of force divided by mean bone strength. The mean force was 49 kgf and 95 kgf (481 N and 932 N) for the outrigger and distracter respectively. There were no reported rod failures and only one reported bone failure, at 40 kgf (392 N), for the twenty cases.

A following study that looked at the outrigger and distraction forces was conducted by Dunn, McBride et al. (1982). They compared the difference between outrigger force for an adolescent and adult group. They found that there were higher forces for the adult group and they attribute this to an increased spinal stiffness with age. In contrast, the adolescents required less force due to their more flexible spines. There was one case of hook "cut out' that was observed at 40 kgf (392 N) in a patient diagnosed with mildly osteoporetic bone. Another interesting point was the relationship found between applied force and final correction obtained. They found that lower initial outrigger forces correlated with lower final correction and it is speculated that if more force had been applied in these cases a better final correction would prevail. Knowing this they suggest taking advantage of the spines viscoelastic properties through periodic re-application of force up to safe levels during preparation of the fusion bed to potentially improve correction as previously suggested by Harrington.

The only recent *in vivo* force measurements are those concerned with insertional torque of pedicle screws. Okuyama et al. (2000) measured the insertional torque of pedicle screws and compared them with bone mineral density and also tried to predict screw loosening. They found no significant difference between the mean insertional torques measured for the groups with and without screw loosening. Therefore, they felt that insertional torque could not affectively predict screw loosening. The mean insertional torque for the 250 screw measured was 1.45 ± 0.35 Nm. Values greater then 1.96 Nm, which exceeded the limitations of the torque wrench, were recorded in 16 screws.

2.4 Chapter Discussion and Future Directions

The literature review has shown that there are many biomechanical complications with scoliosis surgery. Even though the systems have changed from the Harrington rod system to the CD system, the most common failure mode is still hook pullout at the superior end vertebra.

In order to get an understanding of the failure loads of the CD system, a number of *in vitro* biomechanical tests have been performed. Though these tests do vary in their results, they give a good base as to what level of force is critical. Tensile pullout is an appropriate means to evaluate the mechanics of a pedicle construct. The range for screw pullout is between 345-1650 N, while hook pullout was observed between 464-809 N. In the majority of clinical studies and the previous bench top tests, the mode of failure of sublaminar hooks has been shown to be tensile pullout through the lamina. As previously mentioned, in the patient the majority of the failures tend to occur at the end vertebra. This is believed to be due to flexural bending resulting in large tensile forces at the end vertebra. These tensile forces have not yet been measured *in vivo* and it is the goal of this thesis work to design tools to measure the forces present during the surgical procedure. For example, if there is a large pre-loaded tensile force on the end vertebra, it may be due to inadequate rod contouring. Giving the surgeons real time feedback, as to the amount of tensile force on the end hooks, could allow them to modify the rod with *in situ* bending trying to minimize the pre-load at the end instrumentation.

In the past, *in vivo* forces applied during the Harrington rod procedure were measured. These measurements give some efficacy to the measurement of *in vivo* forces. Waugh (1966) has shown that a distraction force greater then 294-392 N should not be exceeded. A continuous recording of the forces was advantageous over systems that rely on a pointer scale. The work of Elfstrom (1973) showed that the maximum forces were recorded during surgery and that they decreased over time, stabilizing to 25% of their maximum at around day twelve.

There has been no attempt to measure the amount of *in vivo* force applied to the hooks in the CD system. Existing instrumentation systems have changed drastically to address the three-dimensional nature of scoliosis. There is a need to better understand the biomechanics of these new systems. An understanding of the biomechanics can be used to improve patient safety and reduce the implant failure rate. A better understanding of biomechanics may also result in better surgical correction of the curve. As well, the recorded forces applied during CD instrumentation can be used in spine models to help simulate surgery.

To provide a better understanding of the biomechanics applied with the CD system, two devices have been designed and are discussed in detail in the remainder of the thesis. The first device, called the Gripper, is an instrumented rod rotator capable of measuring the rod rotation force applied during CD surgery. The Gripper provided preliminary information as to the amount of applied force but did not give information as the distribution of the forces. In order to get one step closer to the actual vertebra, hooks have been instrumented to measure axial push-in force, axial pull-out force as well as compressions and distraction forces. The Gripper and the instrumented hooks will provide some insight as to the biomechanics involved in scoliosis surgery.

Chapter 3 The Gripper

3.1 Background

During surgical correction of scoliosis, a rod rotator is used to derotate the spine. The rod rotator grabs on to the rod, which is loosely fixed within the attached hooks and screws. The rod is prebent to the desired final spinal kyphosis. The rod is initially placed at ninety degrees to its final desired position. The goal is to take the scoliotic deformity in the posterior plane and rotate the curve into the sagital plane to maintain the natural thoracic kyphosis. Recently, there has been some doubt as to the effectiveness of the rod rotation maneuver (also called derotation maneuver) in actually improving the rotational deformity of the vertebra (Gray 1991), however, the use of Cotrel-Dubousset (CD) instrumentation undoubtabely improves the scoliotic curve.

Currently surgeons are unable to determine how much force is applied during scoliosis correction. There has been little documented work in measuring forces applied by the surgeon during corrective scoliosis surgery. Most of the work has measured the Harrington-Rod procedure (Waugh 1966, Nachemson & Elfstrom 1969, Elfstrom & Nachemson 1973, McBride et al. 1979). Recently, the more common procedure is the rod rotation maneuver starting with CD instrumentation (Cotrel & Dubousset 1988).

The skill, experience and "feel" of the surgeon control this surgical procedure. There is a risk from overload that can fracture a vertebra by way of bone failure at the hook site or the screws pulling out at the pedicle. If insufficient force is applied, a sub-optimal correction may be achieved. The goal is to balance the risk associated with applying more force with the reward of achieving the desired outcome. In order to better evaluate these risks, the forces surgeons apply during surgery need to be quantified.

Knowledge of the rod rotation force applied during surgery can be used in a variety of ways. The first use is safety, which is the surgeon's primary concern. Once a larger sample of data is collected an average and range can be found. Limits can then be incorporated into a real-time data acquisition system to warn the surgeon when a critical force is attained. Another application is to incorporate the measured forces with

displacement measurements and input these into a computer model of the spine. With this model, the surgical outcome can be better predicted; as well, the necessary force required for a particular outcome can be estimated. These models may improve surgical planning and more optimal correction. Another use is to take recordings with both the Gripper and instrumented hooks (discussed in a later chapter) and compare the output form each to determine if any relationship exists between the two.

3.2 Materials and Methods

A rod rotator was modified and instrumented with a sleeve. This sleeve measures the force and moment applied by the surgeon. The rod rotator together with the sleeve and the acquisition system is called the Gripper. (Figure 3.1)

The sleeve of the Gripper consists of a cantilever beam fixed within a rigid frame that leaves the instrumented beam insensitive to squeezing. On this beam are two pairs of strain gauges located on the top and bottom of the beam at one third and two thirds along its length. The dimensions of the beam, 12.7 x 6.5 x 68.5 mm were selected to avoid plastic deformation assuming the surgeon would apply a maximum force of 440 N (100 lbs.). Each pair of strain gauges is connected to a half bridge circuit housed within the sleeve to provide maximum sensitivity and temperature compensation. (Schematic of bridge circuit in Appendix A). Also housed within the sleeve is an inclinometer. The inclinometer output correlates the position of the Gripper in space. At zero degrees, the Gripper is in the vertical position and it has a range of about 45 degrees to each side.

The strain gauge and inclinometer data were sampled with a data acquisition system (DAQ 1200, National Instruments, Austin, Texas) at a rate of 10 Hz. The voltage outputs were then run through Lab Windows CVI (National Instruments, Austin, Texas), which calculates the loads applied, by the surgeon and the orientation of the Gripper and plots the results in real time. After collection, the data can be viewed in MATLAB.

The force and moments applied by the surgeon are calculated assuming a static case that both the sum of the forces and the sum of the moments are equal to zero. The twist or moment applied directly to the sleeve by the surgeon is calculated assuming the surgeon's force is applied in the middle of the Gripper sleeve. Figure 3.2 shows a FBD

of the entire Gripper system clamped in a vertical position. From this figure it can be seen that the resultant force at the rod, F_r, is equal and opposite to the force applied by the surgeon, F_s:

$$F_r = -F_s \qquad \text{e3.1}$$

while the resultant moment at the rod, M_r, is:

$$M_r = M_s + (F_s D_1) \qquad \text{e3.2}$$

Figure 3.3 shows a FBD of the cantilever beam located inside the gripper sleeve. The strain gauges are located at positions one and two. The resultant force, F_c, and moment, M_c, at the end of the cantilever beam are:

$$F_c = -F_s \qquad \text{e3.3}$$

$$M_c = M_s + (F_s l_3) \qquad \text{e3.4}$$

where: $$l_3 = D_1 - D_2 \qquad \text{e3.5}$$

Once the resultant force and moment at the end of the beam have been found, the classic cantilever beam can be analyzed to find the moments at a specific gauge location, x. Figure 3.4 shows the free body, shear force and bending moment diagrams for a cantilever beam. From Figure 3.4a the moment $M(x)$ along the length, l, of the beam with an end point load is:

$$M(x) = -F_s (l - x) \qquad \text{e3.6}$$

From Figure 3.4b, the moment $M(x)$ along the cantilever beam subjected to an end moment is constant at:

$$M(x) = M_c \qquad \text{e3.7}$$

Using superposition, e3.6 and e3.7 can be combined to give:

$$M(x) = -F_s (l - x) + M_c \qquad \text{e3.8}$$

Since the gauge positions are known and are measured from the right hand side of the beam, for the first gauge let $(l\text{-}x) = d_1$ similarly for the second gauge let $(l\text{-}x) = d_2$. The moments at the respective gauge positions are:

$$M_1 = -F_s(d_1) + M_c \qquad \text{e3.9}$$

$$M_2 = -F_s(d_2) + M_c \qquad \text{e3.10}$$

Now that M_1 and M_2 have been found with respect to F_s and M_c, e3.4 can be substituted for M_c. Following this, equations e3.9 and e3.10 can be rearranged to solve for F_s and M_s.

$$F_s = \frac{M_1 - M_2}{d_2 - d_1} \qquad \text{e3.11}$$

$$M_s = \frac{M_1(l_3 - d_2) - M_2(l_3 - d_1)}{d_1 + d_2 - 2l_3} \qquad \text{e3.12}$$

Using the previous equations F_s and M_s can be found from M_1 and M_2 at the respective gauge locations. M_1 and M_2 can be calculated knowing the voltage output from the strain gauges, various constants for the electronic circuits and the geometry and material properties of the cantilever beam. For the general case, M_i can be found from the following equation:

$$M_i = \left[\frac{2\Delta V_i}{gfGV_{in}}\right]\left[\frac{Ebh^2}{6}\right] \qquad \text{e3.13}$$

Where: ΔV_i = differential voltage from gauges (V)

gf = gauge factor for the specific gauges

G = Gain for the electronic signal

V_{in} = excitation voltage for the half bridge circuit (V)

E = Modulus of Elasticity (MPa)

b = base width of beam (mm)

h = height of beam (mm)

The derivation of e3.13 is shown in greater detail in Chapter 4. The force and moment applied by the surgeon on the sleeve of the gripper can now be calculated simply from the output of two bridge circuits.

3.3 Results

3.3.1 Calibration

Calibration was performed with known weights between 5 and 65 N. The calibration was done by fixing the vice grip in a horizontal position and hanging the weights from the center, front and back of the sleeve. Calibration showed that the system could calculate the forces accurately (R^2=0.96) to within ±3 N. The results of the force calibration are shown in Figure 3.5. Fixing the Gripper sleeve in a vertical position and rotating the sleeve by ±5 degrees increments from its initial starting point calibrated the inclinometer. (Figure 3.6) The resolution of the inclinometer was within ±2 degrees for a range of -50 degrees in one direction and 40 degrees in the other direction.

3.3.2 Surgical Tests

For scoliosis surgery, data was collected during the rod rotation of the rod prior to fixation. Prior to surgery, the Gripper was gas sterilized and this sterilization process had no adverse affects on the electronics. The sleeve of the Gripper can be easily slipped over the rod rotator. This design is non-intrusive to the current surgical procedure. The time added to the surgical procedure was no more than five minutes. Forces and moments were recorded for about 50 seconds at 10 Hz. Since continuous data acquisition of the applied force was employed, the pattern of loading can be found. Three such examples from two different patients are shown in Figures 3.7, 3.8 and 3.9.

Figure 3.7 shows a rod rotation maneuver and screw tightening for one patient, Sample I. To begin with, the sleeve had just been placed on the rod rotator, the force was at zero and the inclination was at about negative 10 degrees. Force was applied to a maximum of about 19 N then held relatively constant while some hex nuts were tightened

into the hooks. During this time the inclination remained constant at about 20 degrees while the force on the Gripper was decreased as the hooks presumably took on more load. The sharp drop in inclination around 48 seconds indicates that the Gripper sleeve was removed, corresponding to the return to zero of the Gripper force.

Figure 3.8 shows a rod rotation maneuver for a second patient Sample IIa. Collection of this data sample begins with the Gripper sleeve resting on the operating room (OR) table. The sleeve in then picked-up by the surgeon and placed on to the rod rotator as indicated by the sharp inclination spike around 15-18 seconds. The force and inclination then both increase until they reach maximum values of 40 N and 40 deg respectively. Pressure was released from the Gripper at 30 seconds, noted in the sharp drop in force, and then the sleeve was removed about two seconds later causing the sharp drop in inclination. The inclinometer was then placed back on the table and the force reading returned to zero. There was no concern that the original and final inclinometer readings are not the same as this difference was due to the position the sleeve is placed on the OR table. Sample IIa was different from Sample I in that no screws were tightened as the rod rotator was removed and then later repositioned for another rotation shown in Sample IIb.

Figure 3.9, Sample IIb is from the same patient as Sample IIa. The rod rotator had been repositioned and the inclinometer motion prior to the five second mark indicates the sleeve being placed on the rod rotator. The applied force was large and reaches about 60 N. The inclinometer reached a maximum of 40 degrees at which point it likely railed. The inclinometer would have likely reached about 60 degrees where it was then held as the hex nuts were tightened into the hooks. The sharp drops in force and inclination at about 35s occurred when the sleeve of the gripper was removed and again, as expected, the force returns to zero.

The pattern of loading was often similar for the other patients. The rod rotation maneuver can be repeated up to four times. By repeating the rod rotation maneuver, it is believed that the flexibility of the spine increases resulting in a better outcome. The first rod rotation maneuver attempts follow a pattern similar to Sample IIa. When the screws are tightened the pattern resembles the pattern shown in Sample I and Sample IIb.

This system was tested on 17 subjects with a pre-op Cobb angle averaging 60 (± 17) deg. The average maximum force applied by the surgeon was 39 (± 14) N ranging from 19-68 N. The resultant torque or moment on the rod was 8 (±3) Nm ranging from 4-14 Nm. This is similar to the peak torque used in three-dimensional models by Gardner-Morse et al. (1994) and Poulin (1998).

Unfortunately the six month post-op x-rays were only available for ten patients, as some of the patients have not yet returned for their sixth month checkup at the time this thesis work was completed. An expected correlation between the amount of Cobb angle correction (Pre-op – Post-op) and the applied force was analyzed. For the ten patients with post-op x-rays, there appears to be a weak linear correlation ($R^2 = 0.46$) between the amount of correction versus applied force as shown in Figure 3.10. However, if the AIS cases were sectioned from this group, the correlation is much stronger ($R^2 = 0.9$) as seen in Figure 3.11.

3.4 Chapter Summary

A device called the Gripper was designed, built and tested to measure the forces during scoliosis surgery. The sleeve of the Gripper can be easily slipped over the rod rotator and is non-intrusive to the current surgical procedure. Gas sterilization has no adverse effects on the electronics of the Gripper. The data acquisition system took a continuous recording of the applied force and the pattern of loading was seen. Measurements from the Gripper indicated an average applied force of 39 N with an accuracy of ± 3 N. The average applied torque was 8 Nm ± 1Nm. A slight linear relation ($R^2 = 0.46$) was found when comparing applied torque to amount of correction for 10 patients. This linearity improved ($R^2 = 0.9$) if only the AIS patients were considered. More data needs to be collected to show if a true correlation exists.

The force measured by the Gripper is only one measure in a complicated, lengthy surgery. To get a better understanding of the forces applied to the vertebra, the design of a transducer to measure the forces at the hooks will be discussed in the following chapter.

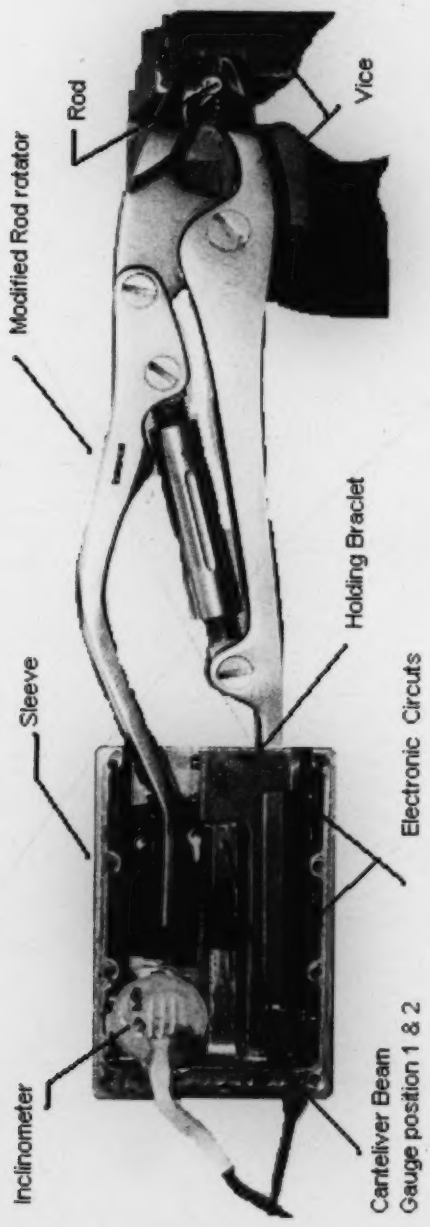

Figure 3.1: The Gripper

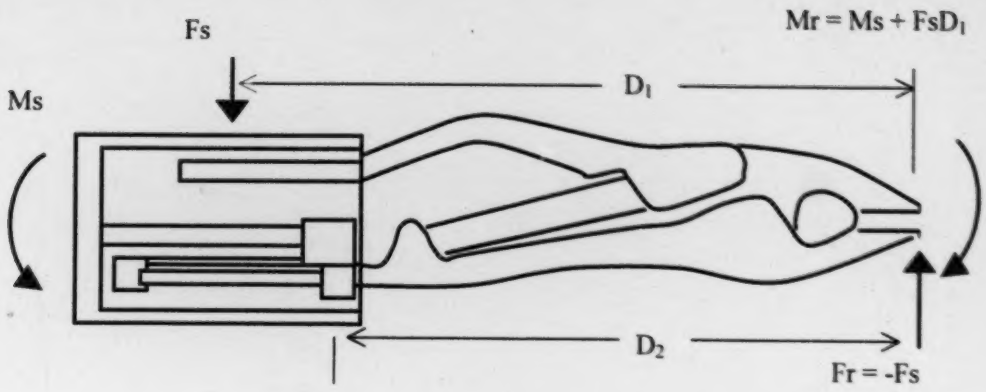

Figure 3.2: FBD of entire Gripper system in horizontal clamped position

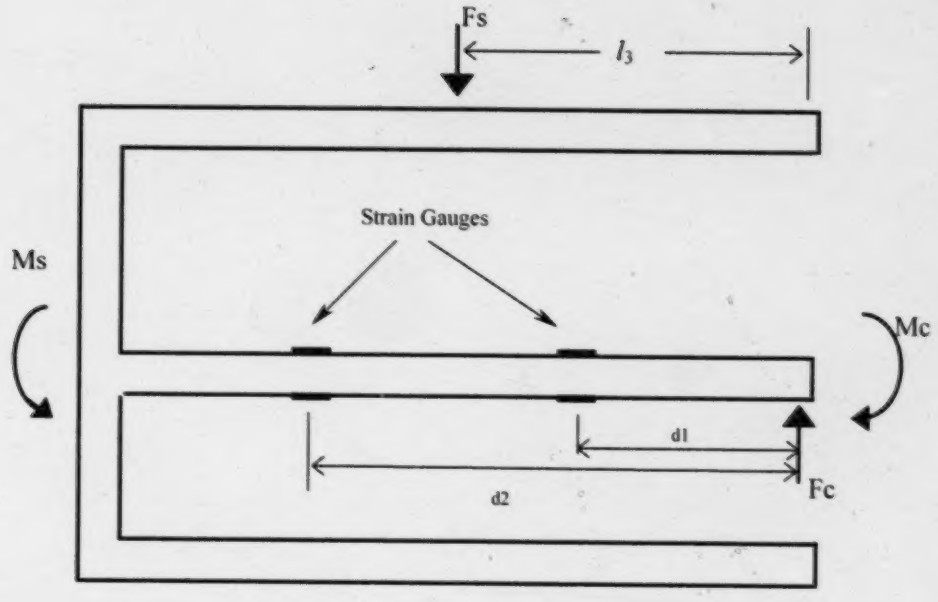

Figure 3.3: FBD of resultant force (F_c) and moment (M_c) within Gripper sleeve

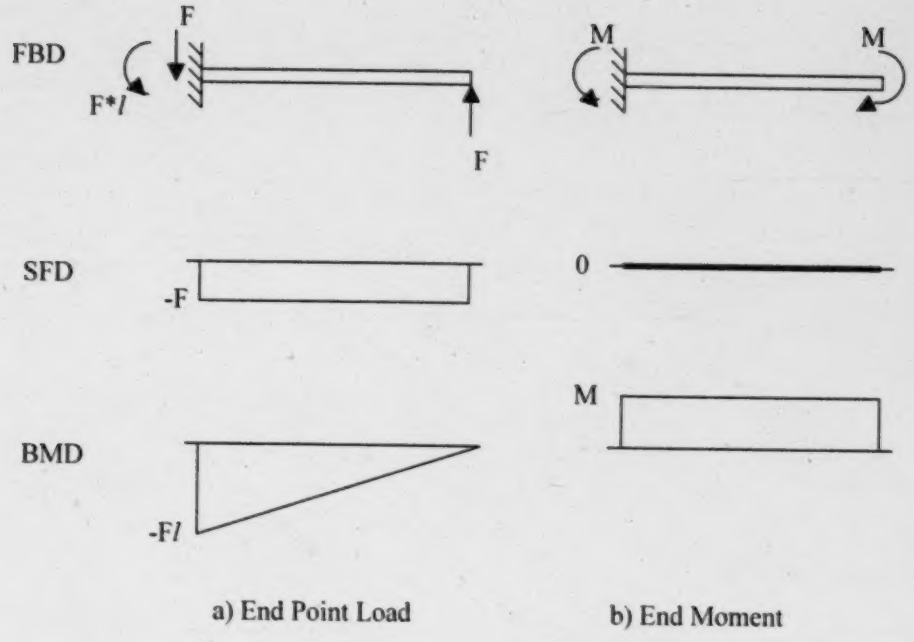

Figure 3.4: Free body, shear force and bending moment diagrams for cantilever beam

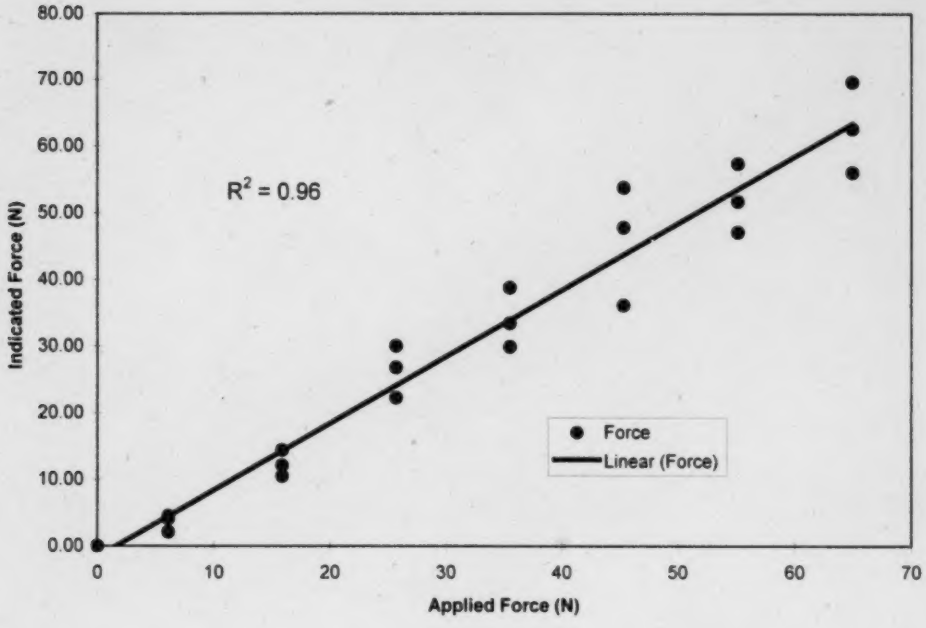

Figure 3.5: Gripper force calibration

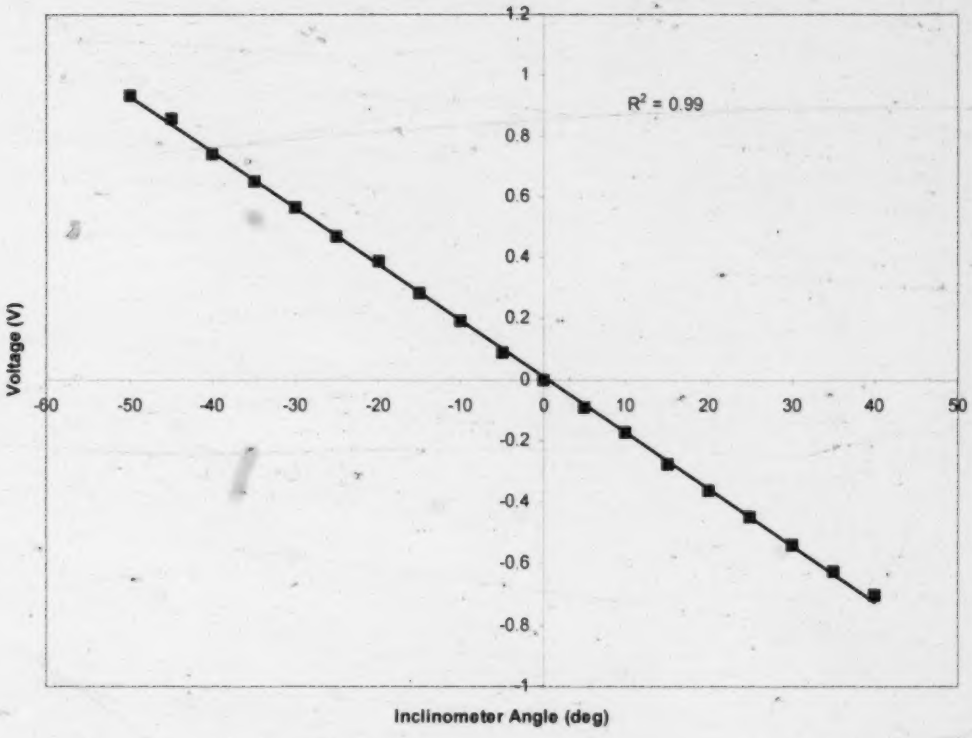

Figure 3.6: Inclinometer calibration

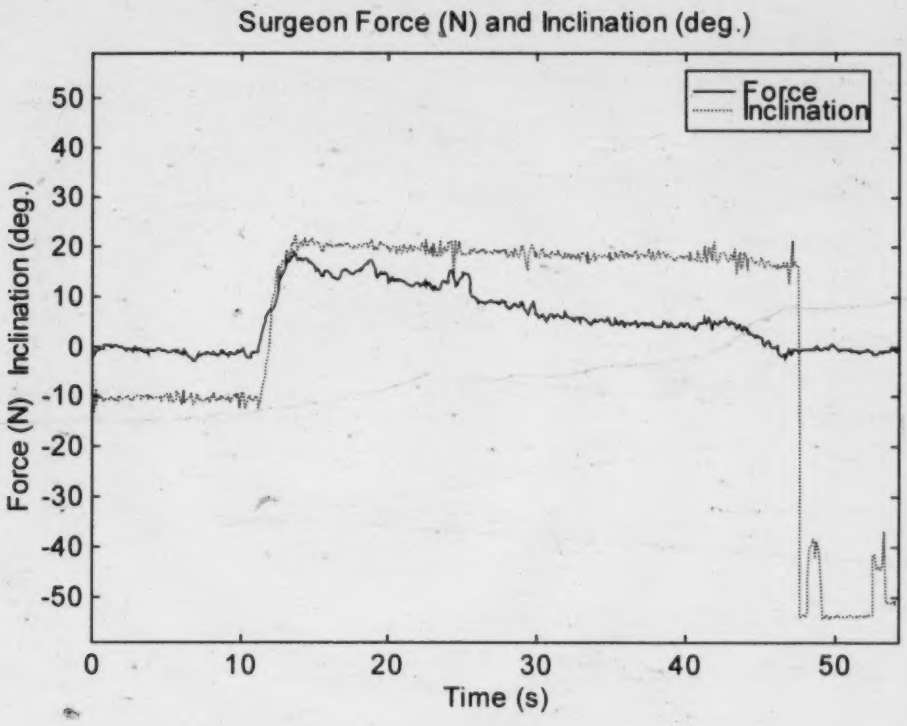

Figure 3.7: Sample I of Gripper force and inclination data

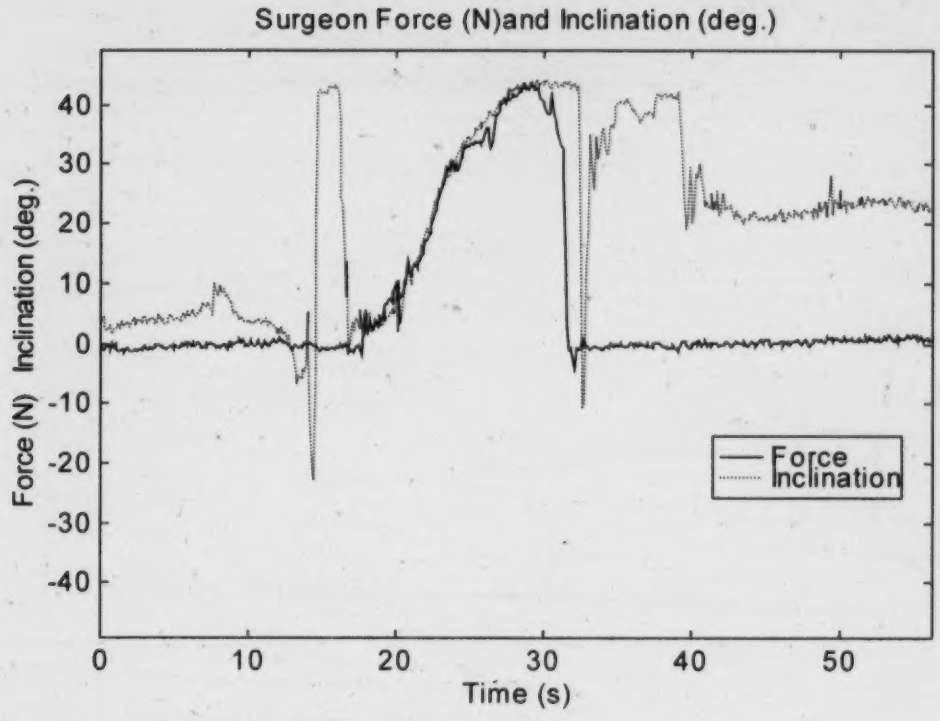

Figure 3.8: Sample IIa of Gripper force and inclination data

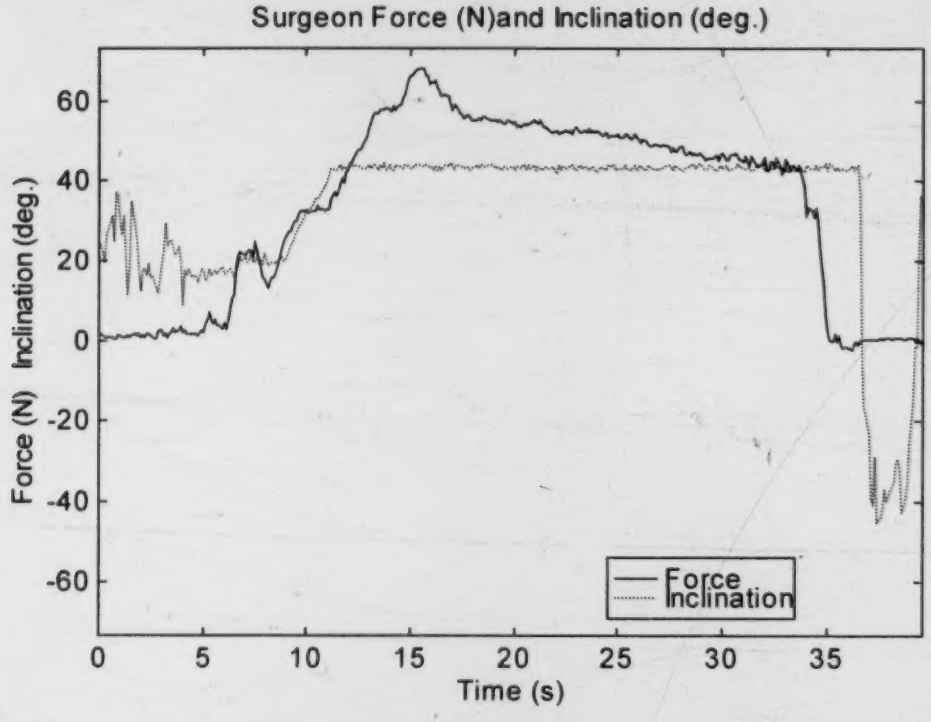

Figure 3.9: Sample IIb of Gripper force and inclination data

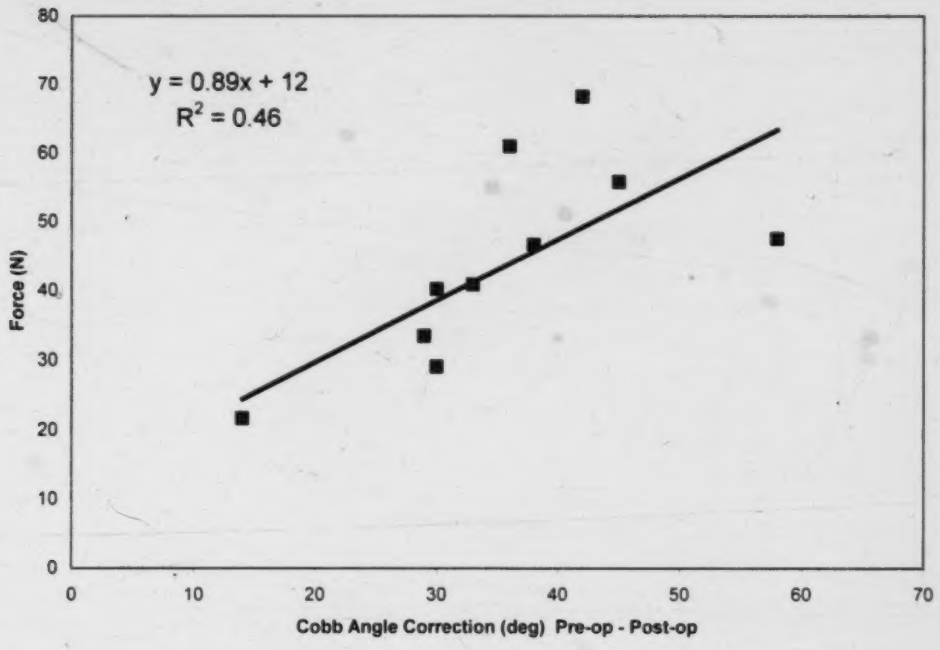

Figure 3.10: Amount of Cobb angle correction vs force

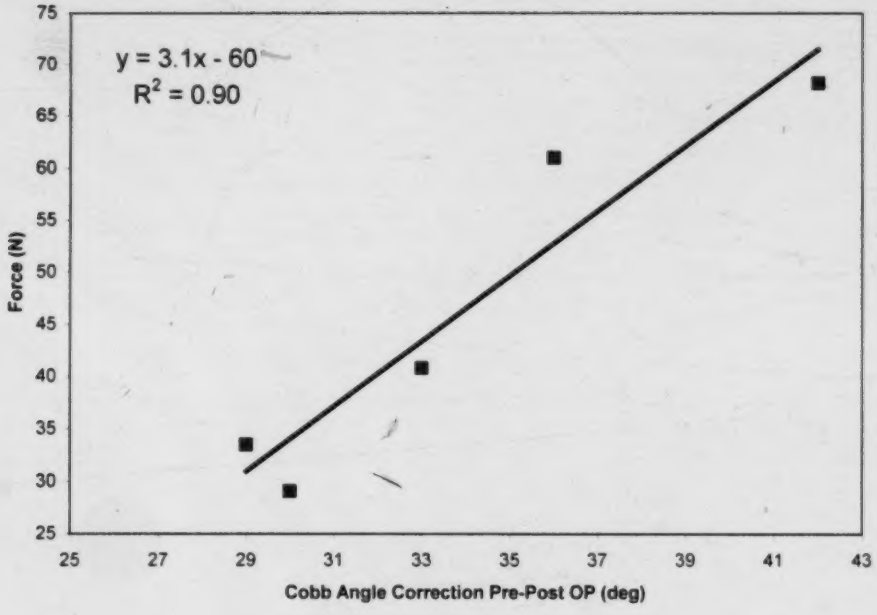

Figure 3.11: Cobb angle correction versus force for AIS patients only

Chapter 4 FEA and Hook Design

4.1 Introduction

This chapter discusses the various steps in the design of a hook capable of measuring the forces applied during scoliosis surgery. The hook will function like a standard CD hook except that it will be capable of measuring forces and moments during the surgical procedure. The design will involve the placement of strain gauges on a hook that will be inserted on the vertebra for the duration of the surgery. After the rod is rotated and the hooks are tightened, the instrumented hook will be loosened, removed and an original CD hook will be put in its place. The switching of the instrumented hook with the original hook will add approximately 15 minutes to the surgery. Ideally the hook would be left in the patient, but due to the risk of infection or hook failure only the approved CD instrumentation will be permanently implanted into the patient.

To design such a hook, finite element analysis (FEA) was a useful tool to determine the sensitivity of three designs. The best design was selected based on FEA results and the following design criteria. First the hook must have minimum strains no less than 35 με calculated where strain gauges are to be placed. This value was selected based on limitations of the data acquisition system with respect to the signal to noise ratio. Secondly, the hook must be able to measure the four predicted forces discussed in Chapter 1, namely: push-in, pull-out, compression and distraction. As well, the strain gauges and wires must be well protected. Manufacturability of the design must also be considered. Finally, the hook must maintain the same functional geometry as an existing CD hook so that it can be used in the operating room.

The hooks were compared based on these design criteria, and one was selected. This design was then further analysed using FEA and classical beam bending theory. The design was manufactured and the predicted and physical outputs were analysed and compared.

4.2 FEA Background

Complex shapes such as the hook are difficult to analyze using classic free body diagrams and simple models. By using FEA, a complex shape can be broken into smaller pieces, called elements, so that a solution can be found. For each element, the force vector, F, and the displacement vector, Q, can be related by means of a stiffness element matrix, K_e. This matrix is an nxn matrix where n is the number of degrees of freedom per element.

$$K_e Q = F \qquad \text{e4.1}$$

For multiple elements, the stiffness matrices for each element are assembled to form the global stiffness matrix.

$$\begin{bmatrix} K_{11} & K_{12} & \cdots & K_{1N} \\ K_{21} & K_{22} & \cdots & K_{2N} \\ \vdots & & & \\ K_{N1} & K_{N2} & \cdots & K_{NN} \end{bmatrix} \begin{Bmatrix} Q_1 \\ Q_2 \\ \vdots \\ Q_N \end{Bmatrix} = \begin{Bmatrix} F_1 \\ F_2 \\ \vdots \\ F_N \end{Bmatrix} \qquad \text{e4.2}$$

The global stiffness matrix, K_G, is based on the material property, geometry and boundary conditions. In most cases the force vector, F, is given and the displacement vector, Q, can be solved. Once Q has been determined the element stresses and strains can be calculated. (Chandrapatla & Belegunda, 1997)

4.3 FEA Materials and Methods

ANSYS 5.6 is a commercial finite element analysis (FEA) software and was used to analyze various hook designs. The modulus of elasticity of the material was 214GPa as the hook was manufactured out of tool steel (Machinery's Handbook, 2000). In order to pick an element type and size, a simple test of element type was done with a cantilever

beam comparing the analytical results to the ANSYS output. (See appendix B) This simple test showed that using SOLID45, SOLID73 or SOLID92 all provided acceptable results. The best results, at less then 1% error, were found with tetrahedral elements containing 10 nodes (SOLID92). This element type was also the only type that could conform to the intricate geometry of the hook making SOLID92 the obvious choice. When using this element, computational time often becomes a problem. However, even for the most complex hook design, the analysis was completed in less than 30 minutes therefore processing time was not a concern.

A structural finite element computer model of the various hook designs determined if sufficient strain was present to measure and distinguish between the four forces. Recall that the strain gauges must be located on the hook in regions that have minimum strains of no less then 35 $\mu\varepsilon$ to be reliably measured and to be distinct from noise present in the system. This value was selected based on the limitations of the available data acquisition system.

To predict strain on the various hook designs, a Sofamor Danek (SD) 84190H pedicle hook shown in Figure 4.1 was modelled and used as the baseline design. The geometry of this hook was measured with vernier callipers to an accuracy of 0.1 mm. Variations of this hook and new designs were modeled in ANSYS to determine the sensitivity of each design. Figure 4.2 shows a FEA model of a standard hook subjected to an applied pressure and constraints. Combined axial and compressive/distractive forces were simulated on the various hook designs. A pullout force of 20N was applied uniformly to each design while constrained with similar boundary conditions. The hook was constrained on the top surface of the hook blade in the x direction, to simulate contact of the hook with the ventral side of the lamina. In order to prevent unconstrained rotation, the hooks were constrained at the tips in the y direction. Assuming no movement of the hook in the lateral direction, the hook was also constrained at the end corners in the z direction. After processing and solving, strain gauges were modelled by selecting an area on the hook the size of a gauge and averaging the strain in this region.

The position of the strain gauges on the hooks must enable them to measure and differentiate between the four major forces outlined in Chapter 1. These four major forces being axial pullout, axial push-in, compression and distraction. The strain gauges

must be well protected to prevent the breaking of wires. The hook must be manufacturable. Finally it must maintain functional geometry so that it can be used with an existing SD instrumentation set.

Three alternate designs were evaluated. The first model was of a CD hook as shown in Figure 4.3a. The second design is called the "moment arm" design. This design maintains the original geometry as the CD hook with the exception of a slice that is removed from the body of the hook (Figure 4.3b). The third design is the "plate" design. This design maintains functional geometry for the body and blade of the hook and includes a plate that connects these two halves together (Figure 4.3c).

4.4 FEA Results of the Three Designs

All three designs were analysed using the five design criteria identified in section 4.1. The results are explained in detail and summarised in Table 4.1.

When analysing the existing hook, (Figure 4.3a) there were immediate problems in meeting the first design criteria because of inadequate strain levels. It was found that the hooks are too stiff to be effectively used as a transducer. When subjected to a simulated axial pull-out force of 20N the strains in the regions of interest were insufficient for our measurement purposes. The easiest location to mount the gauges was axially along the body of the hook, resulting in a strain of only 7 με. The area of maximum strain during the computer simulation occurred at the bend of the hook blade, resulting in 55 με. The strain gauges in both of these locations are unprotected. In fact, in a preliminary test in the cadaver lab, a hook instrumented at the 55 με region experienced pulling off of the gauge. With the gauges mounted on the body of the hook, where they are less likely to fall off, this design was not sensitive to axial push-in force. The positive notes on this hook were minimum manufacturing costs as only slight modifications were made to an existing SD hook. Due to only slight modifications the hook maintained full functional geometry.

The second design, referred to as the "moment arm" design, (Figure 4.3b) includes axially placed strain gauges. These were placed about a third of the length down along either side of the moment arm. This design increased the hook sensitivity so that

the strains in the area of interest were about 150 με for a 20N applied pullout force. However, the sensitivity of the computer modelled strain gage was still not sufficient to be physically recorded during the application of an axial push-in. For this design, two of the four gauges were protected. Manufacturing this design was not difficult and the functional geometry could be maintained.

The third, and most strain sensitive design, was the "plate" design. (Figure 4.3c) With an applied 20 N of force and a plate of 0.8 mm thick, the FEA predicted strain was 155 με. This design is versatile in that the plate thickness can be varied to adjust its sensitivity to strain. This is a useful feature since the magnitude of the force applied directly to the hooks is presently unknown. The strain gauges are mounted on the plate and can differentiate between all four major forces. Since the plate is fastened to the blade of the hook and then slides into the body, the gauges and wires are well protected. This design is manufacturable while maintaining functional geometry of the CD hook.

Table 4.1: Summary of three hooks and design criteria

	Design Criteria				
Hook Type	*Strain*	*Differentiate Forces*	*Gauges Protected*	*Manufacturable*	*Functional Geometry*
Existing SD	Too Low	3 of 4	no	Yes	Yes
Moment Arm	Within Range	3 of 4	some	Yes	Yes
Plate	Within Range	4 of 4	yes	Yes	Yes

FEA provided an easy method for analysing the strains in the three hook designs. Colour plots of the strain could quickly show where areas of high strain were and where potential gauge mounting locations could be. Based on this analysis, the Plate design was selected as the best hook design.

4.5 FEA of Plate

FEA was used to consider the plate design in detail. Figure 4.4 shows the boundary conditions and the application of axial force uniformly distributed on the bottom of the washer. For analysis of the plate alone, the knife-edge ends of the plate

were fixed in the x direction to prevent vertical movement. To eliminate physical slipping of the plate and rotation about the x axis it was constrained in the y direction at two corners. Finally to prevent slipping in the z direction it was constrained at one corner in the z direction. For the bending moment case, a uniform pressure was applied on the sides of the washer to create a moment. One of the main advantages of the plate design is that it is able to differentiate between four different forces. The differentiation of the four forces was first validated with FEA and is schematically represented in Figure 4.5.

In the first image in Figure 4.5a, the hook is subjected to a distraction force causing a moment at the center of the plate. This moment causes the plate to bend into a 'S' shape which provides a positive output from the gauge located on the left half of the beam and a negative output from the right half of the beam. The second image, Figure 4.5b, represents compression. In this case it can be seen that the outputs are reversed, that is a negative output from the gauge located on the left half and a positive output from the gauge located on the right half. The third image, Figure 4.5c, shows axial push in force on the plate this results in negative outputs from the gauges on both ends of the plate. Contrary, the fourth image, Figure 4.5d, shows axial pullout force that results in positive outputs from the gauges on both ends of the plate. This test on the plate alone provided validation that the plate would be able to differentiate the four different forces.

4.6 Magnitude of Plate Strains

For the axial pullout case the force on the plate was varied so that it could be compared with theory and actual gauge output. The plate had a total of 1368 nodes. The axial forces applied were 5, 10, 25, and 200 N and they were distributed as pressures over the bottom of the plate washer to minimize localized 'hot spots'. The time required to solve the loaded plate was only 30 seconds. In order to analyze the strains on the plate, five "hard points" were created, one at each of the corners of the gauge location and one in the center. These hard points were then integrated in the meshing of the object. This made the post processing easy as the strains at these five specific points could be easily found and averaged. The resultant average strains at the gauge location for the 5, 10, 25 and 200N loads were 30, 64, 151, and 1206 με respectively. The standard deviation for

each gauge was calculated and reported in Table 4.3 where comparisons of the three methods are made.

4.7 Analytical Formulas for the Plate

FEA is a useful method of thoroughly determining the stress and strains in an object, however, this method can be time consuming and the results are not always intuitive. In order to support the FEA of the plate, fundamental equations for beam bending theory can be used. Theoretical calculations provide a very quick method for comparing the results of varied parameters. Analytical formulas also provide a method of algebraically separating the moment and load applied to the plate.

Starting with the simplest case, which is a pure axial load on the simply supported plate. The beam load, shear force and bending moment diagrams are shown in Figure 4.6a. With a centrally located load F, the magnitudes of the reaction forces at the ends of the beam are $F/2$. From this, the transverse shear force diagram is created. Integrating the area under this curve yields the bending moment diagram. The moment $M(x)$ can be derived from this diagram as a function of x along the length, l, of the beam.

$$M(x) = \frac{-Fx}{2} \qquad 0 < x < l/2 \qquad \text{e4.3}$$

$$M(x) = \frac{-Fx}{2} - \frac{Fl}{s} \qquad l/2 < x < l \qquad \text{e4.4}$$

The next case is the simply supported beam with a centrally located moment M_o. The beam load, shear force and bending moment diagrams for this loading are shown in Figure 4.6. In a similar manner, the moment $M(x)$ as a function of x along the beam length l was found.

$$M(x) = \frac{-M_o x}{l} \qquad 0 < x < l/2 \qquad \text{e4.5}$$

$$M(x) = M_o - \frac{M_o x}{l} \qquad l/2 < x < l \qquad \text{e4.6}$$

Finally, consider the combined case where both moment and force are applied to the center of the plate. Using superposition and rearranging the following equations are found:

$$M(x) = \frac{-Fx}{2} - \frac{M_o x}{l} \qquad 0 < x < l/2 \qquad \text{e4.7}$$

$$M(x) = \frac{-F(l-x)}{2} + M_o - \frac{M_o x}{l} \qquad l/2 < x < l \qquad \text{e4.8}$$

Since the placement of the strain gauges is at known distances d_1 and d_2, let $x = d_1$ for the one side of the beam ($0 < d_1 < l/2$) and let $x = d_2$ for the other side of the beam ($l/2 < d_2 < x$).

Making the $x = d_1$ substitution into e4.7, the moment at the first strain gauge location is:

$$M_1 = -d_1\left[\left(\frac{F}{2}\right) + \left(\frac{M_o}{l}\right)\right] \qquad \text{e4.9}$$

Similarly substituting $x = d_2$ into e4.8 the moment at the second gauge location is

$$M_2 = d_2\left[\left(\frac{F}{2}\right) + \left(\frac{M_o}{l}\right)\right] - \left(F\frac{l}{2}\right) + M_o \qquad \text{e4.10}$$

Equations e4.9 and e4.10 are useful for predicting the expectant moments M_1 and M_2 at a particular point based on the applied load F and moment M_o. However, with the strain gauges it is possible to calculate the strains at points d_1 and d_2 from the gauge voltage output. The strain can then be converted into stress and finally moments at point d_1 and d_2. M_1 and M_2 are needed to calculate the applied force, F, and moment, M_o, based on the gauge output. It is for this reason that equations e4.9 and e4.10 need to be combined and rearranged to give the applied force F, and moment M_o in terms of M_1, M_2 and geometric parameters.

Combining e4.9 and e4.10 to solve for F and M_o respectively we have:

$$F = \frac{M_2}{d_2 - l} - \frac{M_1}{d_1} \qquad \text{e4.11}$$

$$M_o = \frac{\left[M_2 - \left(M_1\left(\frac{l - d_2}{d_1}\right)\right)\right]}{\left[2 - \frac{2d_2}{l}\right]} \qquad \text{e4.12}$$

As previously mentioned, the moments M_1 and M_2 are calculated from the strain gauge output. They are both calculated the same way so let's look for a general moment, M_i, at position *i*. First, the following equation is used to find the stress, σ_i, due to bending in the beam.

$$\sigma_i = \frac{M_i y}{I} \qquad \text{e4.13}$$

where $I = \frac{bh^3}{12}$ moment of inertia for a rectangular cross section e4.14

$y = \frac{h}{2}$ distance from neutral axis to point of interest e4.15

(gauge location on plate surface)

Substitute e4.14 and e4.15 into e4.13 and rearrange to get

$$M_i = \frac{\sigma_i b h^2}{6} \qquad \text{e4.16}$$

Having calculated M_i in terms of stress, σ_i the relationship between stress, σ_i, and strain, ε_i can be used:

$$\sigma_i = E\varepsilon_i \qquad \text{e4.17}$$

Where E is the modulus of elasticity for the material.

The strain, ε_i, can be calculated from the voltage output from two gauges which are mounted in a half Wheatstone bridge circuit on the top and bottom of the plate at location d_i along its length. This configuration of the strain gauges on the plate provides temperature compensation.

$$\varepsilon_i = \frac{2\Delta V_i}{gfGV_{in}} \qquad \text{e4.18}$$

Where: ΔV_i = differential voltage from gauges (V)

gf = gauge factor for the specific gauges

G = Gain for the electronic signal

V_{in} = excitation voltage for the half bridge circuit (V)

Finally, substituting e4.17 and e4.18 back into e4.16, M_i, the moment at a gauge location can be found,

$$M_i = \left[\frac{2\Delta V_i}{gfGV_{in}}\right]\left[\frac{Ebh^2}{6}\right] \qquad \text{e4.19}$$

Now, the differential voltage outputs ($\Delta V1$ and $\Delta V2$) from Wheatstone bridge 1 and 2 can be substituted into e4.19 to yield the respective moments M_1 and M_2. M_1 and M_2 are then used to solve for the applied force and moments given the output from the strain gauges.

$$F = \frac{M_2}{d_2 - l} - \frac{M_1}{d_1} \qquad \text{e4.11}$$

$$M_o = \frac{\left[M_2 - \left(M_1\left(\frac{l-d_2}{d_1}\right)\right)\right]}{\left[2-\frac{2d_2}{l}\right]} \qquad \text{e4.12}$$

4.8 Probable Error

It is possible to make an estimate of the error or the probable uncertainty of a variable based on the error of the other variables in an equation. The question is what is the certainty of the calculated force based on the uncertainty of the other variables?

Generally speaking, if an equation is purely multiplicative the error, *e*, can be found as follows:

If

$$Q = AG^a H^b I^c \qquad \text{e4.20}$$

then the error in Q is:

$$\left(\frac{eQ}{Q}\right)^2 = a^2\left(\frac{eG}{G}\right)^2 + b^2\left(\frac{eH}{H}\right)^2 + c^2\left(\frac{eI}{I}\right)^2 \qquad \text{e4.21}$$

The previous equations are given in the Mechanical Measurements course notes (1994).

Of greatest concern is the error in the calculated applied force, *F*. It is very difficult to calculate the error in *F* since it is built from various equations, each with an inherent error. The variables involved in the calculation of *F* and their respective errors are summarized in Table 4.2. The respective errors are found a variety of ways. When possible, the manufacturer's specifications were consulted. This was the case for the gain, gauge factor and excitation voltage. The error in gauge location was selected to reflect the difficulty in accurately placing the gauges. The error in bridge circuit voltage is dependent on any outside noise but the value of 0.3 mV was measured from a ground

wire in quiet ambient conditions. The error in modulus of elasticity reflects the ranges given for tool steel. Finally the errors in plate geometry, base and height, was 10% of the smallest major division on a vernier caliper.

Table 4.2: Variables and their respective value and errors.

Variable symbol	**Definition**	**Value**	**Error**
d_i	Distance to gauge location	2.5 mm	0.5 mm
M_i	Moment at gauge location	Variable Nmm	Calculated from εi
ε_i	Strain from bridge circuit	Variable	Calculated from Vi
V_i	Bridge circuit voltage	Variable	0.0003 V
G	Gain	100	0.5
gf	Gauge Factor	2.09	0.02
V_{in}	Excitation Voltage	3 V	0.01 V
E	Modulus of Elasticity	214000 MPa	14000
b	Base of plate	8 mm	0.01 mm
h	Height of plate	0.8 mm	0.01 mm

The error in strain is found from:

$$\left(\frac{e\varepsilon_i}{\varepsilon_i}\right)^2=\left(\frac{eV_i}{V_i}\right)^2+\left(\frac{eG}{G}\right)^2+\left(\frac{egf}{gf}\right)^2+\left(\frac{eV_{in}}{V_{in}}\right)^2 \qquad \text{e4.22}$$

The error in M_i is found from:

$$\left(\frac{eM_i}{M_i}\right)^2=\left(\frac{e\varepsilon_i}{\varepsilon_i}\right)^2+\left(\frac{eE}{E}\right)^2+\left(\frac{eb}{b}\right)^2+2^2\left(\frac{eh}{h}\right)^2 \qquad \text{e4.23}$$

The error in F is then found from:

$$\left(\frac{eF}{F}\right)^2 = \left(\frac{eM_1}{M_1}\right)^2 + 2*\left(\frac{ed_1}{d_1}\right)^2 + \left(\frac{eM_2}{M_2}\right)^2 \qquad \text{e4.24}$$

It is apparent that there is no single answer for the error in F since the error is dependent on many changing variables. The error is, in fact, dependent on the voltage output from the bridge circuit. Taking the expected voltage output for 10 N of force and calculating the error in F we find that it is 3.08N or about 30% error. Another way to get an idea of the amount of error in the system is to calculate the error during one of the tension compression calibration procedures described in the next chapter. Calculating the error throughout this range produces an average error of 30% with a standard deviation of 2.3%. 30% is a large amount of error however, the calculated force can only be as accurate as the sum of its components without any calibration. The largest component contributing to error is d_i or the accuracy of the placement of the gauges on the plate. The calibration procedure is described in the next chapter and after calibration, a high correlation exists between the applied force from an Instron testing machine and the strain gauge output.

4.9 Comparison of FEA, Analytical and Gauge Output of the Plate

After manufacturing of the hook was complete, there were three methods to determine the strain at the gauge location. Manufacturing and calibration are discussed in the next chapter. The first method is to use FEA, second is to use fundamental beam bending theory equations and third is to measure the output strain from the gauges while subjected to a known force. A plate of 0.8mm in thickness was manufactured and this was subjected to actual forces of 5, 10, 25 and 200N of tension in an Instron machine to determine the difference between the three methods. Table 4.3 tabulates the results from these three methods. The value in brackets shows the respective errors for each method.

Table 4.3: Strain results from three methods. Error/standard deviation in brackets.

Force (N)	Strain FEA (μs)	Analytical Strain (μs)	Strain Gauge Output (μs)
5	30 (6)	34 (8)	42 (14)
10	64 (13)	68 (15)	86 (23)
25	151 (31)	171 (38)	143 (35)
200	1206 (246)	1368 (304)	1263 (96)

It can be seen from this table that the strains are not equal and that there is a large window of error for each case. The FEA strain was calculated by averaging the absolute strain values at the five hard points for the four gauge locations on the top and bottom and right and left and sides of the plate. The error in brackets was one standard deviation for this data.

The analytical strain was calculated by combining and rearranging e4.16, e4.17 and e4.9 to get:

$$\varepsilon_t = \frac{-6d_1\left(\frac{F}{2}+\frac{M_o}{l}\right)}{Ebh^2} \qquad \text{e4.25}$$

for which the error was calculated from:

$$\left(\frac{e\varepsilon_t}{\varepsilon_t}\right)^2 = \left(\frac{ed_1}{d_1}\right)^2 + \left(\frac{eE}{E}\right)^2 + \left(\frac{eb}{b}\right)^2 + 2^2\left(\frac{eh}{h}\right)^2 \qquad \text{e4.26}$$

The strain gauge output was difficult to calculate since the output from the Instron machine was noisy at lower values. However, if the Instron output data were averaged in groups of ten, a definite increase in applied load was seen. Therefore, the Instron forces were averaged in groups of ten until an average equal to the desired force was found.

The corresponding mean strain gauge output for this group of ten was calculated and one standard deviation is recorded in brackets as the error.

Overall, the calculated strain output for the three methods gave similar results over the range of forces. Using a confidence interval of 95% and comparing the different methods to one another at the four different forces there was no significant difference found between the three cases.

Figure 4.1: Sofamor Danek CD pedicle hook

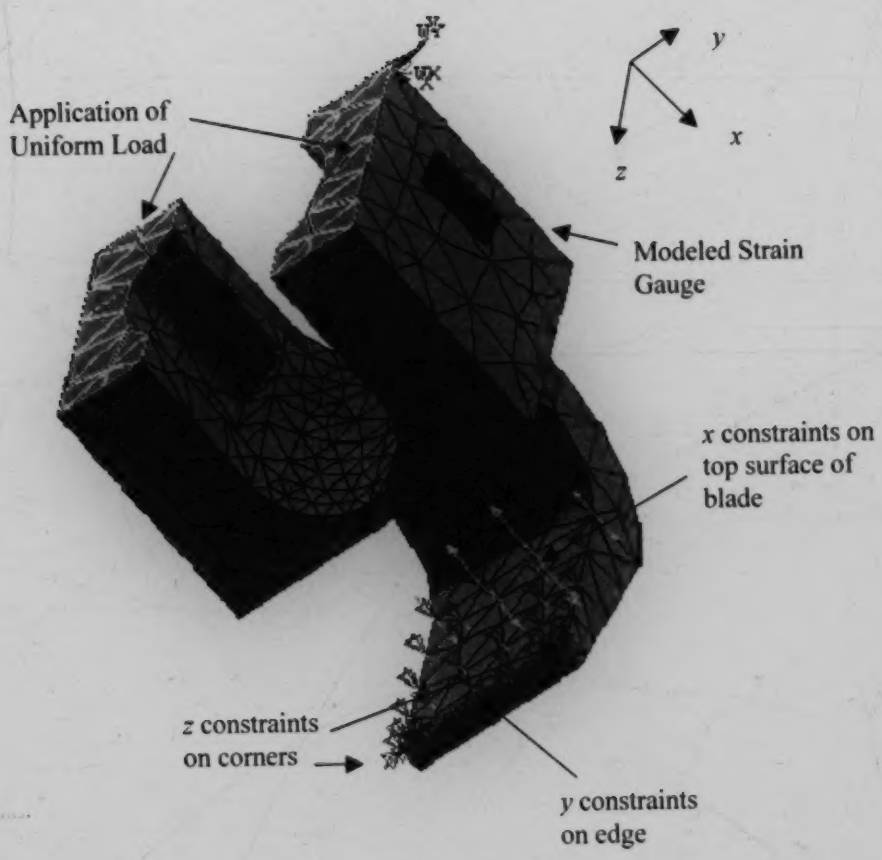

Figure 4.2: The force and constraints applied to the standard CD hook

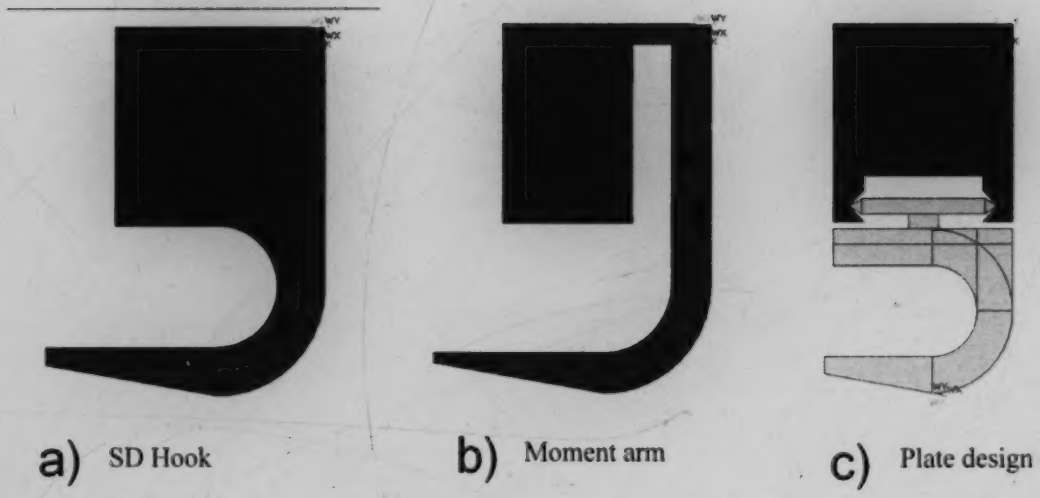

Figure 4.3: The three FEA modeled designs

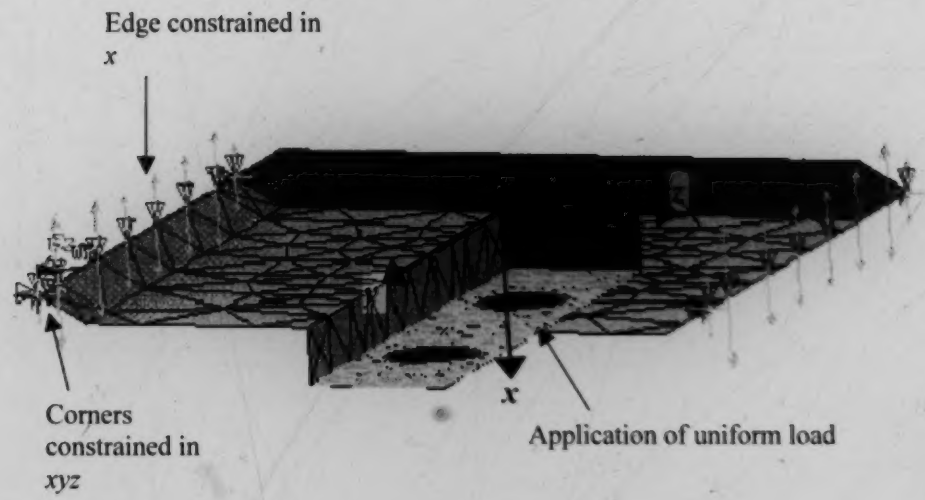

Figure 4.4: The constrained membrane

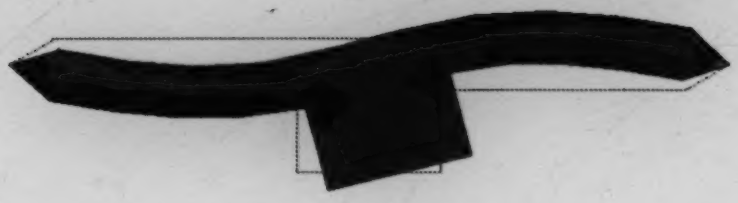

a) Bend/Distraction

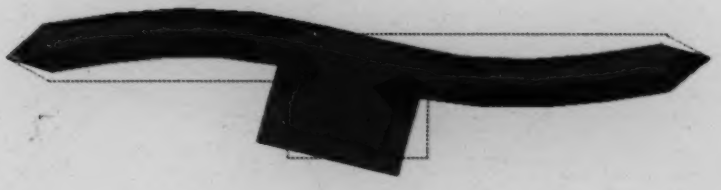

b) Bend/Compression

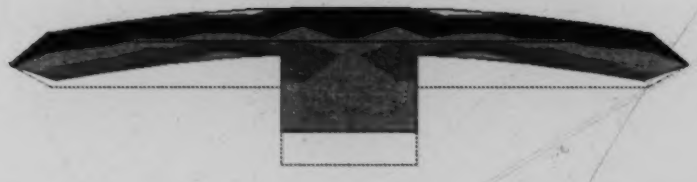

c) Anterior Push-in

d) Posterior Pull-out

Figure 4.5: Schematic representation of plate subjected to four major forces

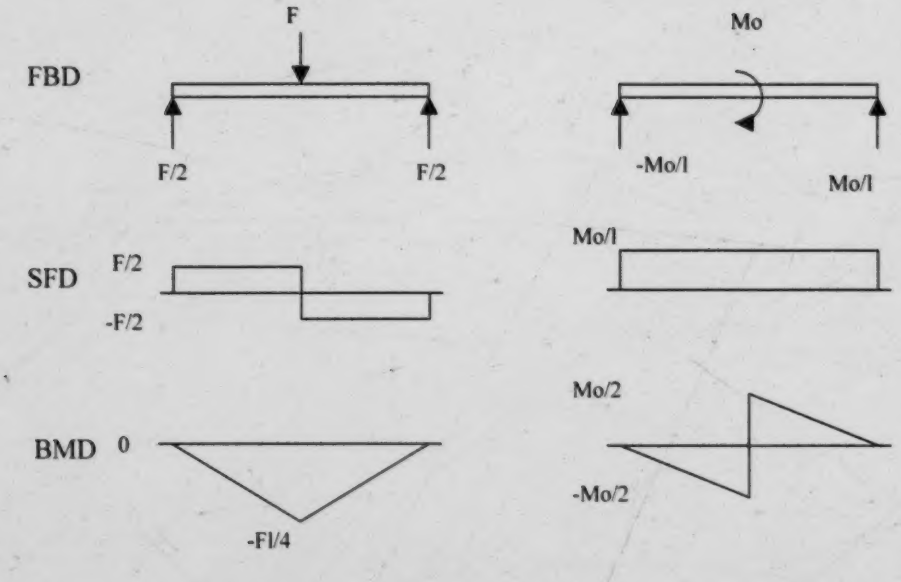

a) Central Axial Load

b) Centrally Located Moment

Figure 4.6: Free body, shear Force, and bending moment diagrams for simply supported beam

Chapter 5 Using the Plate Hook

5.1 Introduction

This chapter discusses the manufacturing and material selection of the hook. Initial results, to verify hook sensitivity to the four forces, are then displayed. A discussion of the calibration procedure and the sensitivity and accuracy of the hook follows. The results of *in-vivo* operating room (OR) trials are discussed as well as the failure of the plate.

5.2 Manufacturing of the Hook

5.2.1 Material selection

The load cell hook was manufactured from tool steel. Tool steel was selected because it is designed to handle high specific loads (Machinery's Handbook, 2000). The sharp tip on the plate edge called for such a material. The hardness of tool steel generally falls within a 50-66 Rockwell hardness range (matweb.com). Converting this to a Brinell hardness (540-770) the ultimate and yield strength can be predicted from:

$$S_u = 490H_B \qquad \text{e5.1}$$

$$S_y = 1.05S_u - 30{,}000\,psi \qquad \text{e5.2}$$

The ultimate and yield strength range from 1800-2600 MPa and 1700-2500 MPa respectively (Juvinall, 2000). Due to the fact that there are strain gauges on the plate it would be undesirable for it to undergo yielding. Knowing the material properties the

geometry of the plate can be selected and the force and moment applied before yielding can be calculated and avoided.

5.2.2 Hook Geometry

The plate hook was manufactured to maintain the same functional geometry as a CD pedicle hook (Figure 5.1). The threads at the top were matched so that a CD hex screw could be inserted during surgery. The gripping holes on the body of the hook enable the hook to be inserted and removed using specialized CD instruments. In order to insure a point contact, the angle of the plate tips are 60° while the angle of the body slot is 90 °. The plate thickness is variable and three different prototype plates were designed. A summary of mechanical properties of the three plates is given in Table 5.1.

The first plate, plate A, designed from O1 tool steel had a yield strength of 1500 MPa and an ultimate strength of 1690 MPa (matweb.com). The plate was 1mm thick allowing maximum axial forces of 800 N and maximum applied moment of 4000 Nmm before yielding. To allow clearance of the screws that attach the plate to the hook blade, holes 0.5 mm deep were counter sunk into the top of the plate. Due to this counter sinking, the relative thickness of the plate was reduced to 0.5mm. This design affected the maximum applied yield force and moment to 200 N and 1000 Nmm respectively ultimately causing a premature failure (discussed later in this chapter).

The second plate, plate B, was also made from O1 tool steel, however, its thickness was reduced to 0.8 mm to increase sensitivity at the gauge locations while the counter sunk holes for the screws were eliminated. Given this geometry this plate should be able to withstand 512N of axial force and 2560Nmm of moment before yielding.

The third plate, plate C, was made from D2 tool steel with higher yield and ultimate strengths of 2300 MPa and 2400MPa respectively. This plate maintained the 0.8 mm thickness of the second plate. Given this geometry and material properties, this plate should be able to withstand 780 N and 3935 Nmm of axial force and bending moment respectively before yielding. The ultimate force and moments are 820 N and 4100 Nmm respectively. Recall that in Chapter 2, Section 2.2.3, the range for hook pull-out for *in vitro* testing was between 464-809 N. The design of plate B, which can withstand an

ultimate force of 820N, should be able to record the applied force until failure if that were to in fact happen in the OR.

Table 5.1: Mechanical properties of three plates

Plate	Yield Strength S_u (MPa)	Ultimate Strength S_y (MPa)	Axial Yield Force (N)	Ultimate Axial Force (N)	Applied Yield Moment (Nmm)	Ultimate Moment (Nmm)
A	1500	1690	200	225	1000	1127
B	1500	1690	512	577	2560	2885
C	2300	2400	786	820	3925	4100

5.2.3 Other Design Concerns

One major concern was the pulling off of the fine lead wires during the surgical procedure. In order to avoid this, a relief plate was screwed to the body of the hook. The function of this plate is twofold. First it securely fastens the wire to the body of the hook so that the relief plate resists any tugging on the wire. Second, the relief plate hangs down preventing the plate from slipping out of the body of the hook.

5.3 Calibrating the Hooks

5.3.1 Initial Results

A prototype of the "plate" hook was manufactured, shown in Figure 5.1, and tested. A DAC 1200 data acquisition system with Lab View and MATLAB were used to record and analyze the data shown in Figure 5.2. The data show the output from the plate being bent in one direction, bent in the other direction, then axially pushed and axially pulled. The raw voltages in Figure 5.2a alternate in sign with these various maneuvers. Figure 5.2b shows that the force remains relatively close to zero during bending then positive force is recorded for the push test and negative for the pull test. On the contrary, Figure 5.2c shows that during the two bending tests, moments are primarily applied so the output is first positive then negative. During the push pull test, as expected, the moment output remains around zero. From preliminary bench top trials the plate had the sensitivity to measure axial force in increments of 115g (1.13N).

5.3.2 Axial Calibration Procedure

Though the calibration procedure was similar for all three plates, only the results of Plate C are presented here since this design was chosen for further use. Plate C was fixed to the small calibration block as shown in Figure 5.3. The top body of the hook was slid over the plate. A hex nut was inserted into the top body of the hook and both the hex nut and the calibration block were fixed to Instron attachment pieces.

The calibration apparatus was loaded in the Instron machine, which provided 50 lbs (222 N) of tension and compression force. The DAC system was used to simultaneously measure three channels, two channels from the strain gauges and a third from the Instron machine. The tension compression test was applied four times, twice with the apparatus at 0 deg and twice with the apparatus turned 180 deg.

For the analysis of the calibration data the raw data from the three channels was plotted in Figure 5.4. A section of the data at a zero point was averaged for all three

channels to later normalize the voltage readings. The Instron force, F_I, was calculated based on the fact that 500 mV is equal to 50 lbs full scale or using the formula:

$$F_I = (\Delta V_I)100 \qquad \text{e5.3}$$

The plate force was then calculated from the theoretical equations discussed in Chapter 4.

A plot of calculated plate force versus Instron force is shown in Figure 5.5. This graph should be linear, $y=x$. However, there are numerous reasons for such errors, some of which were discussed in Chapter 4, such as inaccuracies in plate geometry, gauge location and errors in electronic components. Others include the possibility that the load from the Instron may not be exactly centred, the digital output from the Instron may not be directly correlated to the force applied, and noise in the DAC also provides error. Another source of error that may result in nonlinearity is the possibility that the tips of the plate resting on the edges create a shorter effective length with increasing load.

To account for the various sources of error, and to find a line that fit throughout the entire calibration, an equation of plate force versus Instron force was found to fit the data so that $R^2 > 0.999$. This equation was found for all four calibration samples and then averaged together to give:

$$Y = -1 \times 10^{-6} x^3 - 9.5 \times 10^{-5} x^2 - 0.7114 x + 0.597 \qquad \text{e5.4}$$

This equation was then termed the polynomial calibration factor and used to recalculate the plate force. The polynomial calibration plate force was then plotted versus Instron Force. The result in Figure 5.6 now shows a linear graph where $y=x$ and linear with $R^2 > 0.999$ for all four calibration data sets. Calibration showed that the applied axial load could be measured with an 8% error and a resolution of ±5 N.

A resolution of ±5 N differs from the initial results that showed the plate could detect a 115g weight. Part of the problem is that the Instron machine is designed for 50,000 lbs (222420 N) and the calibration of the hook only used ±50 lbs (222 N). The

resolution of the plate is therefore limited by the resolution of the Instron machine. In order to determine the resolution of the plate on a smaller scale, various weights from 100g to 3000g were applied to the plate. This calibration was repeated four times and all were linear with:

$$y = 0.915x \quad (R^2=0.99) \qquad \text{e5.5}$$

The error and resolution improved with 5% and ±1N respectively for the range of 0 N to 30 N. The appropriate calibration factors are incorporated into MATLAB to analyse the data.

5.3.3 Moment Calibration

In order to calibrate the plate to applied moments it was set up in the apparatus pictured in Figure 5.7. A pure moment was applied to the plate by applying two equal and opposite forces each at a distance of 3 cm from the centre of the plate. The weights varied from 0 to 1 kg at 50g intervals this resulted in a range of applied moments from 0 to 589 Nmm. Ten and twenty gram weights were also used to check for resolution. The moment calibration was linear (R^2 = 0.995). A small linear calibration factor (1.053) was required to get a better match with the calculated moment values and the actual applied moment values. Calibration showed that the applied moment could be accurately measured within a 7% uncertainty and a resolution of ±6 Nmm.

5.4 Using the Plate Hook

This section describes the use of the hook in chronological order. It begins with the results of the first surgical case using a hook with Plate A. A noise test in an empty OR was then performed. The second surgical case, again using Plate A, is presented. Failure tests on hooks containing Plate B and C are performed.

5.4.1 Surgical Case 1

The first case used a hook equipped with plate A measuring 1mm in thickness and having the 0.5 mm counter sunk screw holes. This OR case was a success in that the surgeon found the hook easy to use and it integrated with the existing CD system. The numerical results were difficult to interpret because of a large amount of noise in the system. The recorded voltages can be seen in Figure 5.8. The large spikes that are visible on the graph are not due to large forces but due to the fact that the connection between the wire and the circuit box was loose. If the data is edited and these spikes are removed the data looks somewhat better (Figure 5.9). Due to noise, not much that can be concluded from the applied forces in this data. The maximum moments are visible upon insertion (Figure 5.10) and removal (Figure 5.11) of the hooks. These moments are around 1100 Nmm for insertion and 730 Nmm for removal. There is some force present at about 750-1050 seconds into the procedure at which point it was noted that the rod pusher was being used. Taking a closer look at this part of the procedure, the average force is about 35 N combined with a moment of 125 Nmm (Figure 5.12). However, the noise on the force reading is about ± 20N. This noise is reflected in the fact that the noise on the raw voltage is about 80 mV peak to peak. Though the values of moment, and especially force, are not that large compared to the noise level, this attempt was able to provide some initial results.

5.4.2 Noise Test

Prior to the second case, the system was set-up in an empty OR to test for possible sources of noise. (Figure 5.13) There was little interference from any of the machinery with the exception of the electro cauterizer and the puls-ox emitter, which are only turned on intermittently to prevent blood loss and were not used during the recording period of the previous case. It is however noted, that those systems should not be turned on in conjunction with hook data collection, if they are, the data collected during that time must be disregarded. The noise level is about 10 mV for all the other equipment.

5.4.3 Surgical Case 2

The results of the second case are in Figure 5.14. This case, again using Plate A, didn't last long. The only recorded period was the insertion of the hook at which point the applied moment reached two major peaks. The first was 860 Nmm and the second was 930 Nmm, causing failure of the plate as recorded in Figure 5.15. This applied moment to failure was much less then what was calculated for a plate 1mm thick (4000 Nmm) however, due to the countersinking the effective thickness was 0.5mm at the area of stress concentration. Recall that the moment required to cause yielding for such a plate is 1000 Nmm and the ultimate applied moment to failure is 1200 Nmm. The noise level for this case was around 100mVpp, again much too large to obtain reliable force readings.

One must ask why did Plate A fail at 930 Nmm? One explanation to this question is that the fillet on the plate creates a stress concentration. For the geometry of the plate, this stress concentration is about 1.3 (Peterson 1974). Incorporating this stress concentration, the failure of the plate should occur at 867N. Recall the error on moment recordings is 7% so the recorded failure at 930Nmm could in fact be as low as 865 Nmm, which brings it within the stress concentration failure range. Another question is why did Plate A not fail during the first OR case where the insertional moment was recorded at a maximum of 1100Nmm? This can possibly be explained with fracture mechanics and micro crack propagation. Though fracture mechanics are not the basis for this thesis, a basic explanation is that local yielding even though minute, will cause a loss in local ductility at the vulnerable spot (Juvinal 2000). Since tool steel is already very brittle, this is likely what happened. The initial load of 1100Nmm during the first case caused yielding and upon repeated application of moments close to the yielding range, the plate lost ductility and eventually failed.

5.4.4 Failure of Plate B

After plate A, used in case one and two, broke it was inspected and the design was re-evaluated. The geometry of the plate was modified and plate B was fabricated. The

first modification was to eliminate the countersink for the screw heads. The next change was to actually decrease the overall plate thickness to 0.8mm in order to increase the sensitivity of the strain gauges by a factor of 1.6. Recall that this plate B should be able to withstand 512N of axial force and 2560Nmm of moment before yielding. This plate was sacrificed in the Instron Machine and was able to withstand a force of about 124 lbs (551 N) before failure. (Figure 5.16) This is within 5% of the calculated ultimate failure force of 577 N for the plate B design.

5.4.5 Failure of Plate C

A third and final plate, plate C, was manufactured. This plate was manufactured using an Electric Discharge Machine (EDM). The goal of this machining process was to reduce machining time and increase precision. Although this plate retains the same geometry as plate B it was made out of stronger steel so this plate should be able to withstand 780 N and 2935 Nmm of axial force and bending moment respectively before yielding. The EDM was able to quickly produce six of the plate C design and one was tested to failure in the Instron machine. Plate C failed at 168 lbs (747 N), which is within ten percent of the predicted ultimate failure load of 820N.

5.4.6 Surgical Case 3

In order to reduce the noise that was still apparent during the second OR case, the DAC system grounding was improved as explained in Appendix A.2. Another major source of noise during the two OR cases, was the length of cable connecting the hook to the DAC card. A 3 m cable was used in the OR to distance the laptop from the sterile zone. It was found that this long cable resulted in more ambient noise in the signal than the short, 1 m, cable that was frequently used for lab tests. In the lab, the ambient noise measured with the 3 m cable was about 40 mV peak to peak (pp), while the 1 m cable only had 1.5 mV pp as shown in Figure 5.17. Consequently, to get a better signal to noise ratio, the 1 m cable was used for the third OR case.

The results of the third OR case are shown in Figure 5.18. All three plots have time on the *x* axis. On the *y* axis the output voltage, calculated force and calculated moment are displayed for the first second and third plots respectively. The noise level is acceptable and much lower than the output signal. As observed previously, the maximum moments are during hook insertion as shown at the beginning of the time trace. For this case, the moment reaches 1000 Nmm. There is again a long period of quiet time while the surgeon is placing other hooks along the spine as noted from 50 to 550 seconds. From the 550 to 600 second marks, the hex nut was being loosely tightened into the hook as noted by the changing force and moment recordings. From about 600 to 750 seconds, the surgeon was "tugging" on the spine and rod to increase flexibility and properly fit the rod. This tugging resulted large hook loads; a maximum force of 370 N was reached, while the maximum moment was close to 500 Nmm. At the 750 second mark the rod rotation maneuver began and continued through to 900 seconds. During rod rotation the force carried by this hook gradually decreased while the moment fluctuated around zero. At this point, the hex nut was briefly tightened and the force levels off to about 250 N. The hex nut was then loosened and the hook was removed as evident from the 300 Nmm moment spike around the 980 second mark. After removal of the hook, the force and moment return to zero. The 370 N load experienced during the "tugging" of the spine was larger then anticipated however, the surgeon did report that he expected a large amount of preload on the hook before the rod rotation maneuver. The collection of data from future cases is required to determine if this high pre-loading pattern is typical.

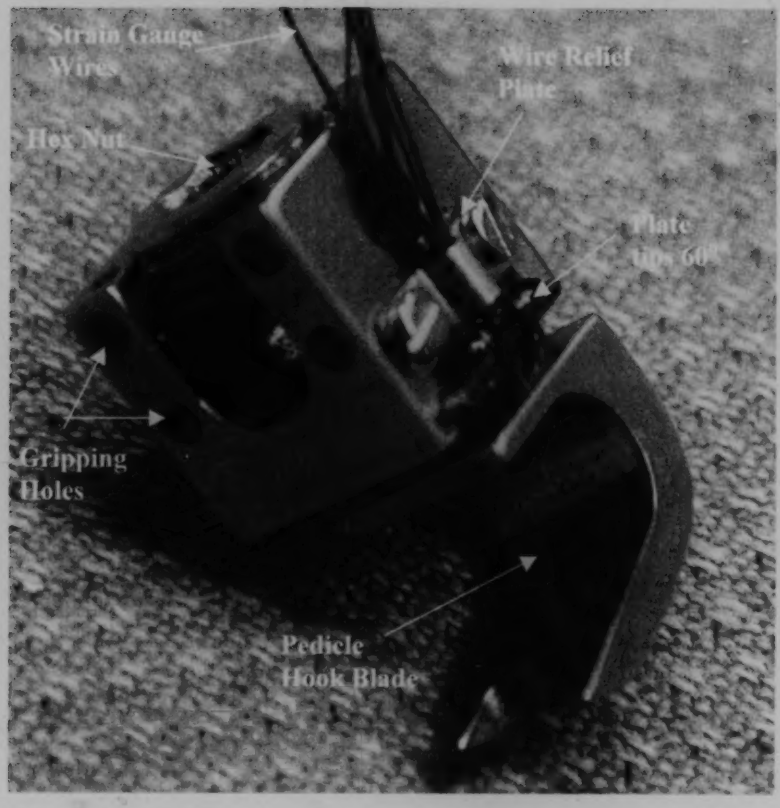

Figure 5.1: Prototype "plate" hook

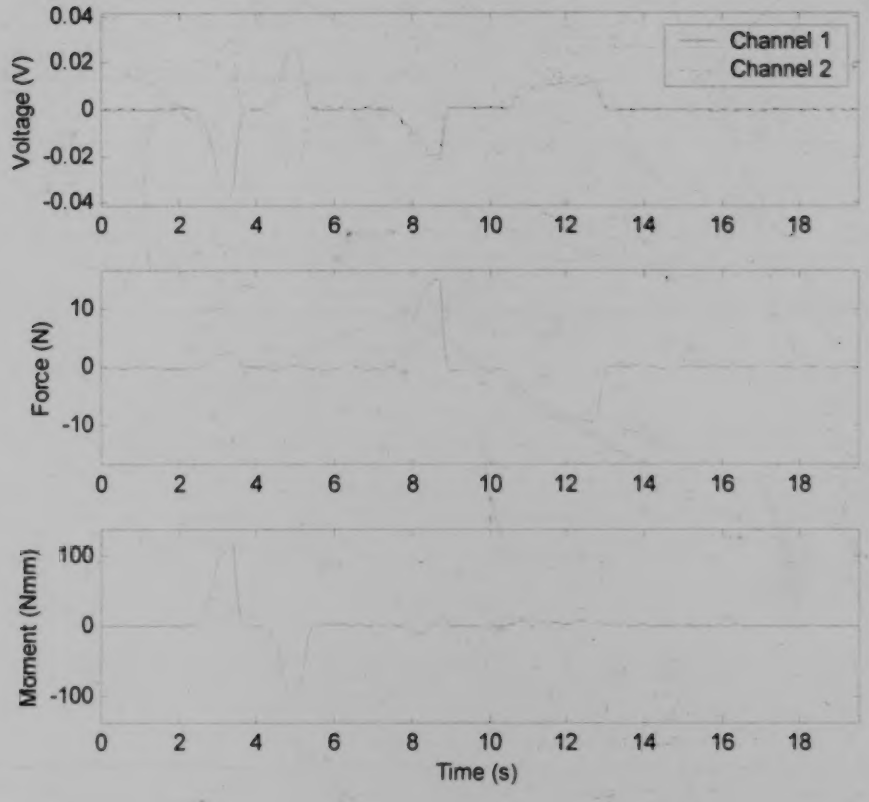

Figure 5.2: The raw voltage, resultant force and moment for bend, bend, push, pull test

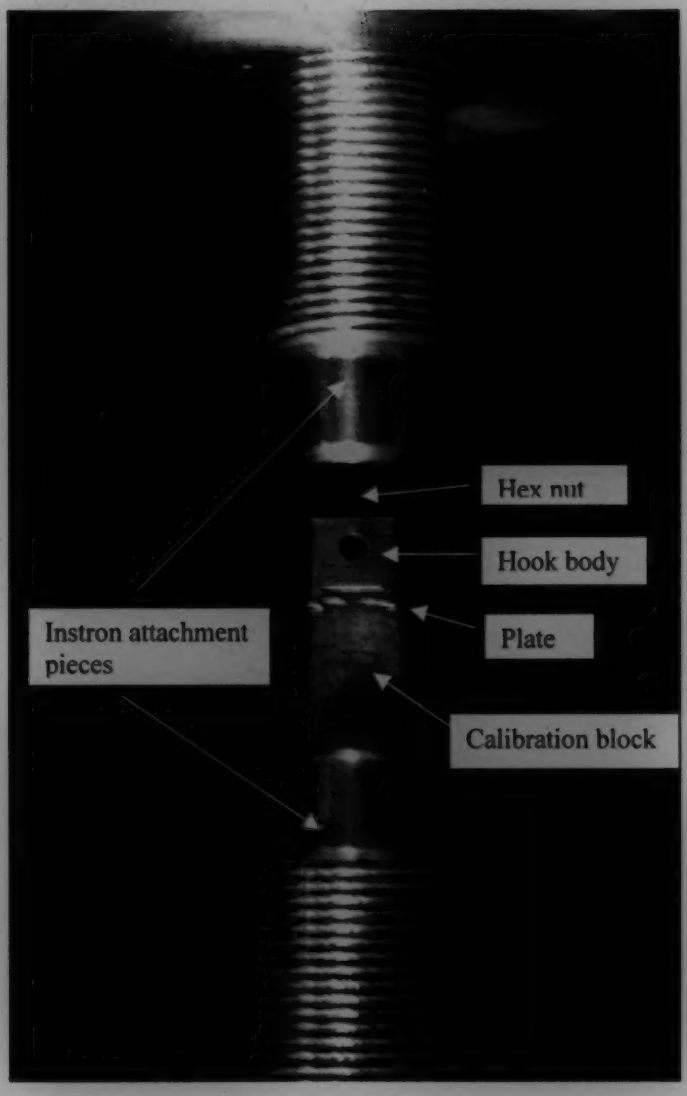

Figure 5.3: Calibration setup

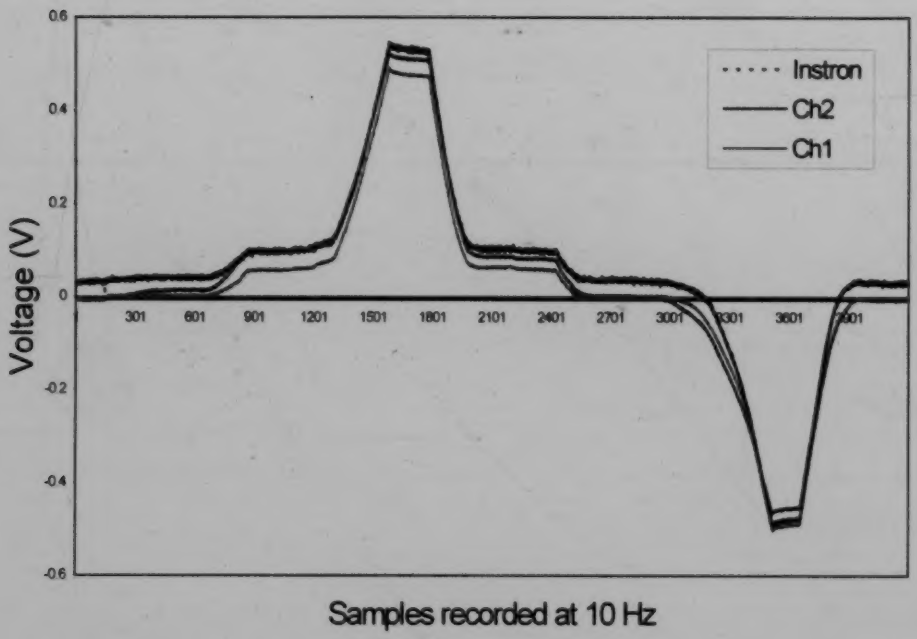

Figure 5.4: Raw voltage from tension, compression axial calibration

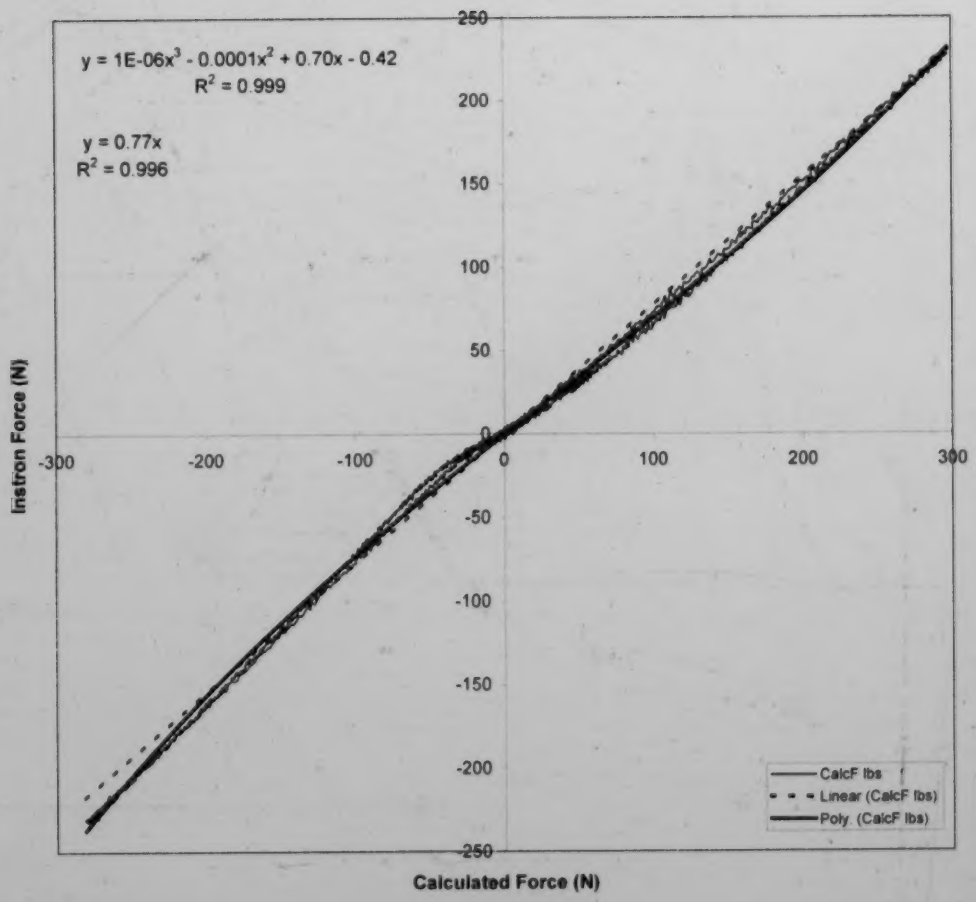

Figure 5.5: Calculated plate force vs applied Instron force

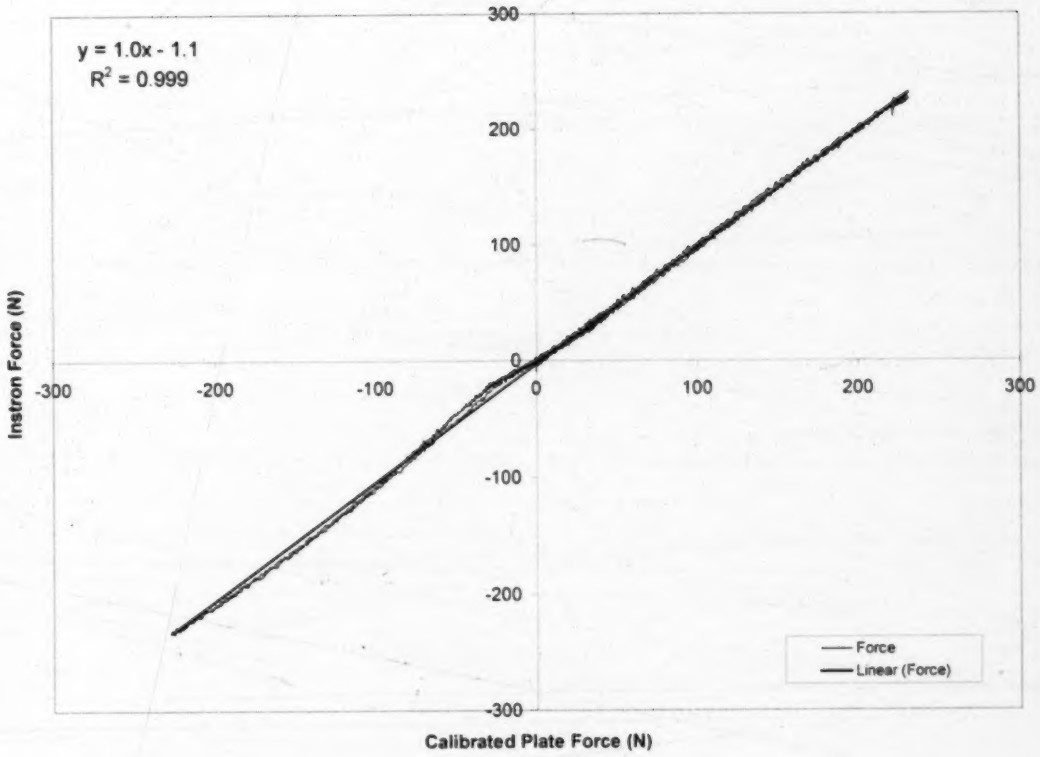

Figure 5.6: Calibrated plate force vs applied Instron force

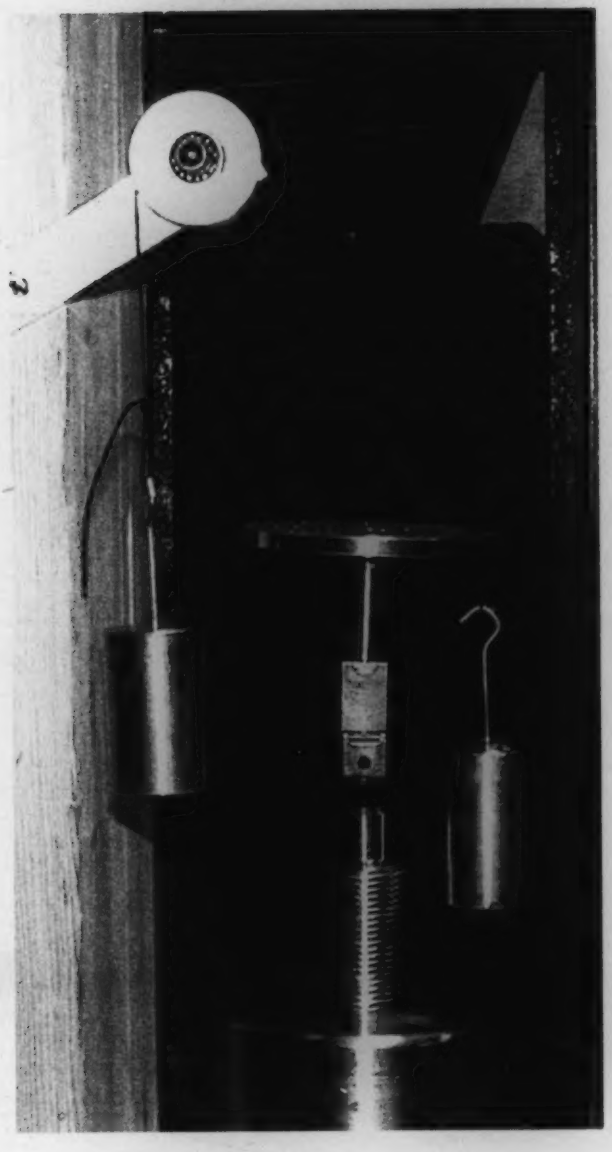

Figure 5.7: Moment calibration set-up

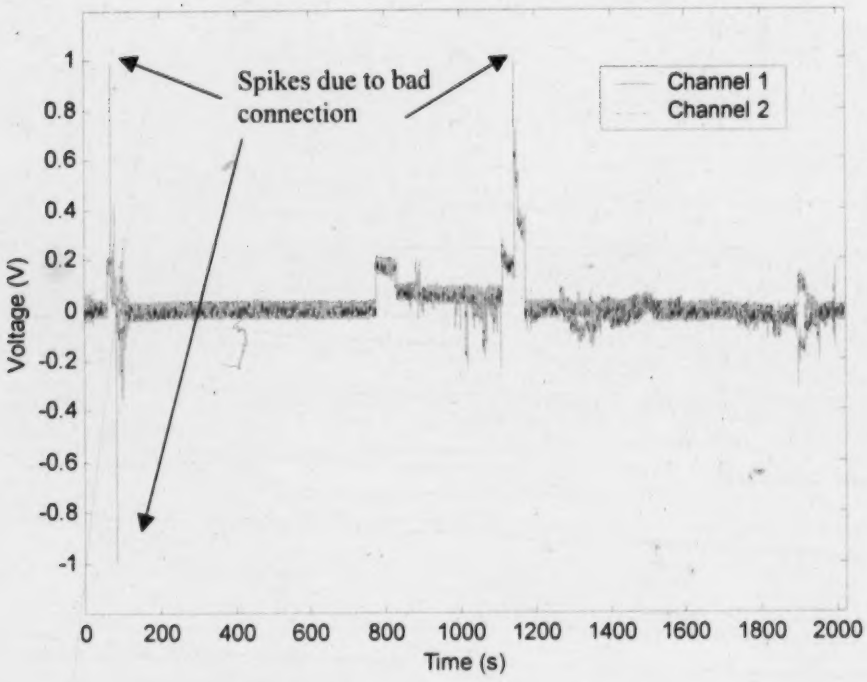

Figure 5.8: Raw voltages from Case 1

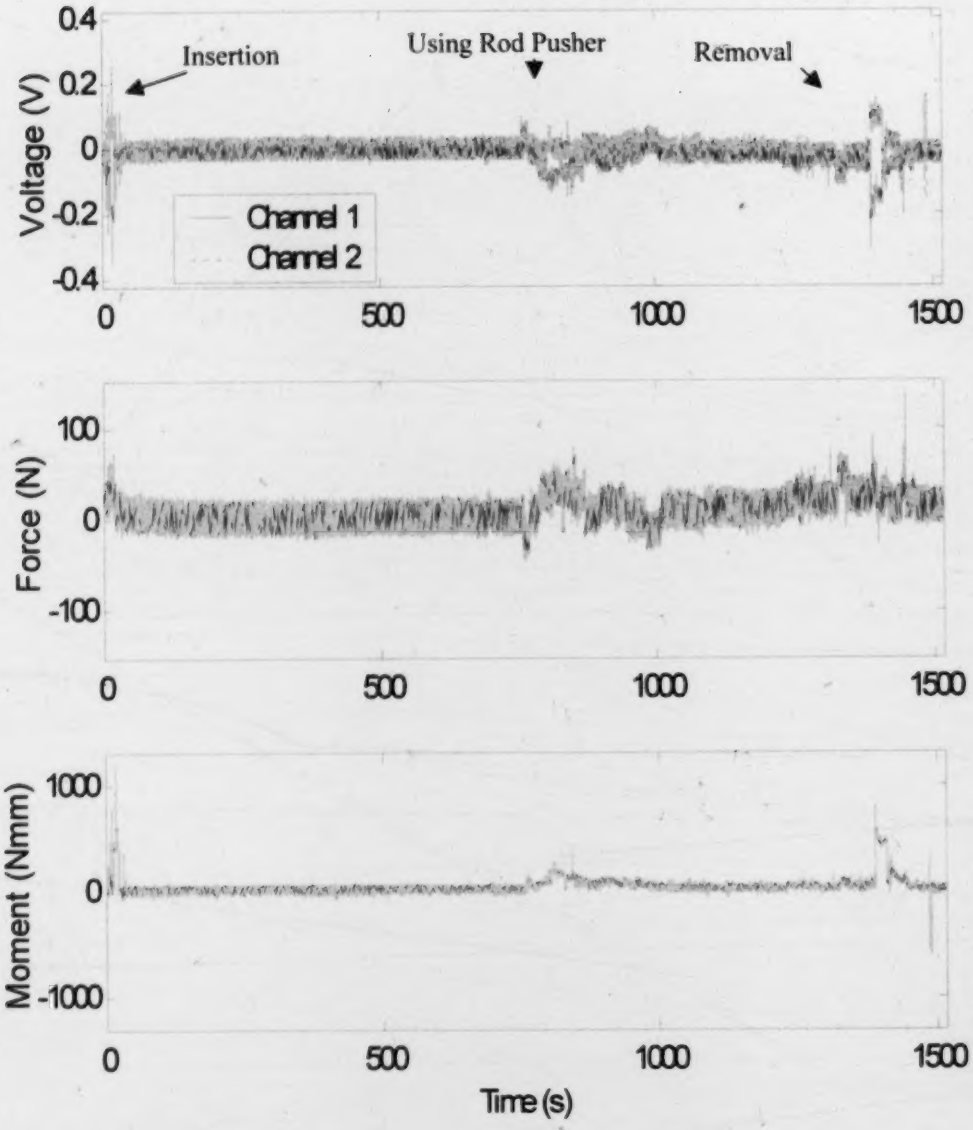

Figure 5.9: Edited results from Case 1

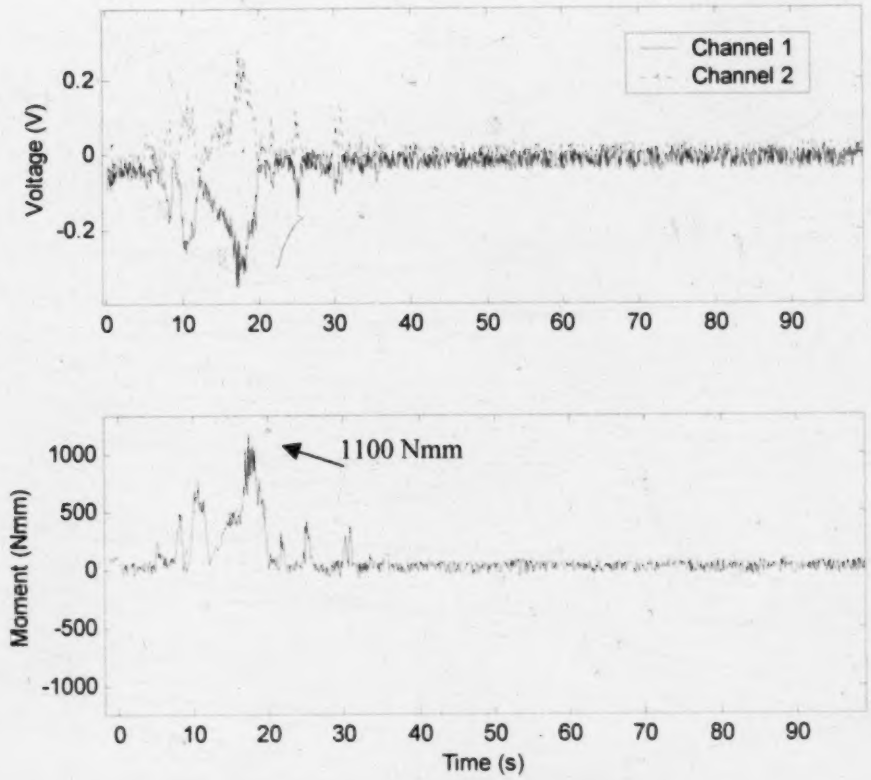

Figure 5.10: A close up look at the moments applied during hook insertio

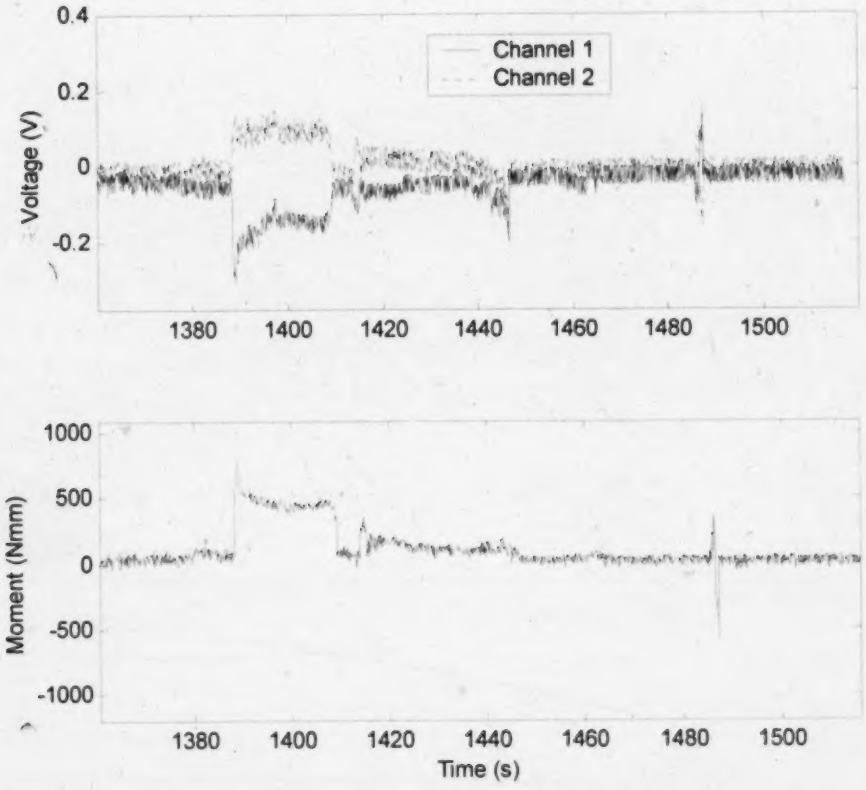

Figure 5.11: The moments and force present on removal of the hook in Case 1

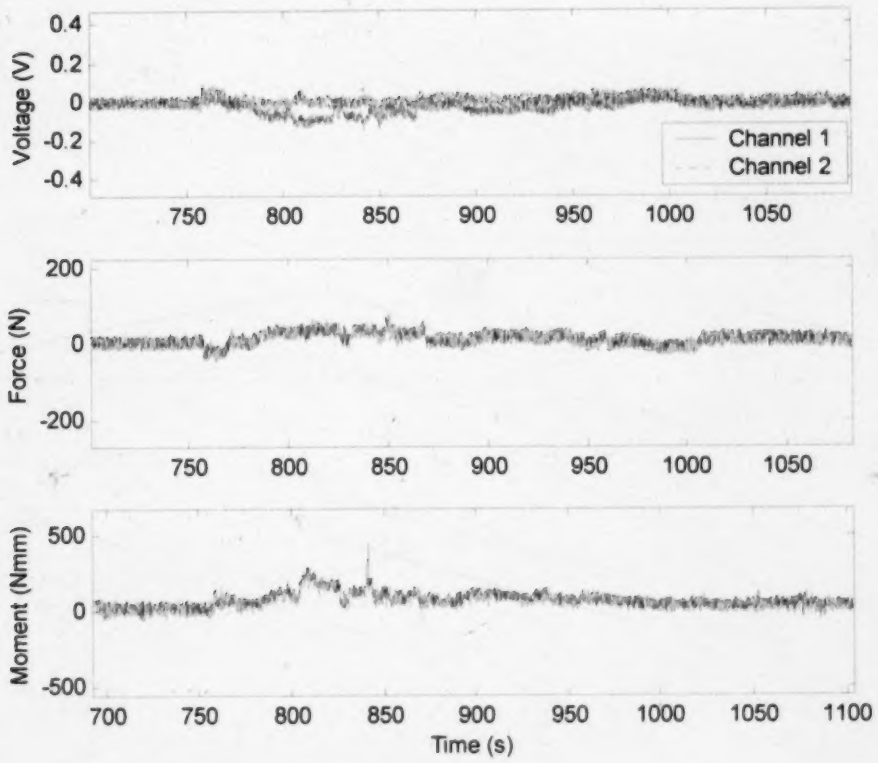

Figure 5.12: Force present while rod pusher is used

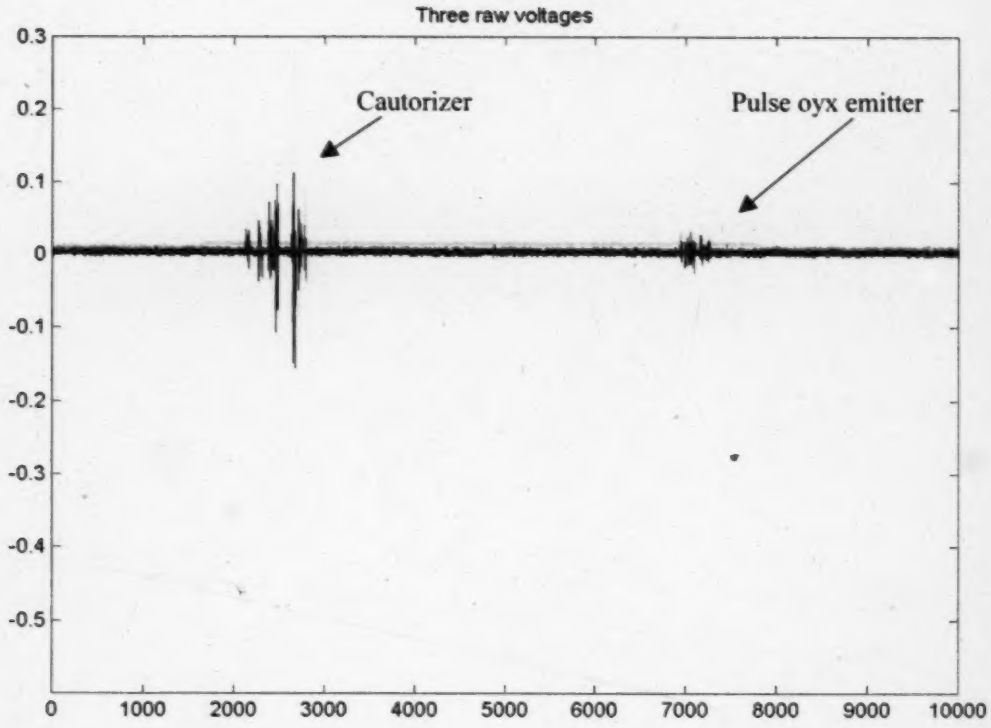

Figure 5.13: Noise test with various equipment in empty OR

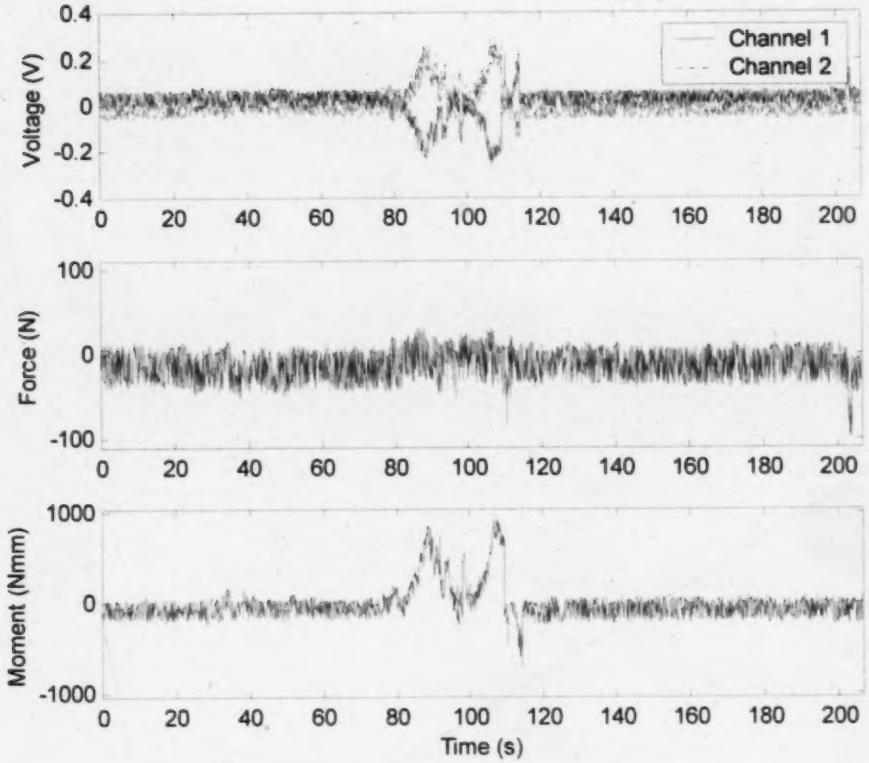

Figure 5.14: Raw voltages, calculated forces and moments from Case 2

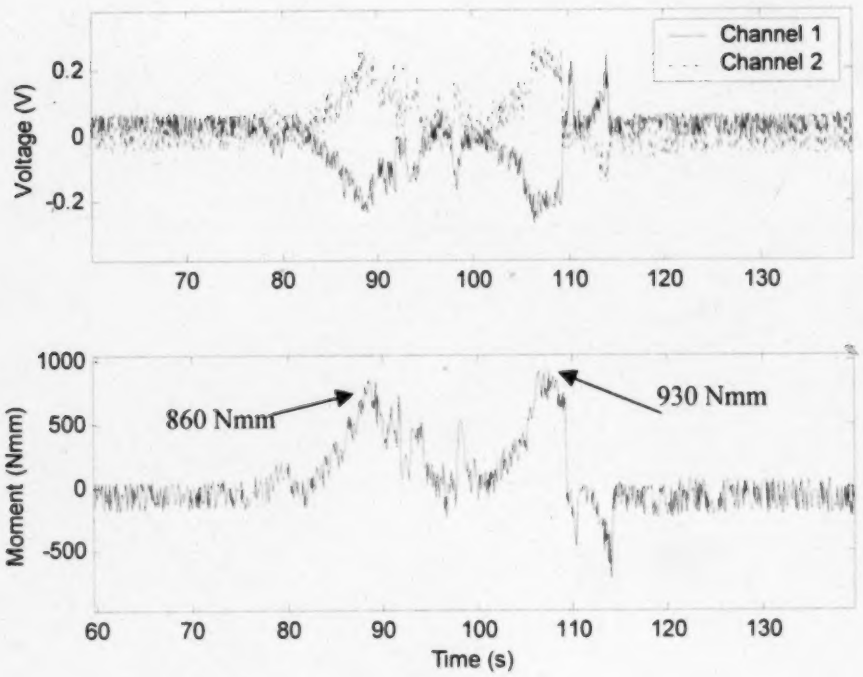

Figure 5.15: Insertional moment and failure of Plate

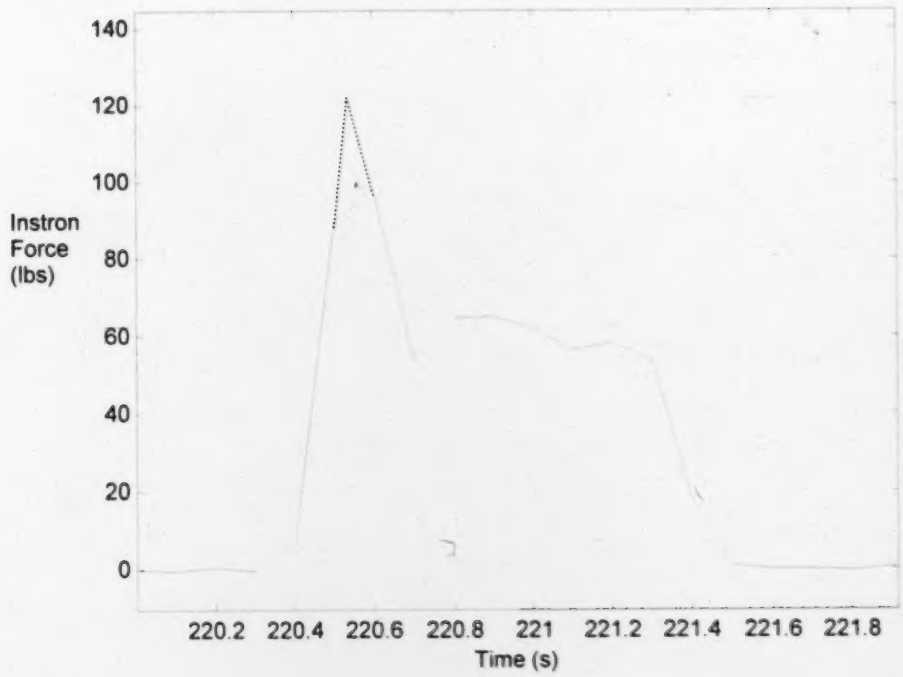

Figure 5.16: Test of Plate B in Instron Machine. The failure point was > 100 lbs and was off scale so the actual point was interpolated at 124 lbs.

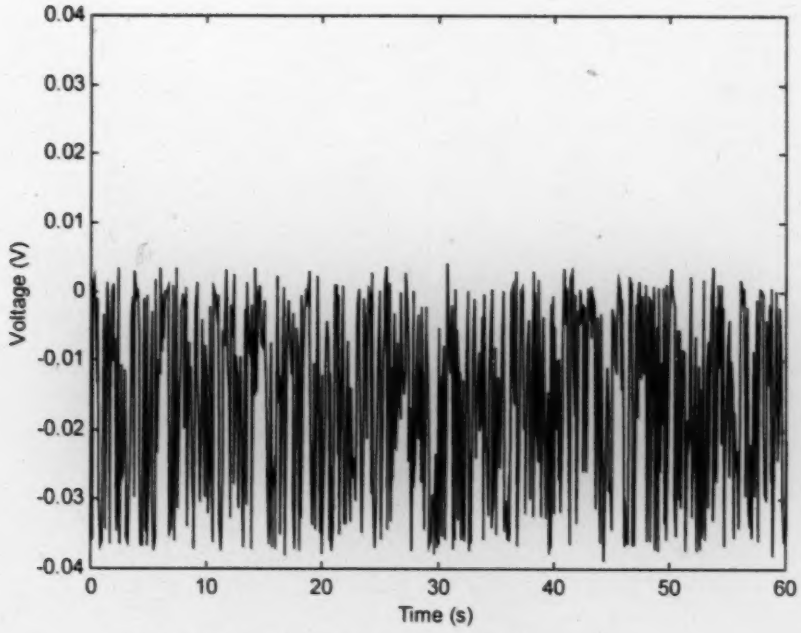

a) Ambient noise with 3 m long cable

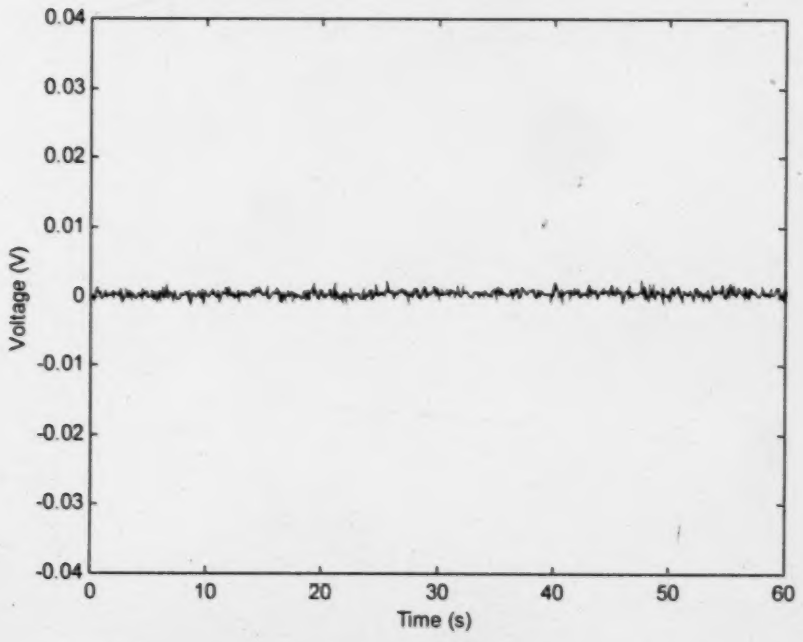

b) Ambient noise with 1 m short cable

Figure 5.17: Ambient noise comparison

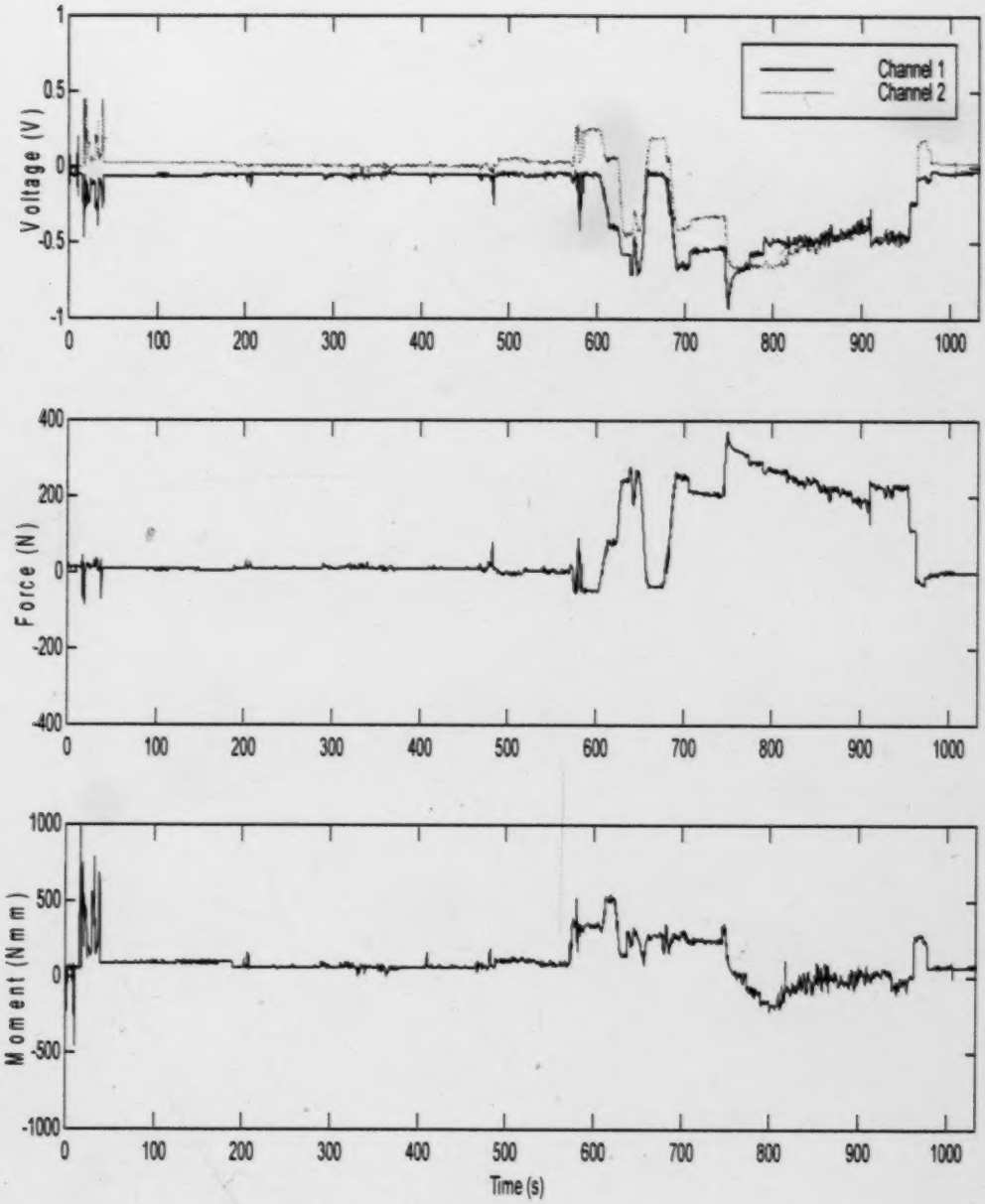

Figure 5.18: Results of OR Case 3

Chapter 6 Conclusions

6.1 Chapter 1

The purpose of this study was to develop tools that could measure the forces applied during scoliosis surgery. The design of such tools is just one step in providing a better understanding of the mechanics involved in scoliosis surgery. Chapter 1 began with a discussion of basic anatomy, scoliosis, surgical procedure and finally a quantitative prediction of the forces applied during surgery. Recall, that during the rod rotation maneuver, force is applied on the rod rotator, which transforms the scoliotic curve into a kyphotic curve. At the level of the hooks, the reaction can be broken into four different forces. These forces are axial pull-out, axial push-in, compression and distraction.

6.2 Chapter 2

The focus of the literature review was in three major areas. The first was to outline some of the complications that have arisen due to scoliosis surgery. It is the hope of this work that a better understanding in the mechanics involved in scoliosis surgery could one day reduce complications and improve patient safety. The second section consisted of a review of *in-vitro* testing concerning instrument failure. The range for screw pullout is between 345-1650 N while hook pullout was observed between 464-809 N. The literature concerning pullout was often contradictory although a rough estimate of the force required for pullout was gained. The third section dealt with a review of previously measured *in-vivo* forces. Since the majority of measurements were done many years ago when the Harrington rod system was used, the quantitative results of such studies are of little use today. The studies do however provide grounds for the efficacy of in-vivo force measurements. One aspect evident from the literature review is that to date, there are no means to measure the forces applied during scoliosis surgery. Until the forces are quantified, there will not be full understanding of the mechanics of surgical correction.

6.3 Chapter 3

6.3.1 Conclusions from Gripper Study

As a first step to understanding the mechanics of surgical scoliosis correction, the instrumented Gripper was designed. The Gripper consists of an instrumented sleeve and modified rod rotator that were used to determine the forces applied by the surgeon during the rod rotation maneuver. The Gripper was calibrated between 5 and 65 N and had a resolution of ±3 N. Housed within the Gripper sleeve is an inclinometer that can measure its position between –50 to 40 degrees from the vertical with a resolution of ±2 degrees. The Gripper was used on a total of 17 OR cases where the average maximum force applied by the surgeon was 39 (± 14) N. Analysing ten of these cases, a slight linear correlation ($R^2 = 0.46$) was observed when comparing the amount of correction (degrees of Cobb angle) to the maximum force applied. Dividing this group of ten into five adolescent idiopathic scoliosis (AIS) patients a larger linear correlation ($R^2 = 0.9$) was observed. There is still not sufficient data to draw strong conclusions from these correlations. The fact that there is a stronger correlation with the AIS patients alone may be due to the fact that the flexibility of the neuromuscular cases is variable depending on their diagnosis. Presumably, all the AIS patients would have similar flexibilities, musculature and ligament and tendon structure. Another interesting point surfacing with the Gripper data is the pattern of loading during the rod rotation maneuver. Most cases follow the curves presented in Sample I, Sample IIa and Sample IIb. These show an increase in force and inclination at about the same rate. Then, depending on whether it is the final rod rotation maneuver or not, there is either a sudden drop in both force and inclination or the inclination remains relatively constant at its maximum while the force gradually decreases as hex nuts are tightened.

6.3.2 Future Work with Gripper

A study is continuing to analyse the flexibility of the patients by looking at their bending radiographs. However it is important to note the diagnosis of the patient and how this may affect the overall forces required to correct the scoliotic deformity. Since a trend is beginning to surface in the pattern of loading during the maneuver this will be

further analysed. A long-term goal of the Gripper project is that force data can be combined with the position changes of the spine to aid in surgical modelling. Another potential use for the Gripper is a real time warning system. The software already incorporates a warning signal to alert the surgeon when an unsafe level of force is applied. After more data are collected, a better understanding of what is unsafe can be implemented into the real time program.

6.4 Chapter 4

The Gripper only provides biomechanical information during one part of the surgery, the rod rotation maneuver. In order to get a better understanding of the forces applied at the vertebral level, a hook capable of measuring the four predicted forces must be designed. FEA provided the initial analysis of three designs enabling the selection of a hook that best fit the criteria. The greatest advantage of FEA was in visualizing stress gradients on the hook designs in order to determine possible hook geometry and gauge locations. Once the plate design was selected, the plate itself was analyzed in greater detail. This analysis was done in two ways, the first with FEA and the second with analytical beam bending theory. The results of the FEA, analytical calculations and physical strain gauge output from a plate were compared. Using a 95% confidence interval there was no significant difference between the three methods. The analytical formulas provide the basis for transforming the strain gauge readings into applied forces and moments.

6.5 Chapter 5

6.5.1 Conclusions of Plate Hook Design

The design of the plate was the most challenging aspect of this thesis work. As evident from Chapter 5, the outcome was not always as anticipated. Initial results were positive and the plate hook was able to differentiate between being bent in two directions as well as axial push-in and pull-out. The greatest surprise was the failure of Plate A during the second OR case. In hindsight, the failure of this plate could be attributed to

the counter sunk holes made for the screws that attach the plate to the blade of the hook. Plate B was manufactured without the counter sunk holes, thus increasing the applied load before yielding. Plate C was manufactured with the same geometry as plate B it however, was made of D2 tool steel with slightly stronger mechanical properties. The body and blade of the hooks were made to conform not only to vertebral anatomy, but also to be used with the existing CD instrumentation. Trials 1 and 2 in the OR demonstrated that the hooks could in fact be used with the CD instrumentation.

Axial calibration in the Instron machine between –50 to +50 lbs (-222 to +222 N) showed that the applied load could be measured with a percent error of 8% and a resolution of ±5N. This resolution was insufficient for the forces anticipated in the OR, so a second calibration was done with weights from 100-3000g (1-30N). This calibration showed that the plate error and resolution improved to 5% and ±1N respectively. The moments were calibrated through a range of 0 to 589 Nmm. The applied moment could be accurately calculated to within a 7% error and a resolution of ±6 Nmm.

The first surgical case showed that the maximum moments were witnessed during insertion and removal of the hook. The moments were 1100 Nmm and 730 Nmm respectively. There was some force present during the time the rod pusher was being used. This force is estimated at 35 N, however the noise was great and this value is questionable.

The second case in the OR again measured high moments upon insertion of the hook. Two major peaks were recorded, 860 Nmm and 930 Nmm. It was on the second peak that the plate failed. Even taking the counter sunk holes into account the ultimate failure moment of Plate A should be 1127Nmm. The fact that the plate A failed at moments lower than predicted can be explained two ways. The first is with the addition of a stress concentration factor due to the fillet of the plate. Another explanation for the failure is that upon repeated application of moments close to the yielding range, the plate lost ductility and eventually failed.

In order to investigate the noise problem, the plate hook and DAC system were tested in an empty OR. This noise test showed interference only when the cauterizer and puls-ox emmiter were being used. In order to improve the noise the DAC system was

better grounded. By connecting the analogue and digital grounds to one another on the connector blocks, the noise in the system decreased.

To better understand the failure of the plate, Plate B and C were tested to failure in the Instron machine. Plate B failed at 551N, which was within 5% of the ultimate failure force of 577N. Plate C was stronger and failed at 747N, which was within ten percent of its ultimate failure of 820N. The ultimate moment applied to Plate C before failure was calculated at 4100 Nmm. Since the maximum recorded moment during surgery was 1100Nmm the design of Plate C has a built-in safety factor of four. This should be sufficient to prevent failure of Plate C during collection of OR data.

Plate C was used during surgical case 3. The noise problem experienced in the first two cases was resolved by using a 1 m cable. Maximum moments around 1000 Nmm were again observed on insertion of the hook. The maximum axial pull-out force of 370 N was observed prior to rod rotation while the surgeon was "tugging" on the rod. More data collection is required to determine if this high loading is typical.

6.5.2 Future Work with Plate Hook

Aside form continuing the data collection, there are more projects in mind for the plate hook. The first is to incorporate the plate design into a screw that can also measure the forces applied during surgery. The DAC and software have the ability to measure the output from up to four hooks or screws. If recordings from four different positions are monitored a distribution of force along the spine can be seen. Similarly to the Gripper, the forces from the hooks and screws can be incorporated into models of the spine.

6.6 Closing Remarks

The Plate hook and Gripper projects are continuing with data collection using the newly designed tools. The main objective of this thesis was met. That was to design tools capable of measuring forces during scoliosis surgery. The Gripper has been extensively used and a pattern in the type of loads applied during the rod rotation maneuver is beginning to surface. As well with more data, a correlation with applied force and amount of Cobb angle correction can be further validated. The three OR cases with the hooks showed that they can be integrated with the existing CD system and were

easy to use by the surgeon. More data collection is required with the hook to determine which levels of applied forces are typical. Continued data collection with the Gripper and the Plate hook will hopefully provide a better understanding of the mechanics involved in scoliosis surgery.

References

Aubin CE, Lobeau D, Labelle H, Maquinghen-Godillon AP, LE Blanc R Dansereau J. Planes of Maximum deformity in the Scoliotic Spine. Technology and Informatics 59: Research into Spinal Deformities 2. ISO Press. P45-48 1999.

Been HD, Kalkman CJ, Traast HS, Ongerboer de Visser BW. Neurologic injury after insertion of laminar hooks during Cotrel-Dubousset Instrumentation. Spine 19(12)1402-1405, 1994

Berlemann U, Cripton P, Nolte LP, Lippuner K, Schlapfer F: New means in spinal pedicle hook fixation. A biomechanical evaluation. European Spine Journal. 4:114-122, 1995

Chandrupatla TR, Belegundu AD. Introduction to Finite Elements in Engineering 2nd ed. New Jersey: Prentice Hall, 1997.

Coe JD, Warden KE, Herzig MA, McAfee PC: Influence of Bone Moneral Density on the Fixation of Thoracolumbar Implants A comparative Study of Transpedicular Screws, Laminar Hooks and Spinous Process Wires. Spine 15(9):902-907, 1990

Cotrel Y, Dubousset J, Guillanat M: New Universal Instrumentation in Spinal Surgery. Clinical Orthopaedics and Related Research. Feb.227: 10-23, 1988

Dubousset J. Three-Dimensional Analysis of the Scoliotic Deformity. In: Weinstein SL, editor. The Pediatric Spine: Principals and Practice. New York: Raven Press Ltd., 1994:479-496

Dunn HK, Daniels AU, McBride GG. Intraoperative Force Measurements During Correction of Scoliosis. Spine 7(5):448-455, 1982

Elfstrom G, Nachemsom A. Telemetry Recordings in the Harrington Distraction Rod: A method for the Increasing Safety in the Operative Treatment of Scoliosis Patients. Clinical Orthopaedics and Related Research. 93:158-172, 1973

Freedman LS, Houghton GR, Evans M. Cadaveric study comparing the stability of upper distraction hooks used in Harrington instrumentation. Spine 11(6):579-582, 1986

Gardner-Morse M, Stokes IAF. 1994. Three-Dimensional simulations of the Scoliosis Derotation Maneuver with Cotrel-Dubousset Instrumentation. Journal of Biomechanics. 27(2): 177-181.

Gray JM, Smith BW, Ashley RK, LaGrone MO, Mall J. Derotational analysis of Cotrel-Dubousset Instrumentation in Idiopathic Scoliosis. Spine 16(8Suppl):S391-393, 1991

Guidera KJ, Hooten J, Weatherly W, Highhouse M, Castellivi A, Ogden JA, Pugh L, Cook S: Cotrel-Dubousset Instrumentation, results in 52 Patients. Spine 18(4):427-431, 1993

Harrington PR. Treatment of scoliosis, correction and internal fixation by spine instrumentation. J Bone Joint Surgery 44A:591-610, 1962

Hasegwa K, Takahashi HE, Uchiyama S, Hirano T, Hara T, Washio T, Sugiura T, Youkaichiya M, Ikede M. An Experimental Study of a Combination Method Using a Pedicle Screw and Laminar Hook for the Osteoporptic Spine. Spine 22(9):958-963, 1997

Heller JG, Shuster JK, Hutton WC: Pedicle and Transverse Process Screws of the Upper Thoracic Spine. Spine. 24(7):654-658, 1999

Juvinall RC, Marshek KM, Fundamentals of Machine Component Design. John Wiley & Sons inc New York. pp.90-92, 2000

Longstein JE. Adolecent idiopathic scoliosis. The Lancet 344(19)1407-1412, 1994

Machinery's Handbook 26th edition. Editor McCauley CJ. Industrial Press Inc, New York pp444-473 pp 521 2000

matweb.com http://www.matweb.com

McAfee PC, Bohlman HH: Complications following Harrington Instrumentation for Fractures of the Thoracolumbar Spine. J Bone Joint Surg 67A(5): 672-685, 1985

McBride GG. Dunn HK. Daniels AU. Force measurements during operative correction of spinal deformities. Biomedical Sciences Instrumentation.
15:19-24, 1979 Apr 23-25.

Nachemsom A, Elfstrom G. A force Indicating Distractor for the Harrington_Rod Procedure. J Bone and Joint Surgery, 51-A(8): 1660-1662, 1969

Okuyama K, Abe E, Suzuki T, Tamura y, Chiba M, Sato K. Can Insertional Torque Predict Screw Loosening and Related Failures? An Invivo Study of Pedicle Screw Fixation Augmentation Posterior Lumbar Interbody Fusion. Spine 25(7):858-864, 2000

Omega, The pressure, strain and force handbook. P E-69, 1994

Peterson RE, Stress Concentration Factors, Wiley, New Your, 1974

Polly DW. Basic Principals of Spinal Instrumentation. SRS spinal deformities handbook SS22 p 1-8, 1996

Poulin F. 1998. Ecole Polytechnique Montreal, Personal Communication

Rittmeister M, Leyendecker K, Kurth A, Schmitt E. Cauda equina compression due to a laminar hook: A late complication of posterior instrumentation in scoliosis surgery. Eur Spine J 8:417-420 1999.

Roach JW, Ashman RB, Allard Rn, The Strength of a Posterior Element Claw at One versus Two Spinal Levels. J of Spinal Disorders, 3(3):259-261, 1990

Ruland CM, McAfee PC, Warden KE, Cunningham BW: Triangulation of Pedicular Instrumentation A Biomechanical Analysis. Spine 16(6): s270-s276, 1991

Tortora Gj, Grabowski SR, Principals of Anatomy and Physiology ninenth edition. John Wiley & Sons inc. 2000.

Van Ooy A, Geukers WGM, Results of CD Operation in Idiopathic Scoliosis. Acta Orthopaedica Belgica, 58(I) 129-133, 1992

Waugh TR, Intravital Measurements During Instrumental Correction of Idiopathic Scoliosis. Acta Orthopaedica Scandinavica. 58-75. 1966

Zeller RD, Dubousset J. CD Horizon Surgical technique for posterior scoliosis correction. SRS spinal deformities handbook p 1-9, 1996

Zdeblick TA, Kunz DN, Cooke ME, McCabe R. Pedicle Screw Pullout Strength, Correlation with Insertional Torque. Spine 18(12):1673-1676, 1993

Appendix A Electronics and DAC System

A.1 Bridge Circuits

The electronics used in the Gripper and for the Plate hook are based on the same principles. Since both cases involve a beam in bending, the strain gauges are mounted on the top and bottom of the cantilever beam for the Gripper, similarly on the top and bottom of the plate for the hook. The gauges are then connected in a Wheatsone half-bridge circuit, which provides temperature compensation. A schematic of the bridge and amplifier circuit is shown in Figure A.1. For the Gripper and the plate, the electronic components are somewhat different. The differences and their values are summarised in Table A.1.

Table A.1: Electronic components

	Gauges (Ω)	Excitation Voltage (V)	Gain	Signal @ Zero Output (V)
Gripper	360	5	1000	2.5 unipolar
Plate	120	3	100	0 bipolar

One major problem encountered with the circuit boards, dealt with the balancing of the bridge. If the resistances of the two strain gauges are not the same, the bridge will be unbalanced. To balance the bridge, one can increase the output offset voltage by adding a resistor in parallel to R2. If the output offset voltage needs to be decreased, one can add a resistor in parallel to R1. For the plate circuitry, a variable resistance potentiometer was placed in parallel so that the unloaded signal could be balanced to zero prior to use.

In order to calculate the strain, ε, the following equation can be used (Omega):

$$\varepsilon = \frac{-2\left(\Delta V / V_{in}\right)}{gf} \qquad \text{eA.1}$$

where: ΔV = differential output voltage

V_{in} = input voltage

gf = gauge factor

It is equation eA.1 that provides the basis for e4.16. Once the gauge signal has been routed through the bridge circuit and amplifier, it is sent to the data acquisition system.

A.2 DAC System

The data acquisition system consists of a DAQCard 1200 from National Instruments. The card has the capability of handling up to eight analogue channels. One important note is that in order to decrease noise and improve the grounding of the card, pins 9,11,13 and 50 should all be connected to one another. The card is also equipped with "software selectable gain" . This term is misleading as the output signal is not in fact multiplied by this gain but the resolution of the output signal is improved. The resolution itself is 12 bits, i.e. 1 in 4096. Table A.2 summarises the software selectable gain. For example, if one was looking at an expected signal of 100 mV on a unipolar range of 0-10V, only 1% or only 40 of the available increments would be used. A better scenario would be to look at the same signal with a 0-200mV unipolar range and then 50% or 2048 increments would be used. If one is unsure of the magnitude of the force applied, the next highest range should always be selected as the signal is clipped once the maximum range is reached.

A few other problems were encountered with the cards. After being unplugged from the laptop numerous times, the pins seem to fatigue on the card and/or cable. The

card has a tendency to overheat when used for long periods of time (>1h). The card comes with a 5 V output voltage that can be sent out from the computer. The consistency of this 5 V is questionable and it is recommended that a separate voltage supply is used as input to the bridge circuits. In general, the DAQCard 1200 was easy to use and, when connected to a laptop, provided a convenient portable data acquisition system.

Table A.2: Software selectable gain

Gain	**Range Unipolar**	**Range Bipolar**
1	0 to 10 V	± 5 V
2	0 to 5 V	± 2.5 V
5	0 to 2 V	± 1 V
10	0 to 1 V	± 500 mV
20	0 to 500 mV	± 250 mV
50	0 to 200 mV	±100 mV
100	0 to 100 mV	± 50 mV

A.3 LabWindows

The application software chosen to collect the data was LabWindows/CVI. The programs written in LabWindows have several features. The programs were able to plot, not only the raw voltages in real time, but also the calculated applied force. Also the data acquisition rate can be adjusted. For both the Gripper and the Plate hook this was 10 Hz. This rate was sufficient to obtain the signal while minimising the file size. The range can be selected for the Gripper it was 0 to 5V and for the Plate hook it was ±1 V. There is a data stop and start toggle button. The data can also be saved directly from a prompt in the LabWindows interface. The LabWindows user friendly interface provides a simple and easy way of collecting data from both the Gripper and the Plate hook.

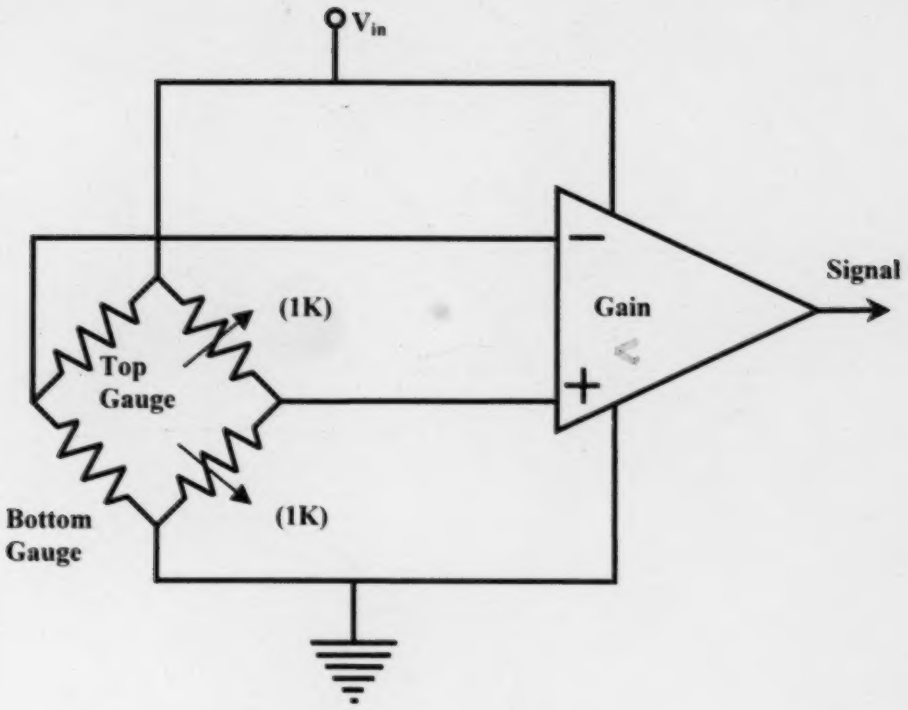

Figure A.1: Wheatstone bridge circuit electronic schematic

Appendix B Finite Element Type Selection

B.1 Introduction

Selection of elements in finite element analysis (FEA) has inherent difficulties. A balance must be reached between accuracy and processing time. Selecting different element types with different numbers of nodes can affect the results. Another option that affects the accuracy and processing time is the element size. To test different elements, a simple object can be modeled where the analytical results are known. From this one can proceed with FEA and test various elements.

B.2 Materials and Methods

ANSYS 5.6 was used to model a simple beam measuring 5 x 10 x 100 mm as seen in Figure B.1. This beam was then fixed by four key points on the corners of the left-hand side of the beam. A zero displacement was set in all degrees of freedom on the four key points making a fully constrained cantilever beam. At first an axial load of 10N was applied to the right end of the beam in the positive X direction with a magnitude of 2.5 N on each of the four key points. This distribution of load over the four key points was selected to reduce a stress concentration at any one point. The stress and strain results of the beam were analyzed. The same beam geometry was loaded but instead a bending load was applied in the negative Y direction. Again this load was 10N distributed as -2.5 N applied to the four key points. The stresses and strains were then solved for this load distribution. This was repeated four times for each load configuration using different element characteristics. The four elements tested include: SOLID45, SOLID72, SOILD73, and SOILD92. SOLID45 is a structural solid cube with eight nodes. SOLID72 is a tetrahedral with 4 nodes. SOLID73 is a structural solid cube with rotations at its 8 nodes. Finally, SOLID92 is tetrahedral in shape with mid nodes giving a total of 10 nodes. The nodal stress and strain were listed for each case and compared with the theoretical values calculated by hand. To reduce any errors from the axial load and constraints the stresses and strains were measured in the center of the beam. For the

bending load resultant stresses and strain were measured 25 mm from the fixed end. Every time the beam was meshed using smart mesh tool with the coarseness set to six. Smart mesh automatically selects the element size based on the coarseness selected. Ten is the coarsest setting while one is the most fine. (Though the size of the elements does affect accuracy this was not tested in this portion of the experiment.) The option exists to mesh both SOLID45 and SOLID73 with hexagonal (hex) or tetrahedral (tet) mesh. Both were tried and the results were compared.

B.3 Results

All four element types preformed equally well in the axial strain and stress calculation. There were, however, marked differences in the resultant bending stress and strain for each case. The total number of nodes ranged from 113 to 433. The percent error in strain measurement varied from 63% to 0.7% while the error in stress varied from 62% to 0.3%. A summary of the FEA calculated stress and strain as well as the percent errors when compared to the analytical results can be found in Table 1.

Table B.1: Bending test results

Element Type	Stress (N/mm^2)	% Error	Strain micro ε	% Error	Number of nodes
Analytical	18.00	NA	90.00	NA	NA
SOLID45 tet	6.87	61.83	33.50	62.78	156
SOLID45 hex	17.43	3.17	87.42	2.87	200
SOLID72	14.07	21.81	59.33	34.07	113
SOLID73 tet	14.83	17.59	64.67	28.15	157
SOLID73 hex	17.56	2.44	88.40	1.78	256
SOLID92	18.06	0.33	90.67	0.74	433

B.4 Conclusion

The error in FEA calculated strain was as high as 63% for the beam meshed with SOLID45 tet. The error was also high for the SOLID73 tet mesh. This shows that, though possible, it is dangerous to mesh a hexagonal object with tetrahedral meshing.

The strain error for SOLID72 was also high at 34%. For this element type there was a warning message stating that "Structural elements without mid nodes usually produce much more accurate results in quad or brick shape." Therefore, it is recommended to use SOLID92 which has mid nodes or use SOLID73hex or SOLID45hex which are brick shape. The error for these three shapes is acceptable with a maximum error of 3.17%. For this reason SOLID45hex, SOLID73 hex or SOLID92 will be selected as the element to use in continued finite element analysis. Because SOLID92 has mid nodes, a quadratic shape function is used providing better stress and strain results. The ability for these three elements to conform to varied geometry as well as processing time will be the ultimate determinant to which one of the three is used.

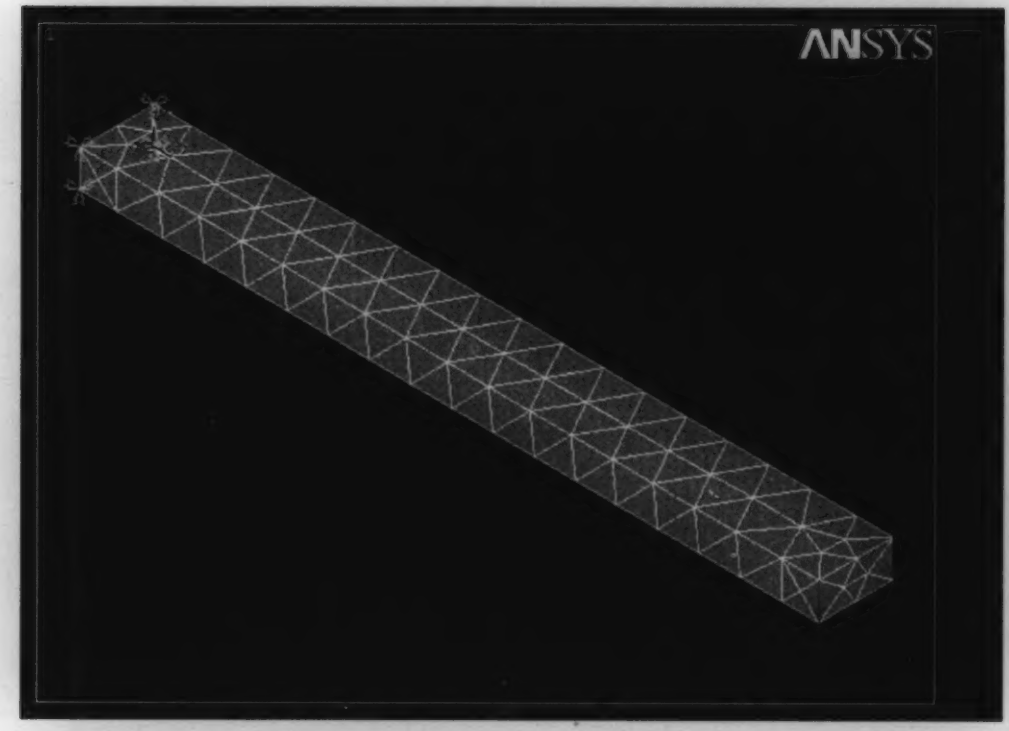

Figure B.1: FEA model of cantilever beam